NASA CR-168167
GARRETT REPORT 21-4269

NASA

FINAL REPORT
FOR
SCALED CENTRIFUGAL COMPRESSOR, COLLECTOR AND RUNNING GEAR PROGRAM

GARRETT TURBINE ENGINE COMPANY
A DIVISION OF THE GARRETT CORPORATION
111 SOUTH 34TH STREET — P.O. BOX 5217
PHOENIX, ARIZONA 85010

PREPARED FOR

NATIONAL AERONAUTICS AND SPACE ADMINISTRATION

NASA LEWIS RESEARCH CENTER
CONTRACT NAS3-22431

1. Report No.	2. Government Accession No.	3. Recipient's Catalog No
NASA CR-168167		

4. Title and Subtitle	5. Report Date
Final Report for Scaled Centrifugal Compressor, Collector and Running Gear Program	March 31, 1983
	6. Performing Organization Code
7. Author(s)	8. Performing Organization Report No.
J. G. Kenehan	21-4269
	10. Work Unit No.
9. Performing Organization Name and Address	11. Contract or Grant No.
Garrett Turbine Engine Company A Division of The Garrett Corporation 111 South 34th Street--P.O. Box 5217 Phoenix, Arizona 85010	NAS3-22431
	13. Type of Report and Period Covered
12. Sponsoring Agency Name and Address	CR, 4/80-12/82
NASA Lewis Research Center and U.S. Army Research and Technology Laboratories (AVRADCOM), Propulsion Laboratory, Cleveland, Ohio	14. Sponsoring Agency Code

15. Supplementary Notes

Project Manager: Richard L. Lantz
NASA Lewis Research Center
Cleveland, Ohio

16. Abstract

The Scaled Centrifugal Compressor, Collector and Running Gear Program was conducted in support of an overall NASA strategy to improve small-compressor performance, durability, and reliability while reducing initial and life-cycle costs. Accordingly, Garrett designed and provided a test rig, gearbox coupling, and facility collector for a new NASA facility, and provided a scaled model of an existing, high-performance impeller for evaluating scaling effects on aerodynamic performance and for obtaining other performance data.

Test-rig shafting was designed to operate smoothly throughout a speed range up to 60,000 rpm. Pressurized components were designed to operate at pressures up to 300 psia and at temperatures to 1000°F. Nonrotating components were designed to provide a margin-of-safety of 0.50 or greater; rotating components, for a margin-of-safety based on allowable yield and ultimate strengths.

Design activities were supported by complete design analysis, and the finished hardware was subjected to check-runs to confirm proper operation. The test rig will support a wide range of compressor tests and evaluations.

17. Key Words (Suggested by Author(s))	18. Distribution Statement
Centrifugal Compressor Scale Test Rig	Unclassified-unlimited

19. Security Classif. (of this report)	20. Security Classif. (of this page)	21. No. of Pages	22. Price*
Unclassified	Unclassified	86	

* For sale by the National Technical Information Service, Springfield, Virginia 22161

TABLE OF CONTENTS

TABLE OF CONTENTS (Contd)

LIST OF ILLUSTRATIONS

LIST OF ILLUSTRATIONS (Contd)

LIST OF ILLUSTRATIONS (Contd)

LIST OF ILLUSTRATIONS (Contd)

LIST OF TABLES

SUMMARY

The Scaled Centrifugal Compressor, Collector, and Running Gear Program (NASA Contract NAS3-22431) has been part of an overall NASA strategy to improve small compressors in turboshaft, turbofan, and turboprop engines used in rotorcraft, fixed-wing general aviation, and cruise missile aircraft. Included in this strategy has been an effort to improve performance, durability, and reliability while reducing both initial and life-cycle costs of components for advanced, small gas turbine engines. And of particular interest has been the potential of scaling as a means of applying advanced technologies developed for large gas turbine engines to small gas turbine engines.

The Garrett Turbine Engine Company supported this NASA strategy by fulfilling a three-fold program objective. First, the program provided a scaled model of an existing, high-performance centrifugal impeller for evaluating the effects of scaling on aerodynamic performance and for obtaining detailed measurements within the blade passages (using NASA-furnished laser anemometry). Second, the program provided a test rig and gearbox coupling for testing compressors in a research facility at NASA-LeRC. And, third, the program provided a facility collector with a flow-control valve.

Garrett performed complete design studies and analyses for the scaled centrifugal compressor, collector, and test rig. The test-rig shafting was designed to operate smoothly throughout a speed range up to 60,000 rpm. Pressurized components (comprising the casing) were designed to operate at pressures up to 300 psia and at temperatures up to 1000°F.

- Nonrotating components were designed to provide a margin-of-safety of 0.50 or greater (based on tensile yield strength). A minimum stress concentration factor of 3.0 was used at cutouts for the evaluation of low-cycle-fatigue (LCF) life.

- Rotating components were designed for a margin-of-safety based on allowable yield and ultimate strengths. The yield allowable stress was 80 percent of the -3σ yield, and the ultimate allowable stress was 64 percent of -3σ ultimate. A stress concentration factor (K_t) of 1.56 was used for all curvic couplings, and a K_t of 3.12 was used for instrumentation access holes in the tiebolt.

Prior to shipment to NASA, a mechanical check-run of the test rig and functional checks of the torque-tube and throttle-valve assemblies confirmed that all hardware was operating as designed. The operating characteristics of the test rig and general test rig "behavior" were as expected. When assembled and installed in the NASA facility, the test rig and throttle valve assembly will provide for a wide range of compressor tests and evaluations.

LIST OF TABLES

SUMMARY

The Scaled Centrifugal Compressor, Collector, and Running Gear Program (NASA Contract NAS3-22431) has been part of an overall NASA strategy to improve small compressors in turboshaft, turbofan, and turboprop engines used in rotorcraft, fixed-wing general aviation, and cruise missile aircraft. Included in this strategy has been an effort to improve performance, durability, and reliability while reducing both initial and life-cycle costs of components for advanced, small gas turbine engines. And of particular interest has been the potential of scaling as a means of applying advanced technologies developed for large gas turbine engines to small gas turbine engines.

The Garrett Turbine Engine Company supported this NASA strategy by fulfilling a three-fold program objective. First, the program provided a scaled model of an existing, high-performance centrifugal impeller for evaluating the effects of scaling on aerodynamic performance and for obtaining detailed measurements within the blade passages (using NASA-furnished laser anemometry). Second, the program provided a test rig and gearbox coupling for testing compressors in a research facility at NASA-LeRC. And, third, the program provided a facility collector with a flow-control valve.

Garrett performed complete design studies and analyses for the scaled centrifugal compressor, collector, and test rig. The test-rig shafting was designed to operate smoothly throughout a speed range up to 60,000 rpm. Pressurized components (comprising the casing) were designed to operate at pressures up to 300 psia and at temperatures up to 1000°F.

- Nonrotating components were designed to provide a margin-of-safety of 0.50 or greater (based on tensile yield strength). A minimum stress concentration factor of 3.0 was used at cutouts for the evaluation of low-cycle-fatigue (LCF) life.

- Rotating components were designed for a margin-of-safety based on allowable yield and ultimate strengths. The yield allowable stress was 80 percent of the -3σ yield, and the ultimate allowable stress was 64 percent of -3σ ultimate. A stress concentration factor (K_t) of 1.56 was used for all curvic couplings, and a K_t of 3.12 was used for instrumentation access holes in the tiebolt.

Prior to shipment to NASA, a mechanical check-run of the test rig and functional checks of the torque-tube and throttle-valve assemblies confirmed that all hardware was operating as designed. The operating characteristics of the test rig and general test rig "behavior" were as expected. When assembled and installed in the NASA facility, the test rig and throttle valve assembly will provide for a wide range of compressor tests and evaluations.

1.0 INTRODUCTION

This document is submitted by Garrett Turbine Engine Company (GTEC), a division of The Garrett Corporation. It presents the Final Report for the Scaled Centrifugal Compressor, Collector and Running Gear Program, hereinafter referred to as the Scaled Centrifugal Compressor Program. This program was conducted from July 28, 1980 through December 22, 1982 for the NASA-Lewis Research Center (NASA-LeRC) under Contract NAS3-22431.

1.1 Background

NASA-LeRC is active in developing both large and small flow-class compressors; however, NASA-LeRC required the specific capability to test and develop 10-lb/sec-flow-class compressors. The Scaled Centrifugal Compressor Program has provided NASA-LeRC with a 10-lb/sec-flow-class compressor test rig and the associated running gear necessary for complete and varied testing of compressors in this flow class. Additionally, a scaled, 10-lb/sec compressor stage was supplied with the test rig as a part of the initial test series for the new NASA-LeRC compressor test facility.

1.2 Relevance and Significance of the Program

The Scaled Centrifugal Compressor Program has been part of an overall NASA strategy to improve small compressors in turboshaft, turbofan, and turboprop engines used in rotorcraft, fixed-wing general aviation, and cruise missile aircraft. Included in this strategy has been an effort to improve performance, durability, and reliability while reducing both initial and life-cycle costs of components for advanced, small gas turbine engines. And of particular interest has been the potential of scaling as a means of applying advanced technologies developed for large gas turbine engines to small gas turbine engines.

The Scaled Centrifugal Compressor Program supported this NASA strategy by providing a scaled centrifugal compressor stage (or, impeller*), an appropriate test rig, and a facility collector capable of evaluating the effects of scaling on aerodynamic performance. [A parallel GTEC program will provide test rig capabilities for characterizing the flow within the rotating blade passages by the use of Laser Anemometry (LA) measurements.]

*Throughout the remainder of this report, the centrifugal compressor stages discussed are referred to as impellers; for simplicity, "compressor" is used to refer to the larger system which includes the impeller.

1.3 Scope of the Program

The program has provided to NASA-LeRC a test rig, facility collector, and appropriate instrumentation for testing a single-stage, scaled centrifugal impeller (also supplied). However, the test rig is designed to accommodate growth to a multistage machine -- i.e., a two-stage centrifugal or a single-stage-centrifugal/two-stage-axial configuration.

GTEC has furnished all labor, services, and materials to design, fabricate, and assemble the scaled impeller, collector, and test rig. The statement of work consisted of the following four tasks:

- Preliminary design of the test rig, facility collector, coupling, and compressor (Task I)
- Final design of the test rig, facility collector, coupling, and compressor (Task II)
- Fabrication, procurement, and assembly of the test rig, facility collector, coupling, and impeller (Task III)
- Design reports and program management (Task IV).

1.4 Purpose of the Program

The objective of the program was three-fold. First, it provided a scaled model of an existing, high-performance centrifugal impeller for evaluating the effects of scaling on aerodynamic performance and for obtaining detailed measurements within the blade passages (using NASA-furnished LA). Second, the program provided a test rig and gearbox coupling for testing compressors in a research facility at NASA-LeRC. And, third, the program provided a facility collector with a flow-control valve.

1.5 Overview of Technical Approach

The Scaled Centrifugal Compressor Program test rig and collector layouts are shown in Figure 1. The compressor is straddle-mounted between a forward roller bearing and an aft thrust bearing, both of which are hydraulically mounted on oil squeeze films. A clearance-control spindle is used to vary the impeller-to-shroud axial clearance through the operating speed range. (This eliminates the need for a test-rig teardown to shim for proper clearance after the mechanical check-run of each build.) A thrust balance piston is used to maintain a constant, low-thrust load on the clearance-control spindle. Lubrication oil, pressurized air, vacuum, instrumentation lead-outs, and other services are supplied through tubes in the test rig exhaust plenum and tubes entering the forward bearing cavity. Instrumentation locations are provided to monitor impeller-to-shroud clearance, thrust load, shaft excursion, and air-seal pressure differentials.

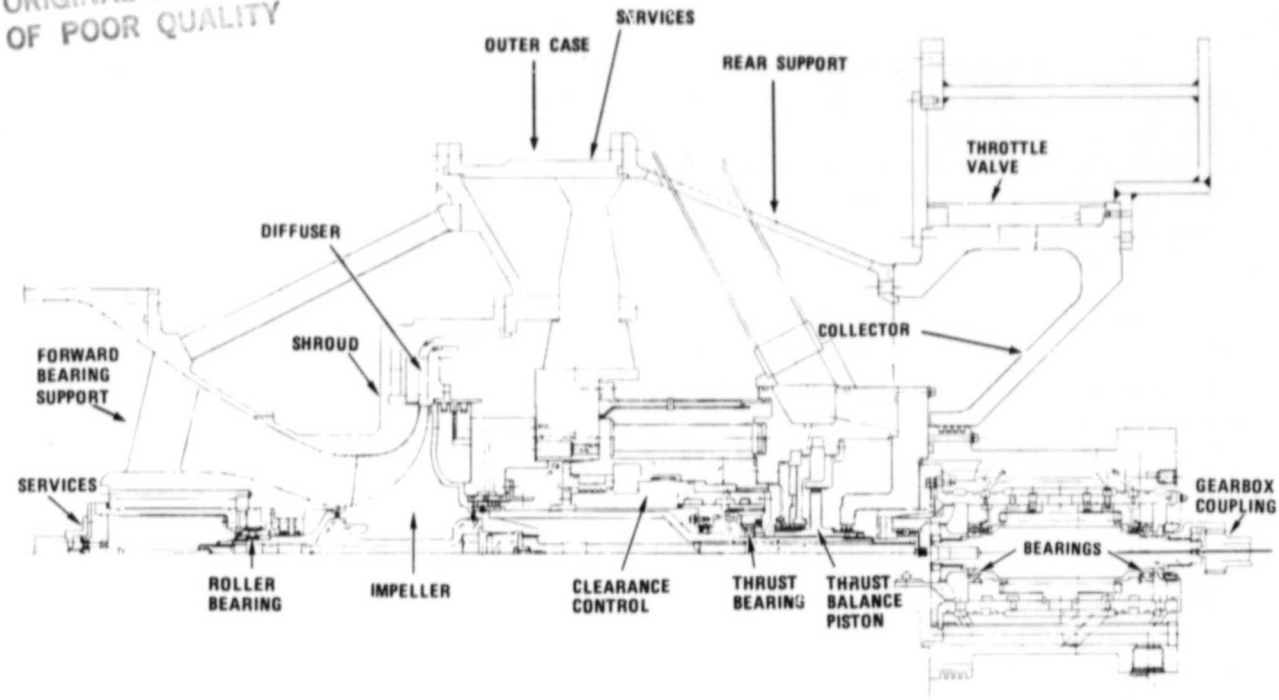

Figure 1. NASA Scaled Centrifugal Compressor Test Rig.

1.5.1 Aerodynamic Scaling

The baseline centrifugal impeller used for this program was designed and tested under Contract F33615-74-C-2006 for the U.S. Air Force Aeronautical Propulsion Laboratory (AFAPL) at Wright-Patterson Air Force Base. [See AFAPL Report TR78-66-21-0820(52)A.] The baseline (AFAPL) and scaled (NASA) impellers are shown in Figure 2.

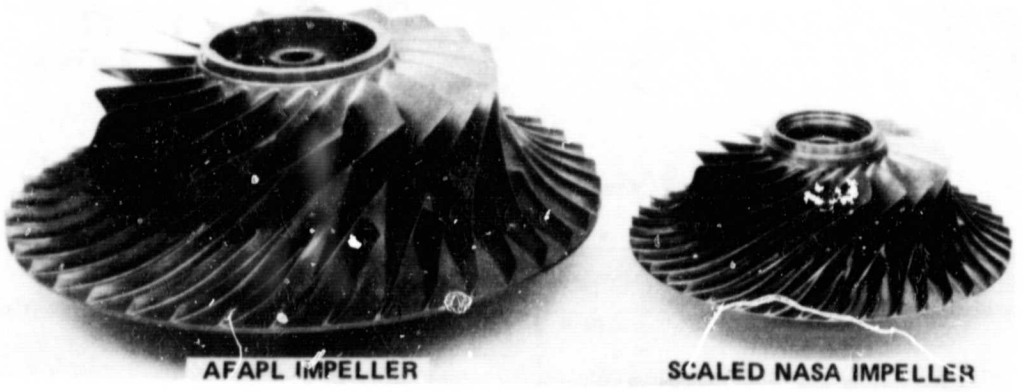

Figure 2. AFAPL 25-lb/sec and NASA 10-lb/sec Impellers.

The configuration of the NASA impeller was generated by applying a scaling factor to the manufacturing coordinates (cold shape) of the baseline impeller; and the impeller-to-shroud running clearance was scaled by the same factor. This scaling factor was calculated by taking the square root of the ratio of the scaled compressor airflow to the baseline compressor airflow and is equal to 0.6325.

An outline of the NASA scaled compressor flow path is shown in Figure 3. The aerodynamic objectives of this compressor include a corrected flow of 10 lb/sec, a pressure ratio of 7.8:1, an efficiency of 82.7 percent, and a design corrected speed of 36,366 rpm. [Refer to AFAPL Report TR78-66-21-0820(52)A for additional information on the aerodynamic design.]

The inlet region of the flow path was designed to accommodate an improved bearing design (compared to that used during testing of the baseline impeller). A comparison of the baseline compressor inlet and the NASA scaled compressor inlet is shown in Figure 4; as shown, the design of the NASA inlet provides for a smooth airflow acceleration to the compressor inlet.

1.5.2 Surface Finish Study

Of significant concern was the possible need to scale the surface finish of the NASA impeller and diffuser to retain hydraulic similarity to the baseline compressor; consequently, a surface-finish study was conducted. Based upon the work of

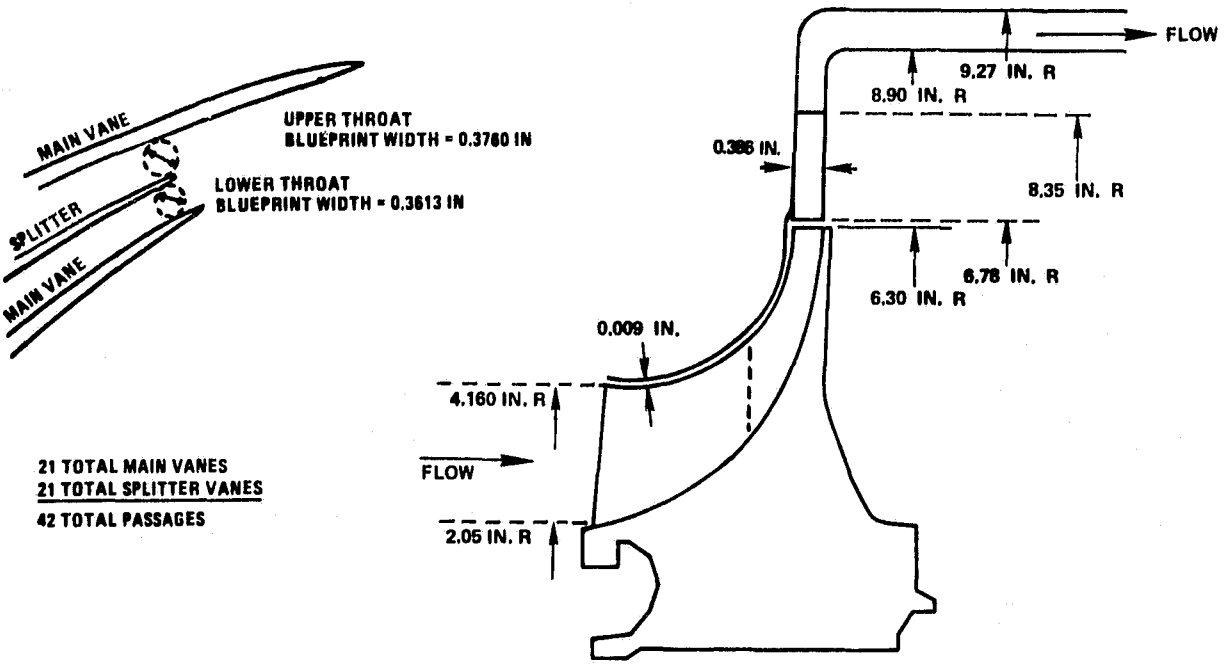

Figure 3. Outline of Scaled Centrifugal Compressor Cold Flow Path.

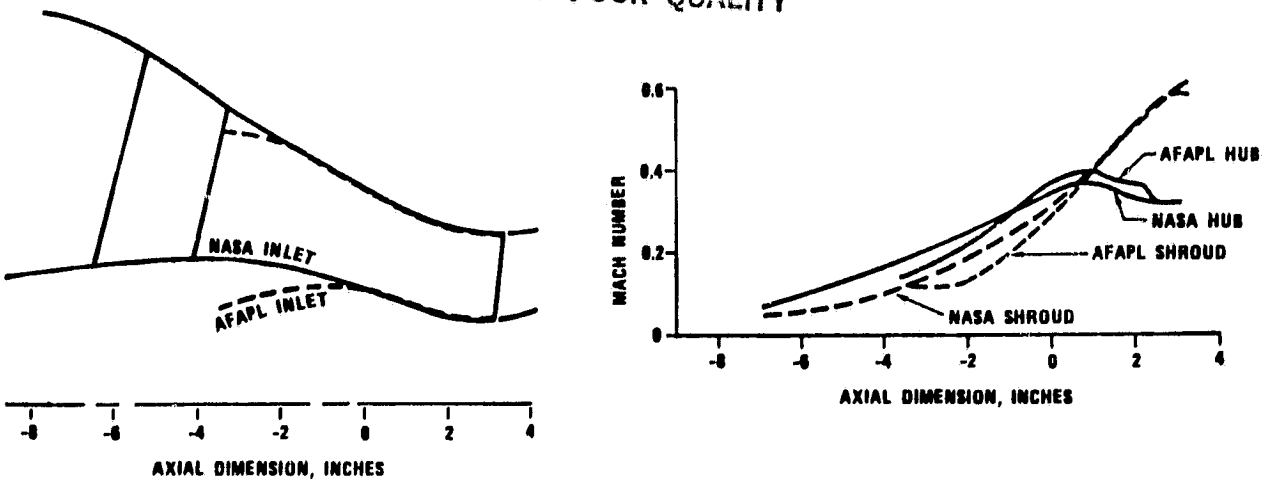

Figure 4. Comparison of Inlet Design and Aerodynamic Performance for the Baseline Versus Scaled Compressors.

Schlichting (Reference 1), the study recognized that, to have a hydraulically smooth surface, the magnitude of the surface finish must be less than that which corresponds to the maximum allowable surface protuberance height (K_{adm}) for a given velocity and density,

where $$K_{adm} \leq \frac{\text{Kinematic Viscosity}}{\text{Free Stream Velocity}} \times 10^2. \quad (1)$$

Since the relationship between K_{adm} and rms surface finish is a function of the shape of the surface waveform (Reference 2), three arbitrarily selected surface waveforms were used to determine the required surface finish for the value of K_{adm} calculated from equation (1).

- For the NASA impeller, the minimum value of K_{adm} is 136.8 μinch; this occurs at the leading edge of the impeller and generally increases as the flow proceeds through the impeller blades. Using sinusoidal, sawtooth, and intersecting arc waveforms, this minimum impeller K_{adm} translated to an rms surface finish of 40 to 48 μinch.

- Similarly, for the NASA diffuser, 61.3 μinch was calculated as a minimum value of K_{adm}. However, this value changes significantly as the flow passes through the diffuser, rising to 183.6 inch at the diffuser exit; in turn, this yield required an rms surface finish of 18 to 22 μinch.

Inasmuch as geometric scaling changes Reynold's number only by changing the diameter, K_{adm} remains unchanged since neither kinematic viscosity nor free-stream velocity changes. Therefore,

as concluded by Schlichting (Reference 1), if the surface finish was hydraulically smooth for the large scale, it also would be hydraulically smooth in the smaller scale (even though the reference Reynolds number changed significantly).

The relationship between loss and Reynolds number was correlated at GTEC. In the correlation, Reynolds number is given by the equation,

$$Rey_N = \frac{\rho_{01} D_T U_T}{\mu_{01}}, \qquad (2)$$

where:

Rey_N	=	Reynolds number
ρ_{01}	=	Inlet stagnation density
μ_{01}	=	Inlet stagnation viscosity
D_T	=	Tip diameter
U_T	=	Tip speed.

As shown by Figure 5, for a hydraulically smooth surface finish, changing the Reynolds number causes the loss to change according to the solid line. For a hydraulically rough surface finish, a similar change of Reynolds number causes the loss to remain unchanged (dashed line).

The region where the hydraulically rough and smooth curves intersect is a transition region, hence it was expected that there would be some curving of the hydraulically rough line as it blends with the hydraulically smooth line. The extent of this transition region could also be affected by the variation in the K_{adm} over the entire compressor blade and diffuser-vane surfaces.

The solid line in Figure 5 can be represented by the equation,

$$\frac{1-\eta}{1-\eta_{Baseline}} = \left(\frac{Rey_{Baseline}}{Rey} \right)^N, \qquad (3)$$

where: η = Efficiency.

Two test-data points taken on the 25-lb/sec compressor at suppressed inlet conditions gave a value of 0.1385 for N. This exponent was lower than the 0.2 power expected from turbulent boundary layer theory, since several contributors to compressor loss (such as clearance, shock, and dump loses) were not Reynolds-number-dependent.

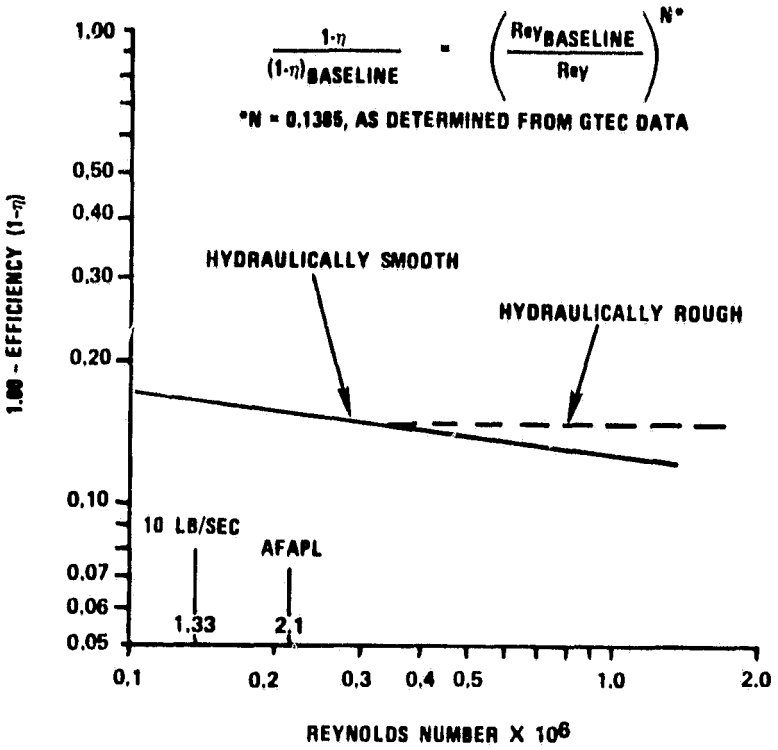

Figure 5. Change in Loss Shown as a Function of Reynolds-Number Change.

The design surface finish of the 25-lb/sec impeller is 16 prior to shotpeen; the measured surface finish averaged 32, as shotpeen will typically deteriorate the surface finish. The surface finish of the 10-lb/sec impeller is 16; the finish was neither measured nor shotpeened. It was concluded that, since the scaled compressor surface finish is the same as the baseline compressor, hydraulic similarity is established. The relationship between Reynolds number and loss is the same for both compressors.

2.0 DESIGN ANALYSIS

GTEC performed complete design studies and analyses for the scaled centrifugal compressor, collector, and test rig. This effort is reported in detail in GTEC Report 21-3907, "Analysis and Data Report for the Scaled Centrifugal Compressor, Collector, and Running Gear," dated October 8, 1981. The primary portions of data are presented in the following paragraphs.

The test-rig shafting was designed to operate smoothly throughout a speed range up to 60,000 rpm. Pressurized components (comprising the casing) were designed to operate at pressures up to 300 psia and at temperatures up to 1000°F.

2.1 Static Components

The nonrotating components were fabricated from AISI 347 corrosion-resistant steel (CRES) and were designed to provide a margin-of-safety of 0.50 or greater (based on tensile yield strength) at the maximum operating pressure of 300 psia. A minimum stress concentration factor of 3.0 was used at cutouts for the evaluation of low-cycle-fatigue (LCF) life.

2.1.1 Collector

The computer model of the collector is shown in Figure 6 with boundary conditions and a pressure drop of 450 psi. Figure 7

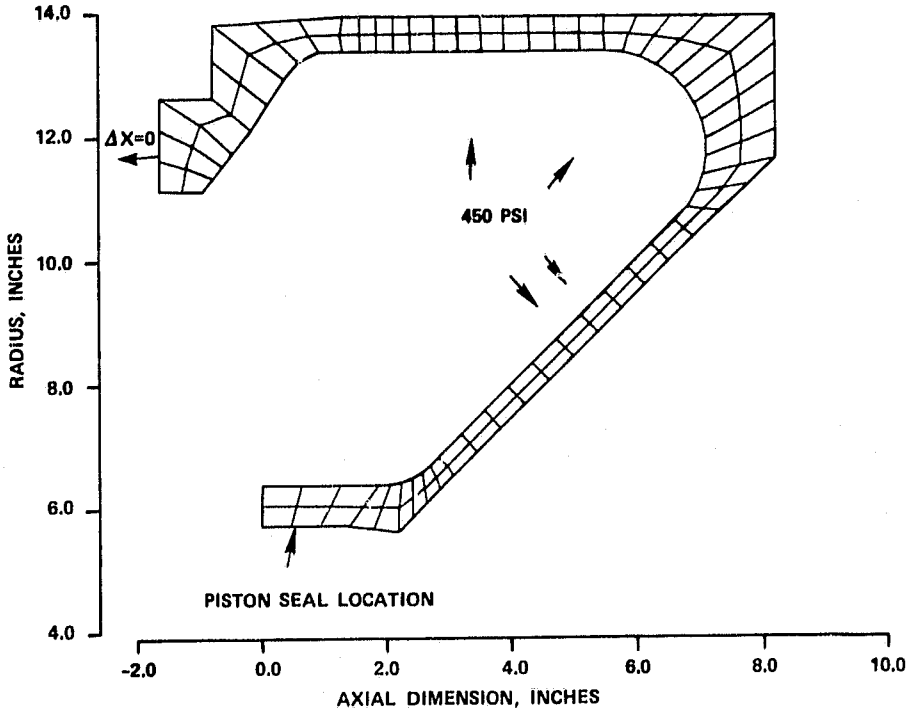

Figure 6. Computer Finite-Element Model of the Test Rig's Facility Collector.

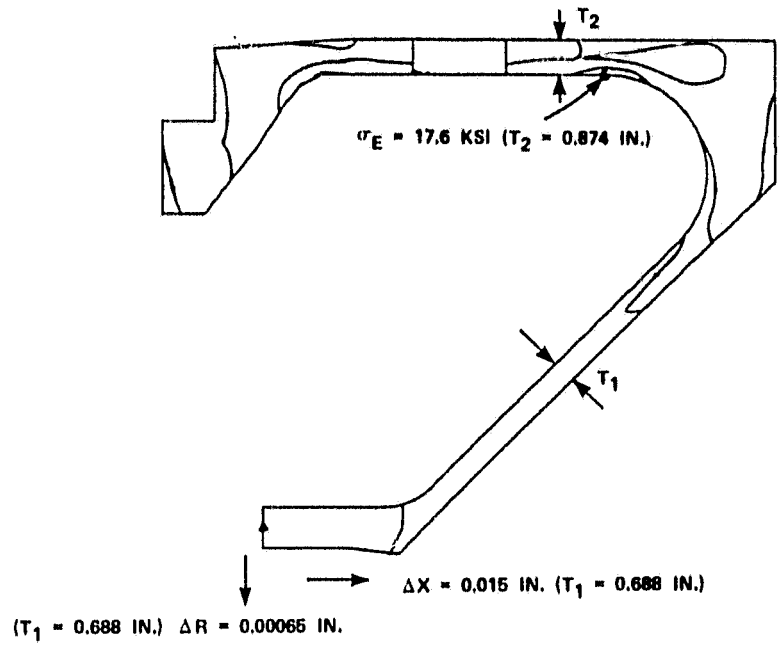

Figure 7. Maximum Effective Stress of the Collector at 450 psi Internal Pressure.

shows the maximum effective stresses and displacements (at 450 psi) obtained for the collector. The wall thicknesses shown are greater than required to meet stress requirements; these thicknesses were increased to control deflections at the piston-ring seal at the inner diameter of the collector.

2.1.2 Collector Support

The test rig and collector mounting configuration was designed with a water-cooled interface for the collector and its support legs. This controls the vertical thermal growth of the centerline of the test rig, thereby maintaining the proper alignment to the test-cell gearbox. (Figure 8 shows the finite-element model used to evaluate the interface area of the collector support. Figure 9 shows the thermal boundary conditions used for the analysis of this area.)

Uneven heating was minimized by the nearly symmetric design of the collector. The design operating temperatures are below the significant creep range of the material, so that residual stresses due to machining or welding do not result in distortions associated with a stress-relaxation process.

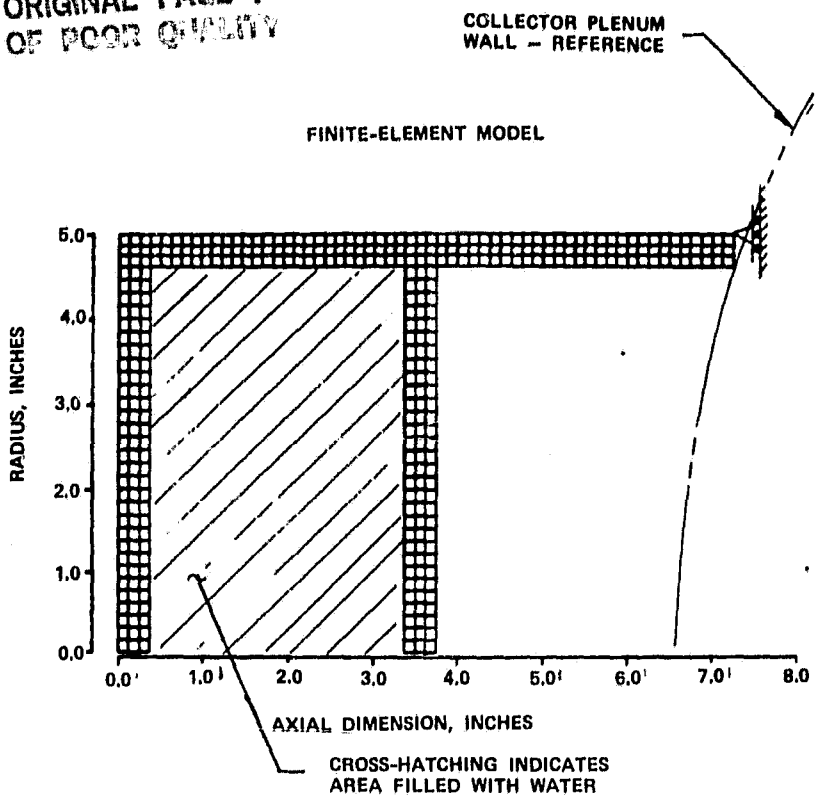

Figure 8. Finite-Element Model of the Support Structure Interface to the Collector Plenum.

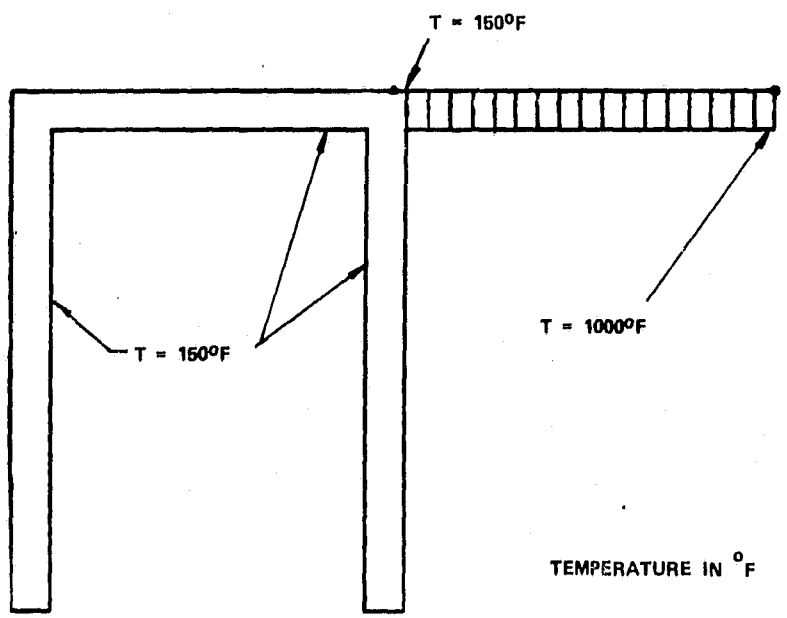

Figure 9. Thermal Boundary Conditions of the Support-Structure/ Collector-Plenum Interface Area.

Figure 10 shows the results of the thermal analysis, and Figure 11 shows the expected deflections. The peak stresses are shown in Figure 12. [This analysis produced data allowing the vertical growth of the test rig to be shown as a function of compressor discharge temperature (Figure 13).] The peak stress of 56,200 psi yields a fatigue life in excess of 10,000 cycles from room temperature to a gas-discharge temperature of 1000°F.

The spring rate for an external side load applied to the collector/plenum assembly at an elevation of 47.6 inches above floor level was calculated to be 1.78 x 106 lb/in. This meant a 5000-pound side load would produce a lateral deflection of

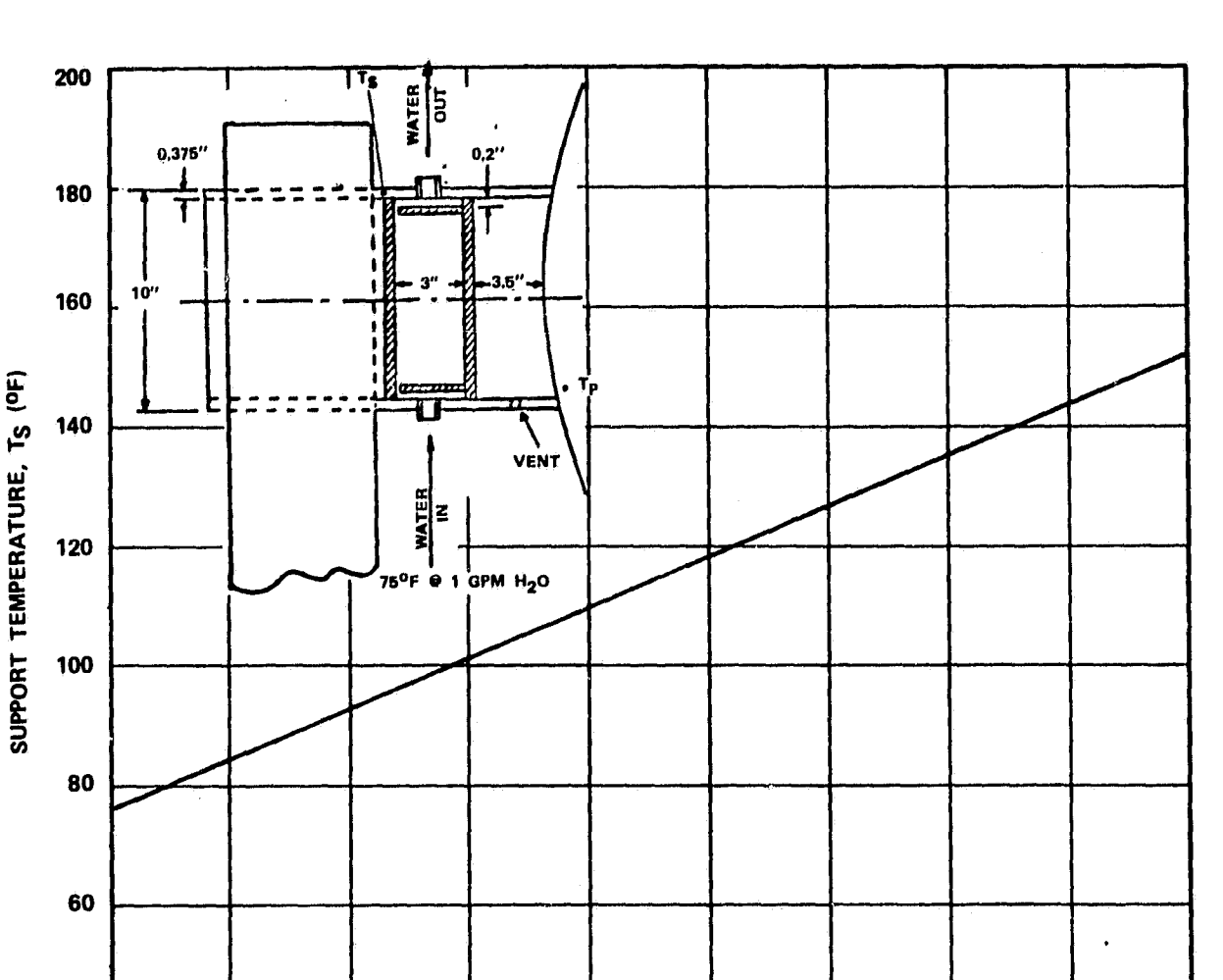

Figure 10. Plenum Support Temperatures Versus Plenum Wall Temperatures.

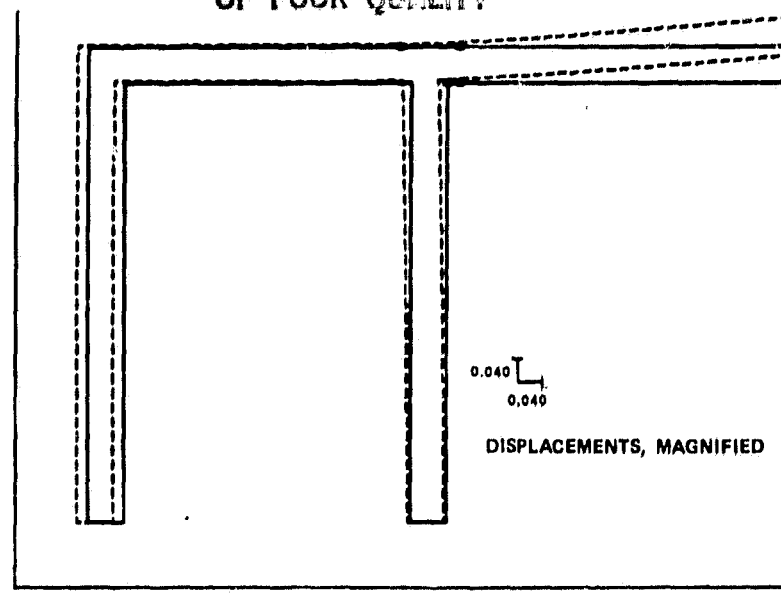

Figure 11. Deflected Shape Calculated for the Support/ Collector-Plenum Interface.

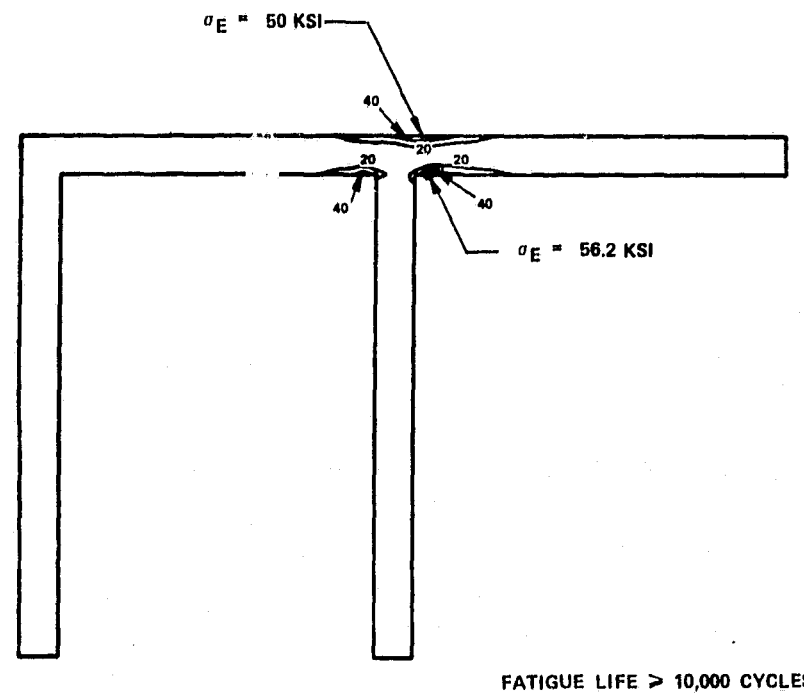

Figure 12. Effective Stresses of the Support/Collector Interface.

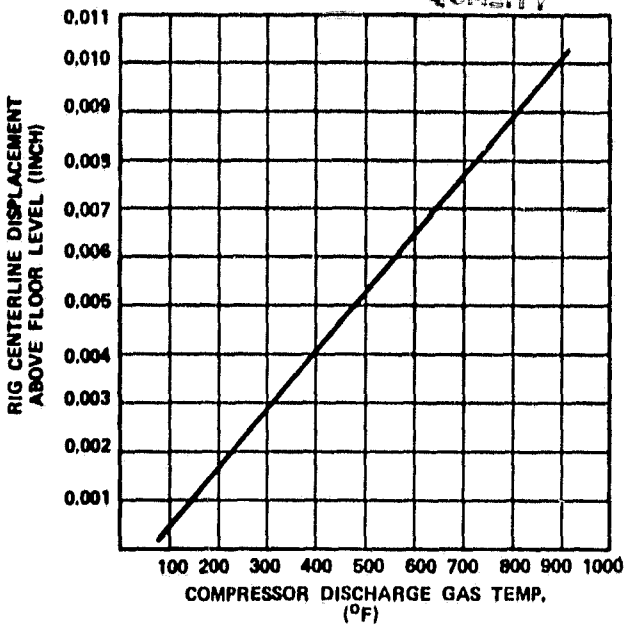

Figure 13. Test-Rig Vertical Thermal Growth.

0.003 inch, which was well within the misalignment capability (0.050 in.) of the coupling shaft.

2.1.3 Flange Loads

Allowable flange interface loads did not (and are recommended not to) exceed the following:

$$\frac{P}{5000} + \frac{S}{6670} + \frac{M}{37,000} \leq 1.0$$

where: P = applied tensile load (lb)
S = applied shear load (lb)
M = applied moment (in-lb).

2.1.4 Outer Casing and Collector Bolting

The results of the bolting analysis are shown in Figure 14 for the various illustrated locations. (The calculations were made based on A286 material and using a conservative hand analysis to compute the kick-loads.) The preload on the bolts was large enough to prevent any flange separation at an operating pressure of 300 psia, since the maximum predicted bolt load at 300 psia is 8,716 lbs.

2.1.5 Rear Support

Figure 15 shows the rear support with flange tapers introduced. With these modifications, the greatest effective stress was 32 ksi, thereby resulting in a 0.16 margin of safety on the 2 percent offset stress for AISI 347 CRES.

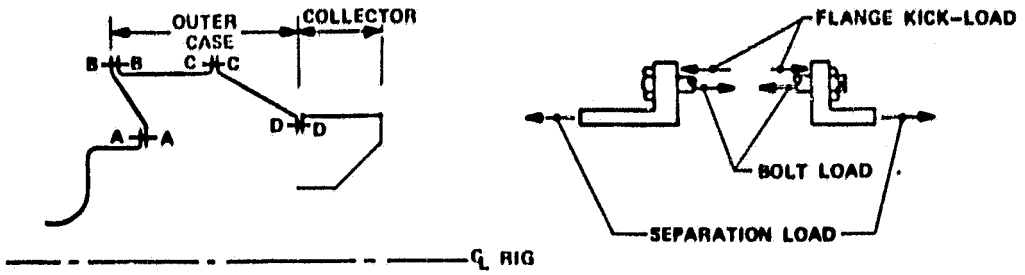

BOLT LOCATION	BOLT DIA. (INCH)	NO. OF BOLTS	SEPARATION LOAD (PER BOLT), LB	FLANGE KICKLOAD (PER BOLT), LB	TOTAL BOLT LOAD, LB	MARGIN OF SAFETY
A–A	0.50	45	3230	7866	11096	0.21
B–B	0.50	90	4283	8430	12713	0.05
C–C	0.50	90	4348	8923	13271	0.01
D–D	0.50	66	2956	10348	13304	0.01

• TABULATED LOADS AND MARGINS OF SAFETY ARE FOR 450 PSI INTERNAL PRESSURE AND YIELD STRENGTH OF A286 BOLTS UP TO 1000°F.

Figure 14. Pressure-Vessel Bolted Joint Summary.

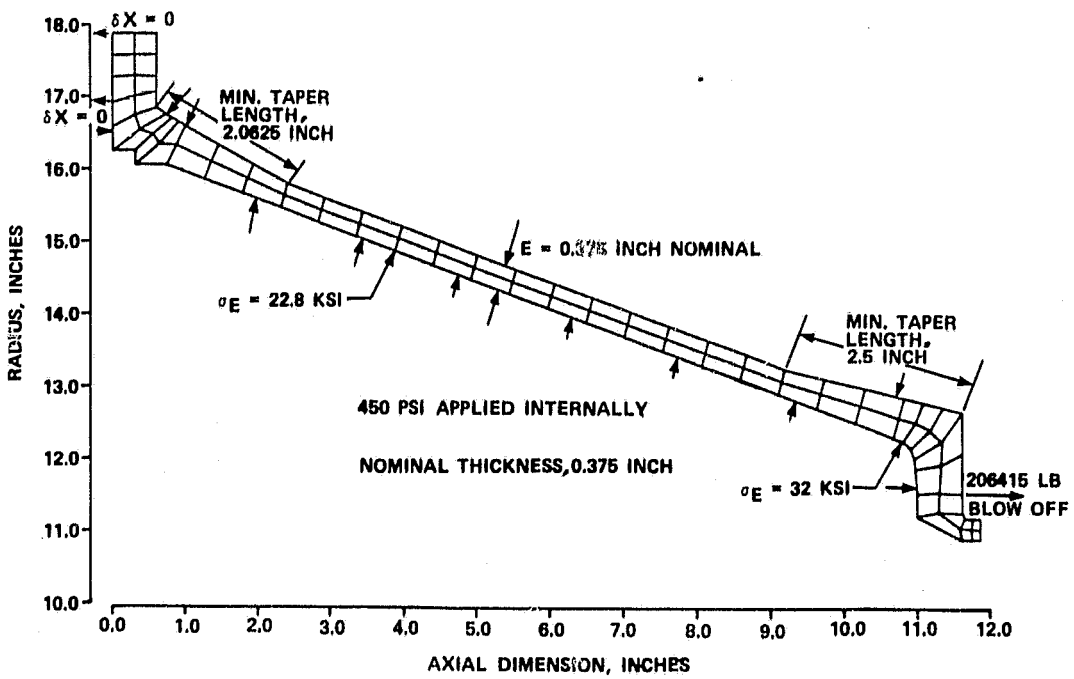

Figure 15. Model of Test-Rig Rear Support (with Flange Tapers Introduced).

2.1.6 Outer Casing

The rig-housing components were originally designed for use in a Garrett-owned compressor rig. The stress analysis of these components was accomplished using the finite-element model shown in Figure 16. The results of the original analysis were reviewed to determine if the internal pressure increase specified for the NASA rig would be acceptable. As a result, the wall thickness of the housing (Part 3553037-1) was increased to 0.45 inch. The stresses calculated for the 0.45-inch-thick wall at 450 psi internal pressure are shown in Figure 17. These stresses were prorated from the original finite-element analysis based on the relationship that stresses are directly proportional to pressure and inversely proportional to wall thickness.

The finite-element model did not include the effect of the overhung load. However, the overhung load was expected to produce a maximum case stress of 400 psi and, since it is not cyclic, was not considered to significantly alter the casing fatigue life.

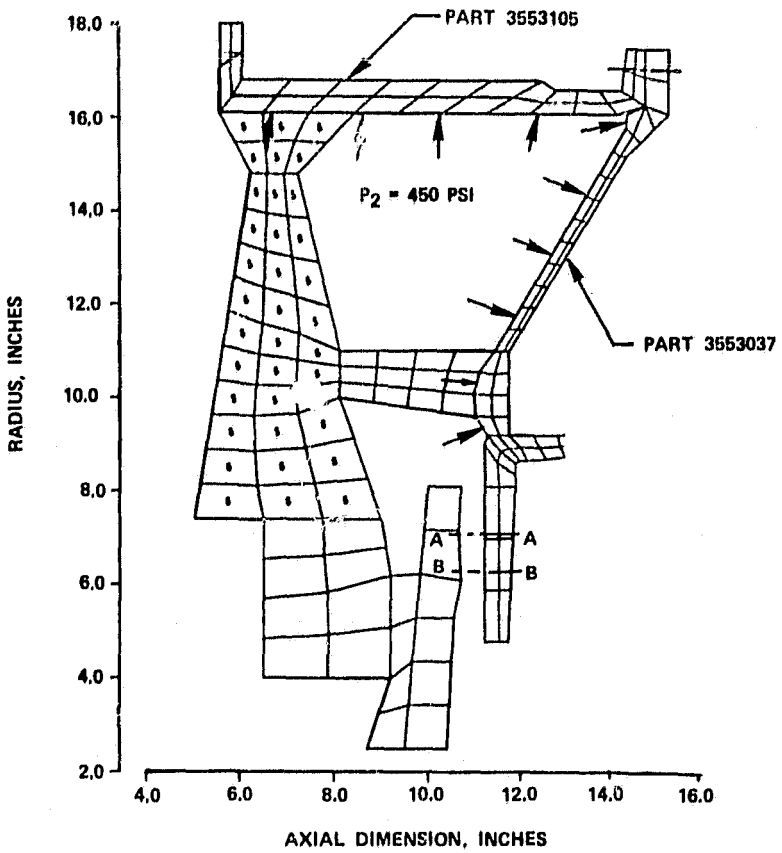

Figure 16. Finite-Element Model and Boundary Conditions for the Outer Case.

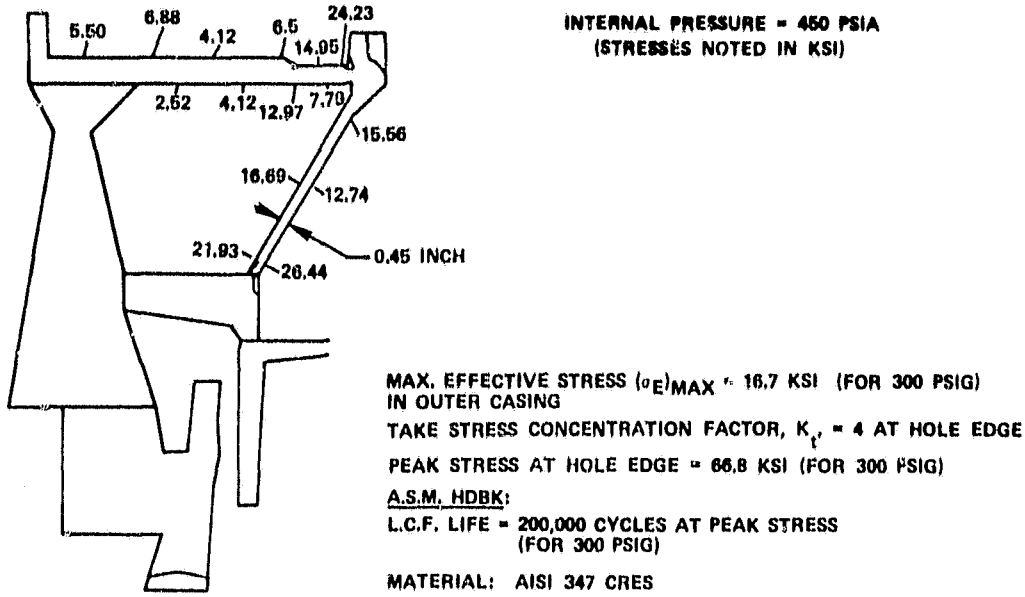

Figure 17. Stresses Calculated for the Outer Case.

The section of the model that did not reflect the NASA rig geometry was not load supporting and did not affect the magnitude of case stresses. Mechanical restraints on the model consisted of an axial support at the outside-diameter flange on the left-hand side of the model. No radial or other axial support was provided. No temperature gradients were used in the analysis, since the rig-housing components are essentially uniform in temperature.

2.1.7 Forward Bearing Support

The forward bearing-support assembly was designed to have adequate radial stiffness to provide desirable rotor-dynamics characteristics and to possess sufficient strength to support rotor imbalance loads created by loss of material from the impeller. The evaluation of stiffness, stress, and fatigue life of the bearing support structure was performed with the three-dimensional finite-element model (Program ISO3DQ) shown in Figure 18.

The model shown in Figure 18 was used to evaluate the stiffness of a three-strut configuration. Similar models were also run to obtain the radial stiffness of both five- and seven-strut designs. Analysis of the calculated deflections indicated that radial spring rate is dominated by strut flexibility, because the inner and outer shells are much stiffer than the struts. Radial spring rates were determined for struts of both 1.5-inch and 2.25-inch chord length, using the elastic modulus appropriate to both 6061-T6 aluminum alloy and AISI 347 CRES. The spring rates for each of these configurations are plotted in Figure 19.

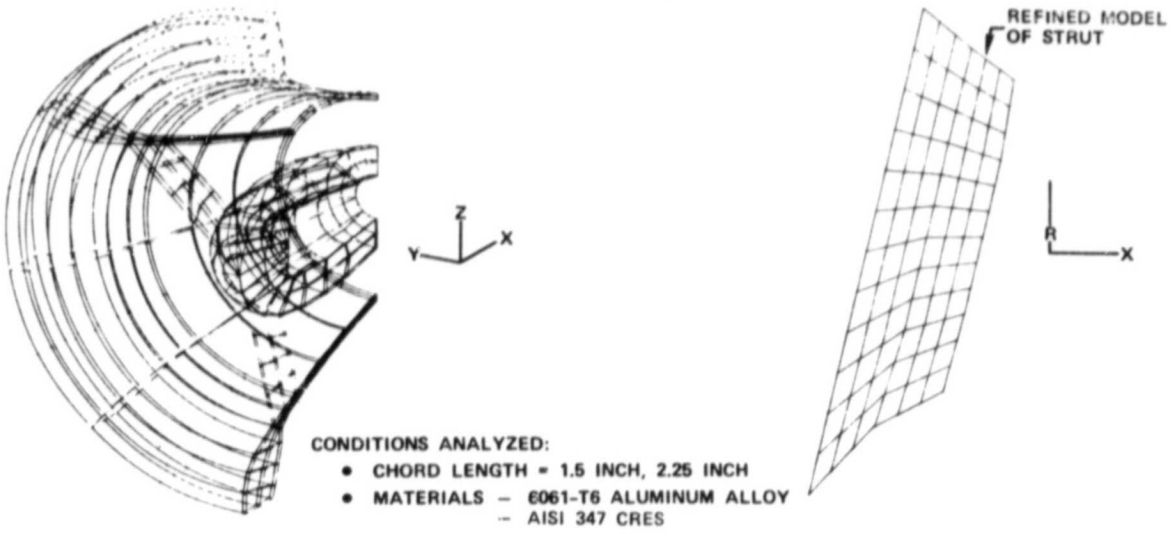

Figure 18. Finite-Element Model of the Forward-Bearing Support Frame.

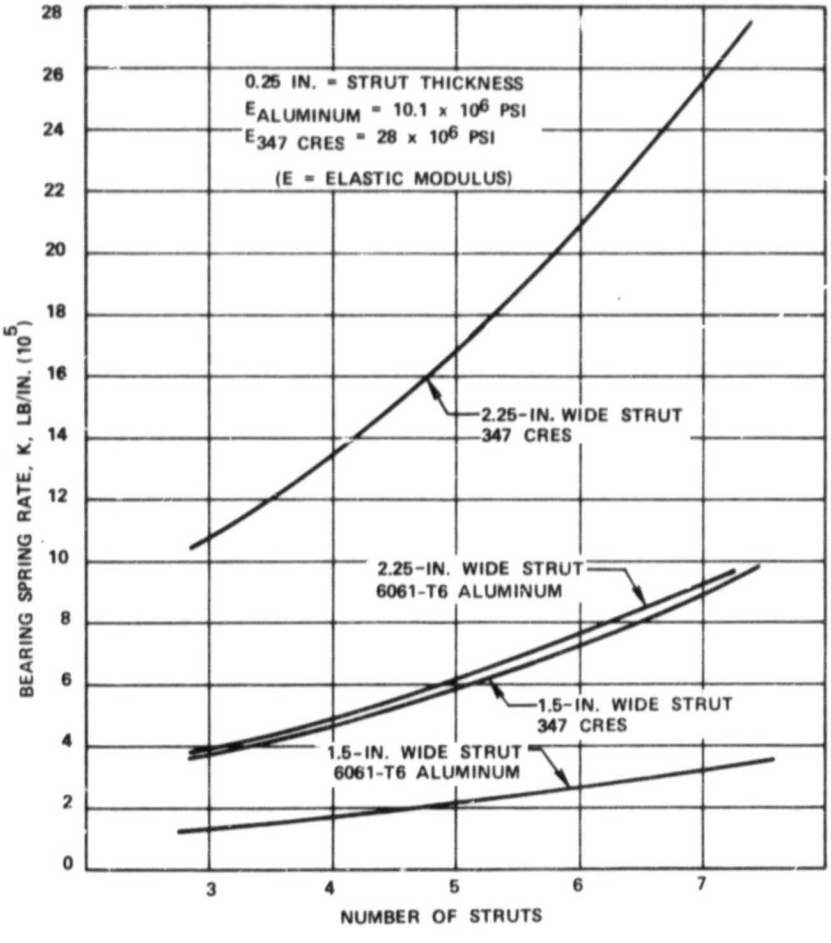

Figure 19. Radial Spring Rates for the Forward Bearing Support.

Normal operating bearing loads were considered to be low and to produce very low stresses in the bearing-support structure. However, since loss of an impeller blade(s) could create large rotating imbalance loads that could produce fatigue failure (typically at the juncture of the struts and inner shell), these stresses were evaluated using the finite-element model shown in Figure 18. Since the large model of the entire frame assembly was relatively coarse, a refined model of the strut was used to ensure that the calculated stresses had converged to the correct solution. Deflections calculated using the large model were used to provide displacement boundary conditions to the refined model of the strut. The fatigue lives of 1.5-inch and 2.25-inch chord length struts, fabricated from both 6061-T6 aluminum and AISI 347 CRES, were calculated and are plotted in Figure 20. (Inasmuch as these struts are subjected to rotating and radial imbalance loads, the lives shown are for a three-strut design. The three-strut design was selected because it simplified the structure in the inlet area, creating less aerodynamic blockage and leaving more room for instrumentation access.)

The final design uses a 2.25-inch chord length and AISI 347 CRES material. It was chosen because it offered significantly greater ability than the 1.5-inch, 6061-T6-aluminum strut to tolerate rotor imbalance loads due to loss of an impeller blade.

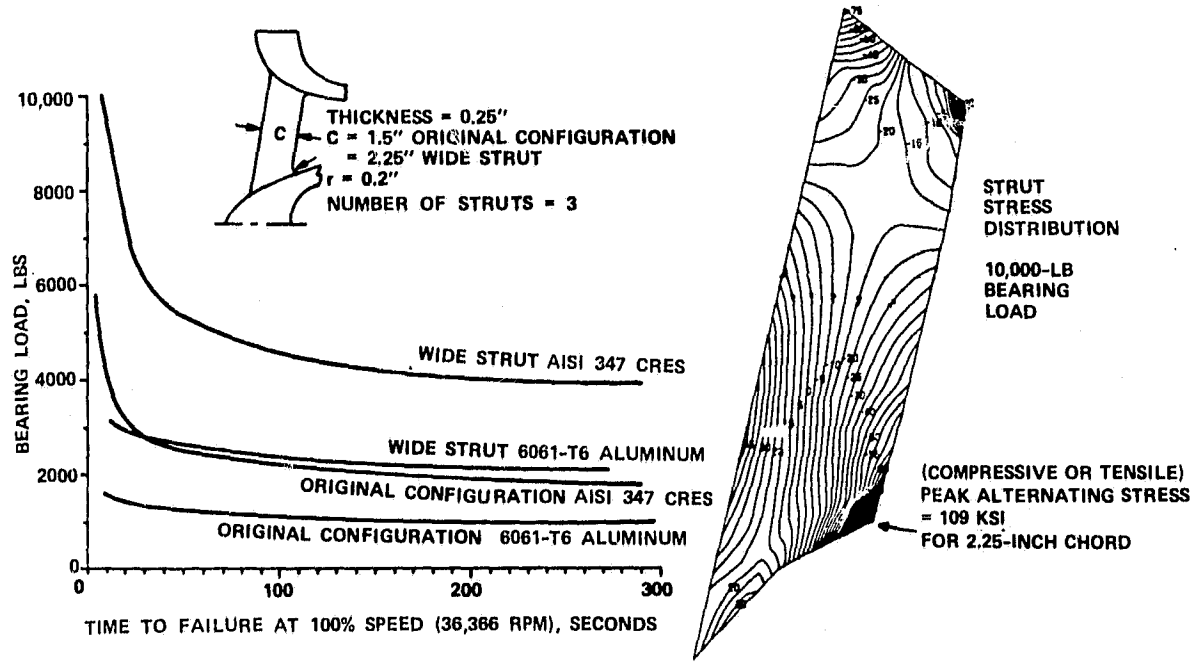

Figure 20. Results of the Stress Analysis Conducted for the Forward-Bearing Support Frame.

2.1.8 Containment

Two different impeller failure modes -- blade failure and disk burst -- were evaluated to determine the rotor energy absorbed by the impeller shroud in order to contain the high-energy fragments within the rig structure.

GTEC studied noncontainment both by penetration of the impeller shroud (wherein a hole is punched in the shroud) and by hoop elongation and ultimate tensile failure of the shroud. Blade penetration was evaluated assuming loss of an entire blade and using the curve shown in Figure 21, which plots blade kinetic energy for AISI 347 CRES (the shroud material) against the product (B) x (Ue)x (t^2), where:

B = Length of released blade = 2.0 in
U = Ultimate tensile strength of shroud = 65,000 psi (600°F)
e = Elongation of shroud at failure = 0.33 in/in (600°F)
t = Minimum thickness of shroud = 0.8 in.

Comparing the resulting product of 27,456 in-lbs to the plot indicated that the shroud was capable of absorbing 430,000 in-lbs of blade energy without a blade penetration. This compared favorably to the 94,245 in-lbs of energy possessed by three full blades and three splitter blades at 105 percent of design speed. (The curve

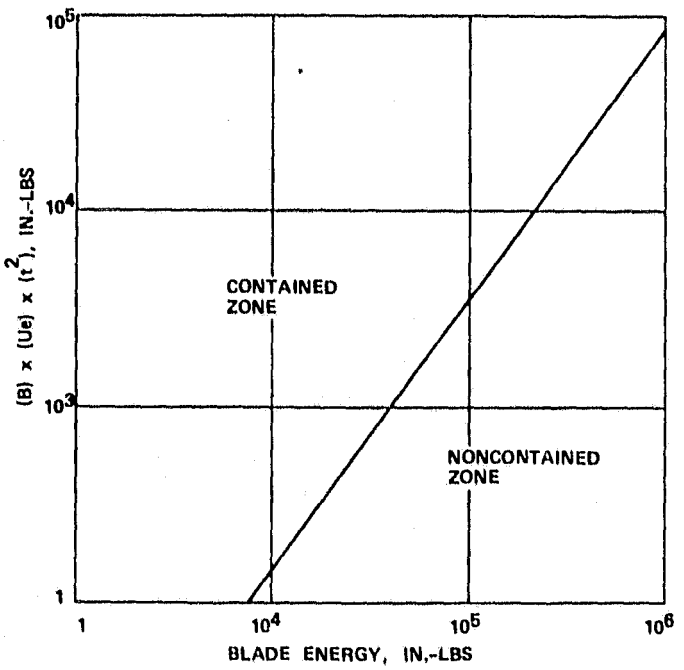

Figure 21. Blade Kinetic Energy Plotted Against Containment Capability.

used for blade penetration-prevention has been verified by fan-blade containment tests on the Garrett Model TFE731 turbofan engine.)

Penetration prevention for disk fragments was investigated using the following empirical relationship developed by whirlpit testing at GTEC:

$$\text{K.E. (in-lbs)} = 2t^2 \ (10^5) \ [\frac{Ue}{12,000}]$$

where:

K.E. = Kinetic energy required for penetration
t = Shroud thickness = 0.8 in
U = Shroud ultimate tensile strength = 65,000 psi
e = Shroud tensile elongation at failure = 0.33 in/in.

The resulting calculated kinetic energy required to produce penetration was 228,800 in-lbs per segment. The rotating kinetic energy of the impeller disk at 105-percent speed (3,672,500 in-lbs) combined with the blade kinetic energy to give a total rotating kinetic energy of 4,300,800 in-lbs. (A three-segment disk burst was considered the most critical condition and would yield a translational kinetic energy per segment of 989,200 in-lbs.)

The second possible shroud failure mode, tensile elongation failure, was evaluated with the following relationship:

$$\text{K.E. (in-lbs)} = \frac{\text{(Volume) x (Ue)}}{0.925}$$

where:

K.E. = Kinetic energy required for tensile failure
Volume = Volume of material in shroud = 139.94 in^3
U = Shroud ultimate tensile strength = 65,000 psi
e = Shroud tensile elongation at failure = 0.33 in/in.

The resulting kinetic energy was 3,245,095 in-lbs.

These results indicated that any possible single- or multiple-blade failure would be successfully contained by the shroud, but that a three-segment disk burst could possibly result in shroud penetration or hoop tensile failure.

2.2 Lubrication System

The required cooling oil flow for the bearings was determined from a computer program (BGLUB2). The program accounted for the bearing geometry, operating speed, type of oil, and "oil-in" temperature. From the given information, the frictional, churning, and viscous losses were calculated. Then, the required oil flow

(assuming an oil delta temperature of 50°F across the bearing) was determined.

The hydraulic mount oil flow was determined based on the bearing excursion, radius, length, and operating speed. (The bearing excursion at a maximum speed of 60,000 rpm was assumed to be 0.0005 inch.) The oil jet sizes were determined from the associated oil flow required, oil-supply pressure, and pressure losses. The scavenge area assumed an oil scavenge velocity of 5 ft/sec or less.

The lubrication oil was specified as hydraulic transmission oil, supplied at a nominal pressure of 100 psig and a temperature of 120°F. The hydraulic mount geometry definitions for the roller and thrust bearing are given in Figure 22, which also shows the bearing oil flow and oil scavenge area requirements. Figures 23 and 24 provide the lubrication and scavenge area requirements for the collector bearings.

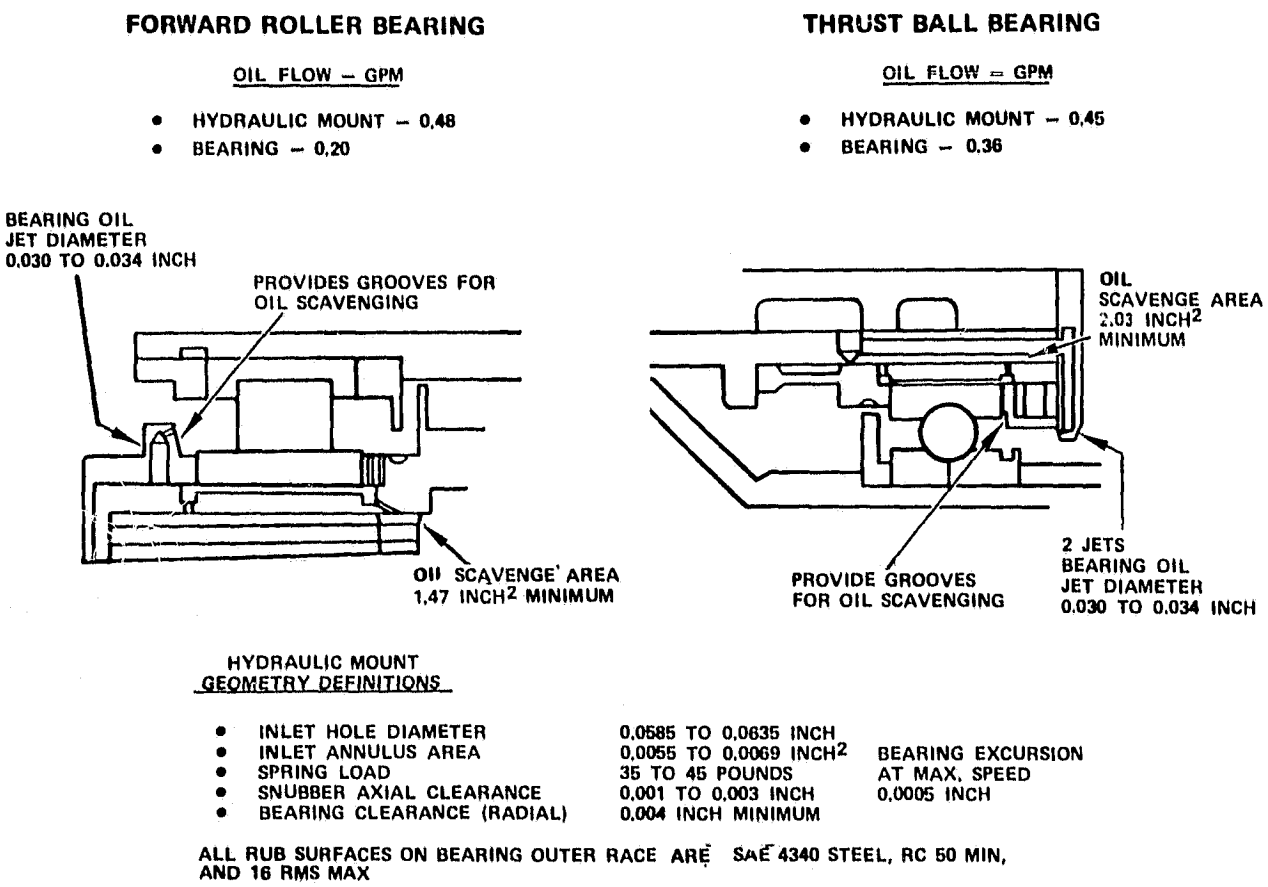

Figure 22. Hydraulic Mount Geometry Definitions for the Roller and Thrust Bearings.

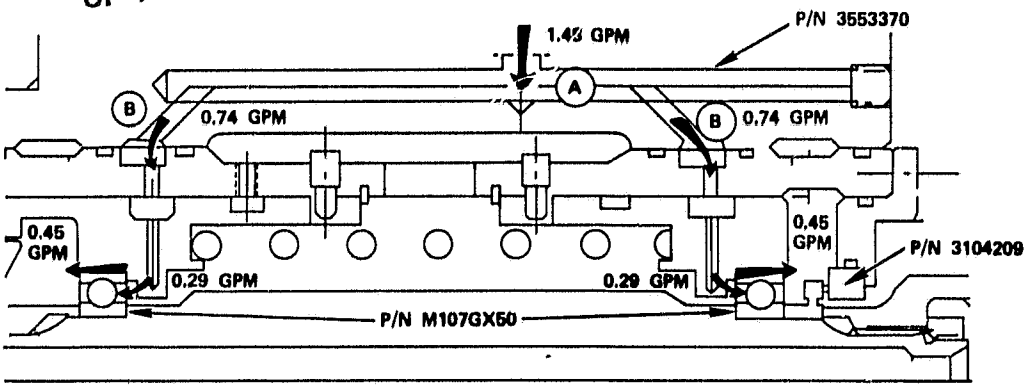

LINE SIZES (MINIMUM)

(A) 0.20 INCH DIAMETER

(B) 0.15 INCH DIAMETER

SPRING LOAD 40 TO 50 POUNDS

OIL JET SIZES

BEARING	0.038 TO 0.043 INCH
OPEN-ENDED HYDRAULIC MOUNT	0.054 TO 0.059 INCH
INLET ANNULUS AREA	0.0046 TO 0.0058 INCH^2

ALL RUB SURFACES ON BEARING OUTER RACE ARE SAE 4340 STEEL, RC 50 MIN, AND 16 RMS MAX

Figure 23. Size Requirements for the Oil Supply Line to the Collector.

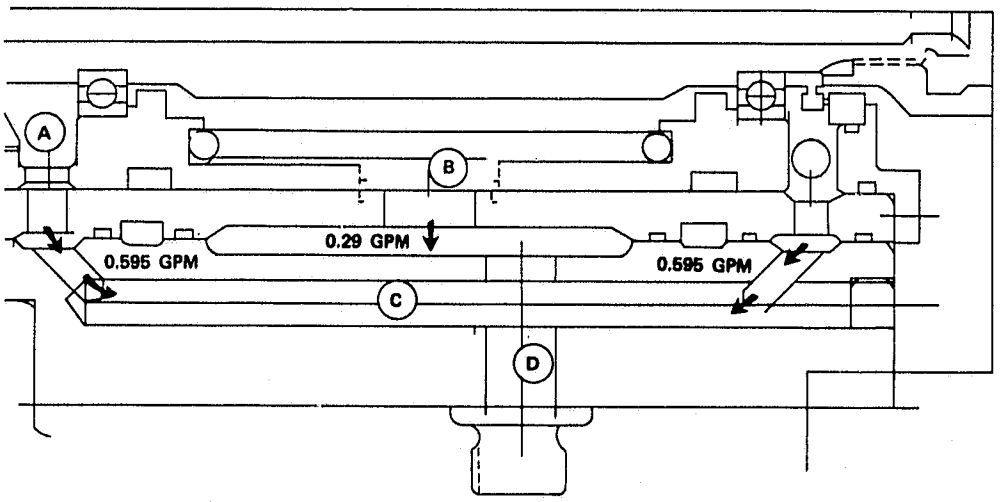

SCAVENGE AREAS (MINIMUM)

(A)	0.038 INCH^2	
(B)	0.019 INCH^2	BASED ON A VELOCITY OF 5 FT/SEC
(C)	0.095 INCH^2	
(D)	0.095 INCH^2	

Figure 24. Requirements for Oil Scavenge Area in the Collector.

The assumed oil system and bearing temperature rise was as follows:

- o 50°F oil temperature rise across the bearing
- o Ball bearing outer-race temperature of 135°F (maximum) above oil-inlet temperature
- o Roller bearing outer-race temperature of 110°F (maximum) above oil-inlet temperature.

Alarm setpoint values were recommended to be set 25°F higher than these limits.

2.3 Seals

The sealing concept for the NASA rig was based on existing GTEC test rigs. Six seals were incorporated into the test rig.

The compressor roller bearing cavity uses a ring seal assembly, shown in Figure 25, which incorporates a third ring for a positive control of airflow direction and sealing capability. The surface speed at the bore of the ring seal at 60,000 rpm becomes 392.4 ft/sec, well below the standard Garrett production seal surface speed of 450 ft/sec for ring seals.

The impeller cavity is sealed by a double labyrinth seal aft of the impeller. The seal is buffered by injecting facility air

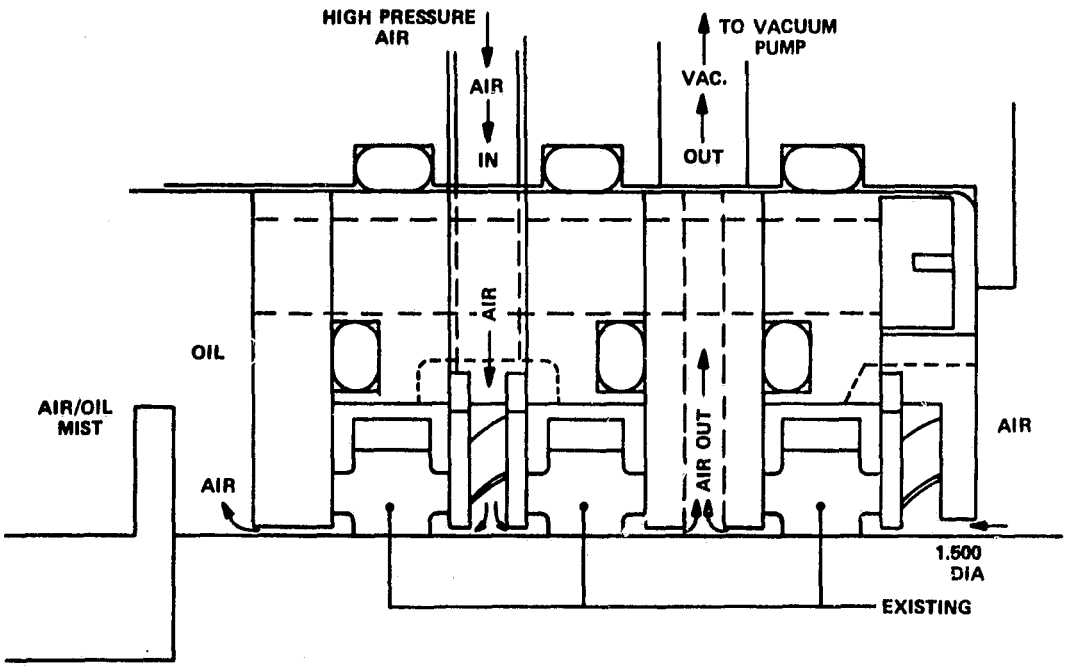

Figure 25. Seal Configuration for the Roller Bearing Cavity.

between the two seals and maintaining an air pressure (between the seals) equal to the pressure upstream -- i.e., on the impeller side -- of the labyrinth arrangement. By buffering the seal and properly balancing the air pressures in this manner, compressor leakage flow is minimized.

The thrust bearing area incorporates a two-stage labyrinth seal. The original design had called for a pneumostatic seal; however, additional Garrett experience indicated that the pneumostatic-seal design could be subjected to unacceptable operating limits during off-design running conditions. Consequently, the labyrinth-seal design was developed to increase durability for the thrust-bearing seal.

Downstream of the balance piston is a 2.35-in-diameter, knife-edge seal. It is designed to separate the thrust balance exhaust air cavity from the torque-tube bearing cavity. (This seal is not susceptible to misalignment or rotor runout and eliminates the possible need to replace the seal during testing.) The pressure differential across this seal is expected to be less than 5 psi and the direction of flow is from the thrust balance exhaust air cavity into the torque tube bearing cavity. Flow is minimal because the scavenge system of this bearing cavity maintains a very low pressure (i.e., close to ambient).

The torque-tube cavity is sealed by a face seal. This seal was originally designed as a compressor-bearing seal for the Garrett TPE331-14/15R turboprop engine with a design speed of 34,904 rpm; it was selected for the NASA rig because of its size and ability to operate successfully at higher speeds. A test rig speed of 45,000 rpm would be within the range of rubbing velocities for similar GTEC production seal designs -- for example, the Garrett TFE731-2/3 turbofan engine No. 5 seal, which also operates at a higher temperature and air pressure. The rig seal operates at a slightly lower rubbing velocity of 395 ft/sec (at 45,000 rpm) in the NASA application.

2.4 Splines

The NASA test rig splines were designed to operate at 1000 hp at 60,000 rpm, 2000 hp at 36,366 rpm, and 3000 hp at 42,000 rpm. All splines and shafting are made of carburized and hardened SAE 9310 steel, except for the outer ring of the ball spline, which is made of carburized and hardened AISI 4330 modified steel. All splines are lubricated by a baked-on dry film lubricant (except for the ball spline, which is oil-lubricated). The temperature limits of this lubrication (baked-on molydisulfide) are -300°F to 600°F.

The NASA test rig uses two different crowned splines -- one on the ball-spline shaft and another on the input drive quill shaft.

These crowned splines were analyzed by computer program "SPLINE". Spline compressive stress and contact pattern overlap ratio result in several thousand hours of crowned spline life in a dry lubricant environment.

Crowned spline lives were roughly approximated by a wear-rate number that depends on the speed of the elliptical contact pattern as it traverses the spline tooth upon misalignment. The approximate spline lives, based on the wear-rate number for the two NASA test rig splines at the two worst operating conditions, are as follows:

	Condition: 3000 hp at 42,000 rpm		Condition: 1000 hp at 60,000 rpm	
Spline Description	Life (hrs)	Sliding Velocity (in./sec)	Life (hrs)	Sliding Velocity (in./sec)
Crowned spline on ball-spline shaft	10,200	401	4300	573
Input drive quill shaft crowned splines	4100	625	3500	893

Spline shear stress was calculated assuming that half the spline teeth are loaded and with the shear area taken at the pitch diameter. Internal spline bursting stress was calculated as the sum of stress created by centrifugal force, tooth bending, and the radial component of force produced by torque. Allowable stresses were modified with life factors that took into account stress concentration, shock loading, and fatigue. Allowable limits of case-hardened steel for shear stress and internal spline bursting stress are 50 ksi and 55 ksi, respectively.

Limits for crowned spline misalignment at 3000 hp, 42,000 rpm operating conditions are as follows:

Spline Description	Misalignment Capability (Radial Offset Between Shaft Centers, inches)
Crowned spline on ball spline shaft	0.032
Input drive quill shaft crowned splines	0.050

Larger shaft misalignments are possible at the other two rig operating conditions because of relatively lower spline tooth loads.

The NASA test rig ball spline was analyzed for outer-ring bursting stress and ball compressive stress. Ball compressive stresses were arrived at by first using computer program "FITUP" to determine clearance growth at speed. Ball contact angles were then calculated, and computer program "JONES" was used to determine ball compressive stresses. Bursting stress from rotational speed, for both the outer ring of the ball spline and the polygon coupling, was determined by the use of computer program "ISOPDQ"; maximum allowable compressive and bursting stresses for the ball spline are 500 ksi and 195 ksi, respectively. The rig polygon coupling was analyzed for outer-ring bursting stress, and bearing stress and torsional capability were evaluated using vendor-supplied design criteria; maximum allowable bursting stress for the polygon coupling is 147 ksi.

2.5 Bearings

The test rig was designed to operate from 0 rpm to 60,000 rpm. The bearings consist of the forward roller bearing and the aft thrust ball bearing, with the same thrust ball bearing used for the torque tube bearings. The roller bearing outer-race temperature was expected to operate at 75°F above the oil-inlet temperature. Similarly, the ball bearing outer-race temperatures were expected to be 100°F above the oil-inlet temperature. (Alarms were set at 25°F above these temperatures.)

2.5.1 Calculation Methods

Computer program "JONES" was used for all bearing calculations. This is a quasi-static program that uses the stress-life reliability method to calculate fatigue life and has been used at GTEC since 1976.

Computer program "FITUP III" was used to calculate the changes of shaft-bearing fit, the inner-ring hoop stresses, and internal bearing clearance changes due to speed, temperatures, interference shaft fit, and axial clamp forces.

2.5.2 Dynamic Bearing Loads

Figure 26 shows the dynamic bearing loads for the roller- and thrust-ball bearings. Figure 27 shows the bearing loads for the torque-tube ball bearings. (In these figures, B1, B2, B3, and B4 stand for bearings No. 1, No. 2, No. 3, and No. 4, respectively.) The B4 support bearing showed excessive loading for the torque tube at 58,000 rpm, requiring that speed be limited so that a 100-lb radial unbalance load not be exceeded.

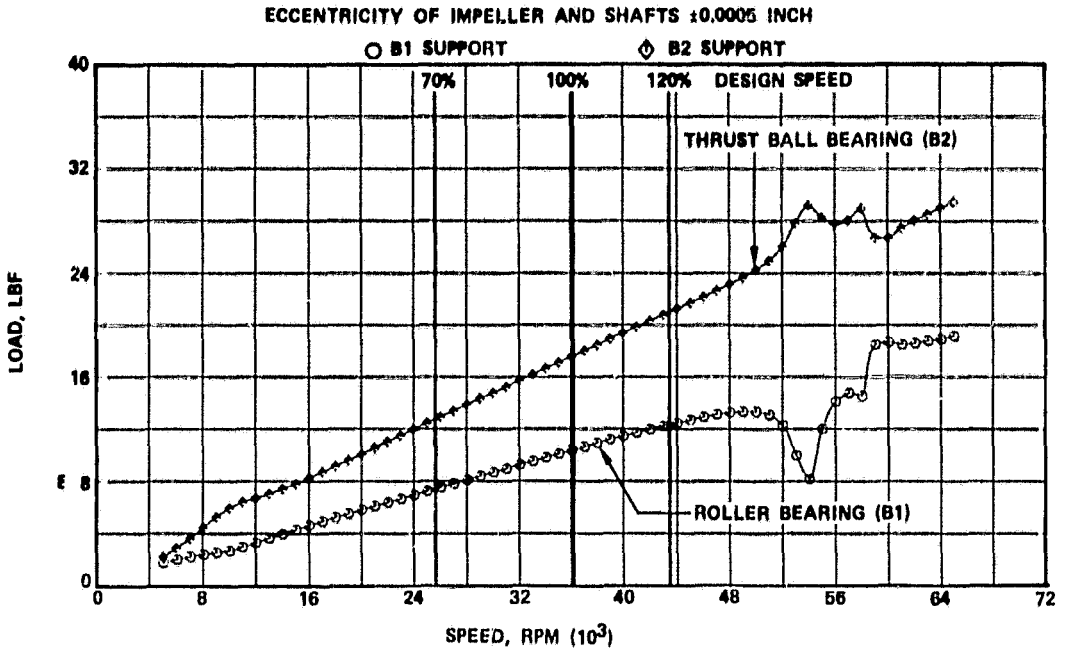

Figure 26. Unbalance Response of Roller Bearing and Thrust Ball Bearing.

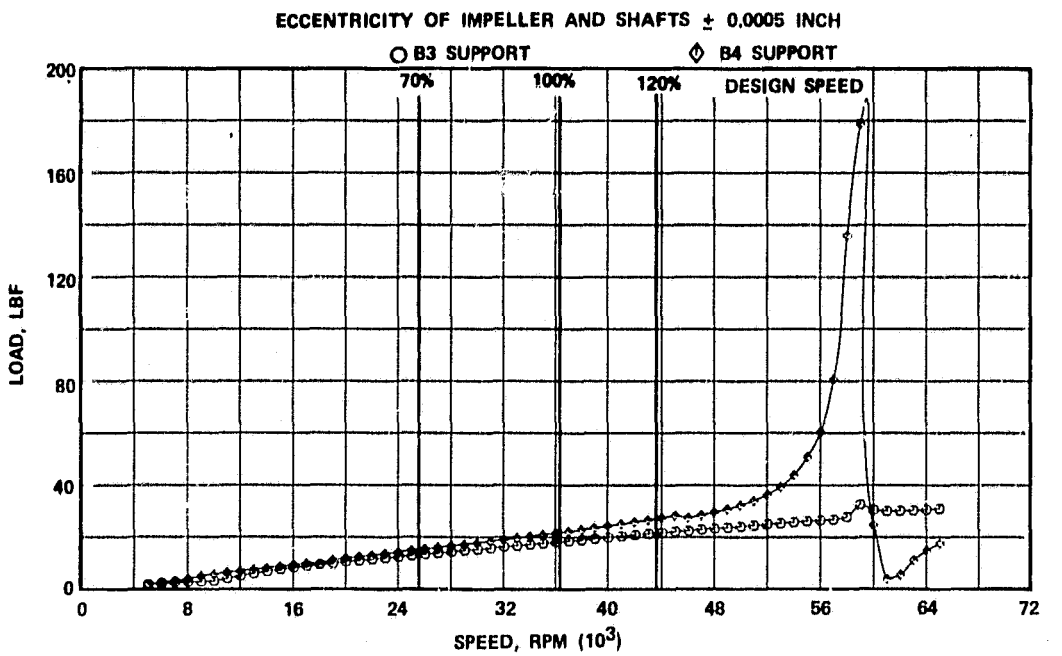

Figure 27. Unbalance Response of Torque-Tube Bearings.

2.5.3 Forward Roller Bearing

The forward roller bearing has an L_1 fatigue life in excess of 10,000 hours. (The radial spring rate for this bearing is shown in Figure 28.) The primary problem was the high skid threshold load on the bearing relative to the sum of the 1-g load and the low dynamic load, as shown in Figure 26. When the drag and drive torques were balanced by use of a constant friction coefficient, the skid threshold loads for the bearing were as follows:

Skid Threshold Load, lbs	Shaft Speed, rpm
60	34,904
65	36,366
86	41,730
177	60,000

The possibility of skidding the roller bearing during very rapid acceleration was not eliminated. However, GTEC experience has been that, if skidding occurs during rapid acceleration, the duration is too short to damage the bearing. (Garrett has 12 million hours of experience with this roller bearing on production turboprop engines using a full complement of roller elements at speeds up to 45,000 rpm.) For the NASA application, the skid threshold of the roller bearing was improved by removing half of the roller elements. The bearings and shafting will have to be reviewed for higher speed applications to ensure compatibility with any new NASA compressor designs.

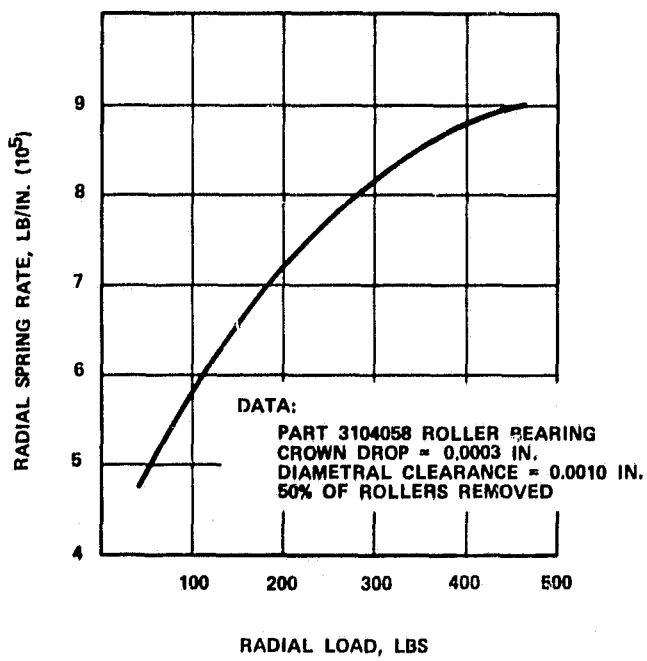

Figure 28. Radial Spring Rate of the Forward Roller Bearing.

The stress analysis of the forward bearing support frame was based on a 10,000-lb bearing load, as already discussed. This load corresponds to a maximum bearing load resulting at the rotor critical speed (transient) with a one-blade-out unbalance condition. The steady-state load at 100-percent speed is only 2500 lbs for the same unbalance condition.

Excessive bearing loads were determined to occur when unbalance exceeds the squeeze film thickness. This situation was found to arise only if more than 30 percent of a full blade loss occurs. Since a full blade loss has never occurred in Garrett's past experience, the design philosophy was to be able to shut down the test rig in a matter of seconds to prevent a bearing failure in the event of a part or full blade loss.

2.5.4 Aft Thrust Ball Bearing

Studies showed that to reach 60,000 rpm shaft speed, a 35-mm bore size was required with smaller ball diameters and a less conforming inner-ring curvature. These bearing features were as follows:

Bore = 35 mm (1.3750 in.)
Outside Diameter = 62 mm (2.4409 in.)
Cross corner = 0.542 ±0.005 in.
Ball size = 5/16 (0.3125 in.)
Ball number = 14
Pitch diameter = 1.96 in.
Contact angle = 23 degrees
Outer-ring curvature = 52 percent
Inner-ring curvature = 54 percent
Outer-race depth = 18 percent
Inner-race depth = 25 percent
Maximum end clearance = 0.013 in.
Separator pilot clearance = 0.009 to 0.015 in.
Separator ball pocket clearance = 0.013 to 0.020 in.
Separator material = Silver-plated 4340 steel
Ring-ball material = M-50 tool steel
Barden Part = M107GX50
Puller groove = None.

At 60,000 rpm, the diameter-times-speed (DN) value of the bearing is 2.1×10^6. This DN value is considered very reliable with the 54-percent inner-ring curvature, since it allows for substantial heat variations between rings without excessive clearance loss that would lead to bearing failure.

Table 1 shows the results of the computer model for this bearing. The bearing variables were within present state-of-the-art technology for test-rig bearings. The only disadvantage of this production bearing is the low fatigue life that results from its opened inner-ring curvatures. However, the fatigue life (L_1) shown

TABLE 1. THRUST BALL BEARING ANALYSIS.

Operating Condition: 60,000 RPM, Thrust Load - 500 Lbs, Radial Load - 50 Lbs

Ball No.	Contact Angle, degrees		Mean Hertzian Stress, psi		Centrifugal Force, lb	Maximum SV Value, psi(ft/sec)
	Outer	Inner	Outer	Inner		
1	-11.761	-31.720	178,930	183,350	89.978	2.97 E06
2	-11.684	-31.773	178,640	182,630	90.066	2.96 E06
3	-11.467	-31.923	177,830	180,610	90.319	2.94 E06
4	-11.151	-32.140	176,700	177,710	90.694	2.90 E06
5	-10.799	-32.381	175,510	174,540	91.124	2.86 E06
6	-10.480	-32.599	174,480	171,700	91.523	2.82 E06
7	-10.259	-32.751	173,790	169,760	91.806	2.79 E06
8	-10.180	-32.805	173,550	169,070	91.908	2.78 E06
9	-10.259	-32.751	173,790	169,760	91.806	2.79 E06
10	-10.480	-32.599	174,480	171,700	91.523	2.82 E06
11	-10.799	-32.381	175,510	174,540	91.124	2.86 E06
12	-11.151	-32.140	176,700	177,710	90.694	2.90 E06
13	-11.467	-31.923	177,830	180,610	90.319	2.94 E06
14	-11.684	-31.773	178,640	182,630	90.066	2.96 E06

in Figure 29 was considered acceptable -- provided the thrust applied to the bearing is monitored during testing and kept between 350 and 700 lbs.

2.5.5 Torque-Tube Bearings

The Barden thrust ball bearing is also used on the torque tube to provide commonality within the rig. A constant 300-lb thrust load was applied to provide an L_1 life of 1,000 hours.

2.6 Rotating Components

Rotating components were designed for a margin-of-safety based on allowable yield and ultimate strengths. The yield allowable stress was 80 percent of the -3σ yield, and the ultimate allowable stress was 64 percent of -3σ ultimate. A stress concentration factor (K_t) of 1.56 was used for all curvic couplings, and a K_t of 3.12 was used for instrumentation access holes in the tiebolt. Elliptical fillets were designed at the impeller blade root; these provide a smooth stress transition from the blade to the disk. (The impeller blades and disk were analyzed with finite-element methods; therefore, stress concentration factors were included implicitly in the analysis.)

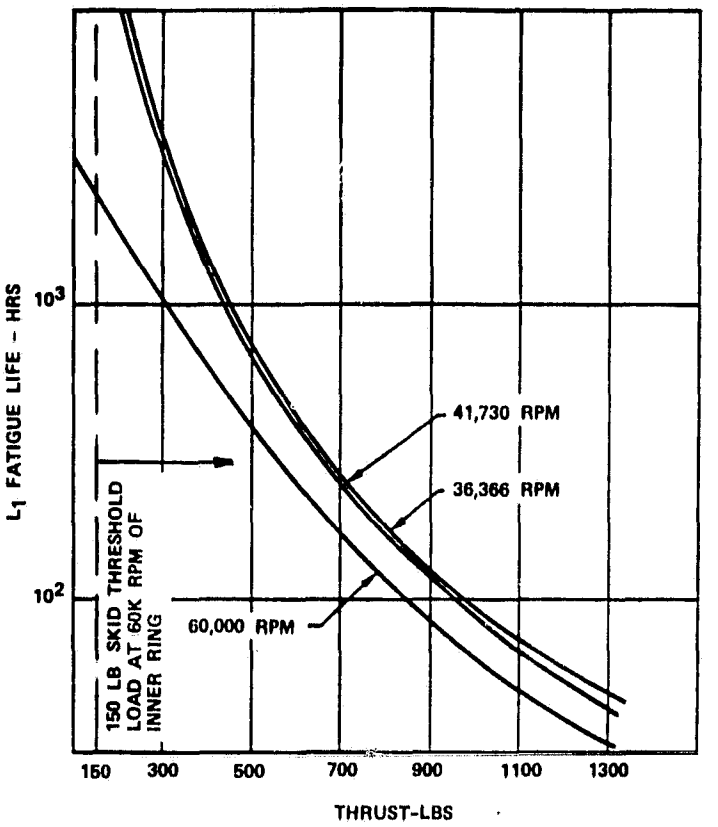

Figure 29. Fatigue Life Versus Thrust Load for the 107-Size, Split-Ring Thrust Bearing.

2.6.1 Rotor Burst Speed Calculation

The impeller burst speed calculations were accomplished with the finite-element model shown in Figure 30, based on use of Ti-17 as the material. The blade inertias were simulated by the plane stress elements of appropriate blade thickness. The disk stiffness was simulated by full-hoop axisymmetric elements.

The average tangential stress calculation was based on integration of tangential stress in the disk elements. The tangential stress distribution is shown in Figure 31. The strength calculation was based on integrating the variation of ultimate strength with temperature.

For the impeller burst speed calculation, 85 percent of the disk section was allowed to approach the ultimate material strength before burst. The resulting calculation was as follows:

$$\text{Burst Speed} = \sqrt{0.85 \left(\frac{\sigma_{ult}}{\sigma_{avg}}\right)} \left(N_{100\text{-percent speed}}\right)$$

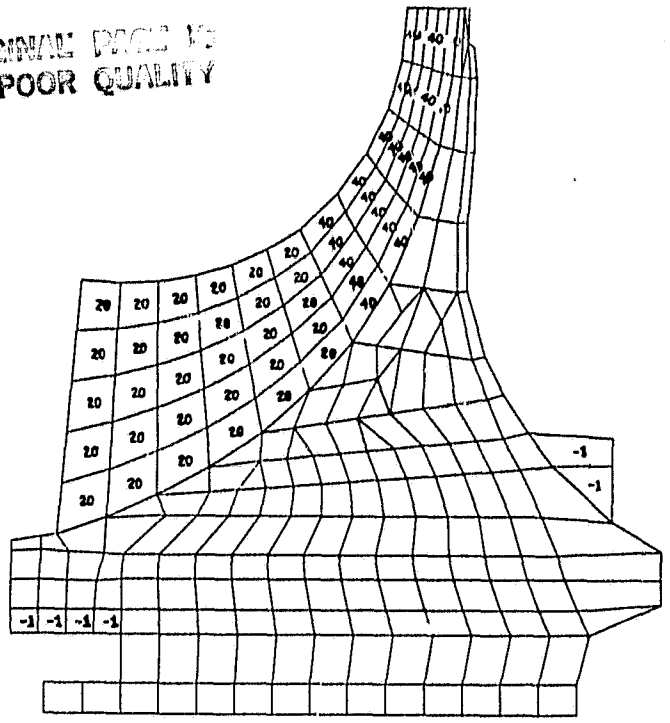

Figure 30. Finite-Element Model for the Scaled Impeller.

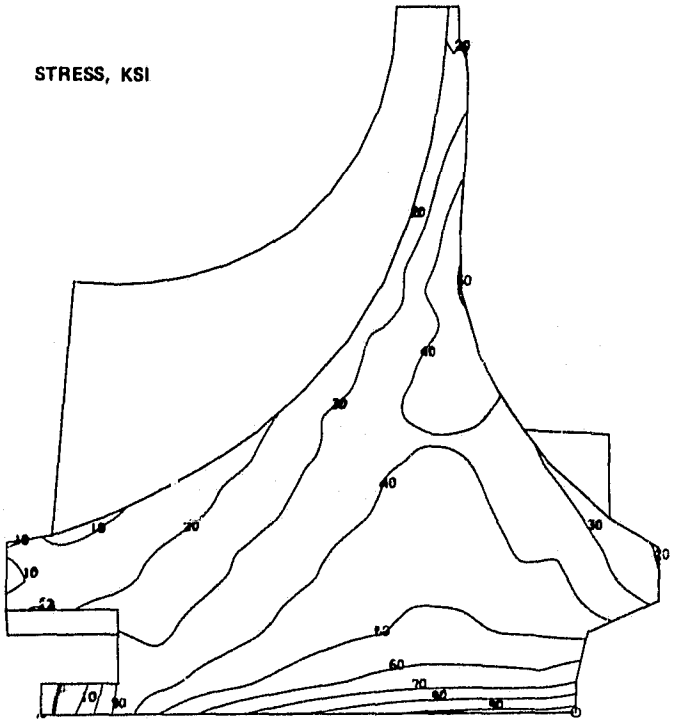

Figure 31. Tangential Stress Distribution for the NASA Impeller at 100-Percent Speed.

where σ_{ult} = ultimate material strength (minimum)
σ_{avg} = average tangential stress
100-percent speed = 36,366 rpm

therefore:

$$\text{Burst Speed} = \sqrt{(0.85)\ \frac{147.3}{43.8}}\ (36{,}366) = 61{,}548 \text{ rpm.}$$

2.6.2 Impeller Stresses

Stress margins were calculated for the maximum blade effective stress, the maximum average sectional stress, and the maximum surface stress that is subject to vibration. These values are summarized in Table 2 for both the blade and the disk.

The impeller blade stresses were calculated with the three-dimensional finite-element model shown in Figure 32, based on 105 percent of design speed. The blade fixity was applied to the hub line of the blade, and Figure 33 shows the calculated stresses.

TABLE 2. Ti-17 DESIGN CRITERIA.

BLADE DESIGN (105-PERCENT SPEED)					
Stress Parameter	Temp (°F)	Yield (or) Ultimate (-3σ) (KSI)	Allowable Stress (KSI)	Actual Stress (KSI)	Margin of Safety*
Max. Effective Surface	390	106.9	$0.8\sigma_{Yield}$ = 85.5	62.9	0.70
Max. Avg. Sectional	390	114.9	$0.64\sigma_{Ultimate}$ = 73.5	49.8	1.31
DISK DESIGN (105-PERCENT SPEED)					
Stress Parameter	Temp (°F)	Yield (or) Ultimate (-3σ) (KSI)	Allowable Stress (KSI)	Actual Stress (KSI)	Margin of Safety*
Average Tangential	150	147.3	$0.55\sigma_{Ultimate}$ = 81.0	43.8	2.36
Max. Effective Bore	135	128.6	$1.0\sigma_{Yield}$ = 128.6	96.4	0.33
Avg. Effective Bore	150	126.0	$0.85\sigma_{Yield}$ = 107.1	80.9	0.56
Max. Effective Web	235	120.0	$0.8\sigma_{Yield}$ = 96.0	72.1	0.66
Avg. Radial Web	265	140.7	$0.64\sigma_{Ultimate}$ = 90.0	45.7	2.08

*Margin of Safety $= \left[\frac{-3\sigma \text{ (Yield or Ultimate)}}{\text{Actual } \sigma}\right] - 1$

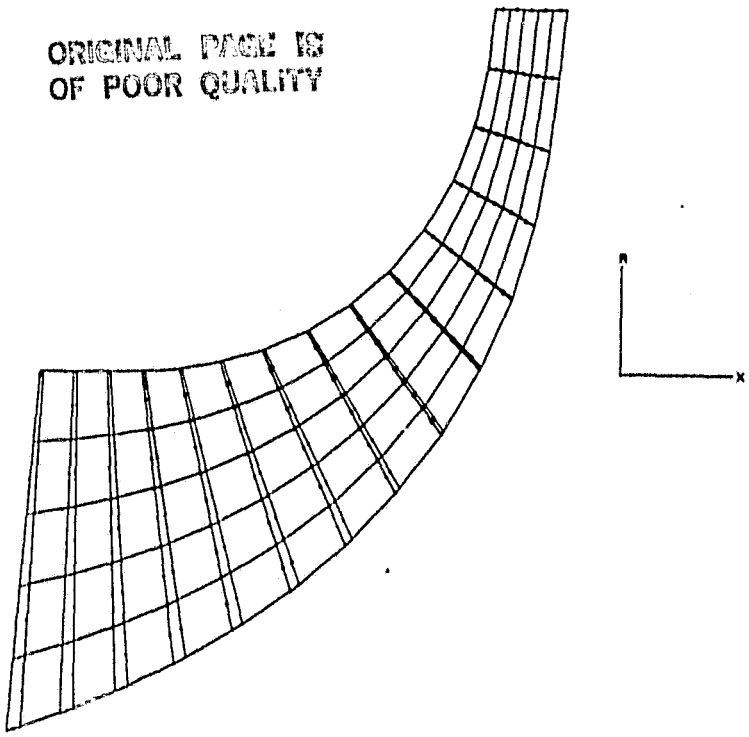

Figure 32. Impeller Stress and Vibration Analysis, as Provided by 3-D, Finite-Element Model.

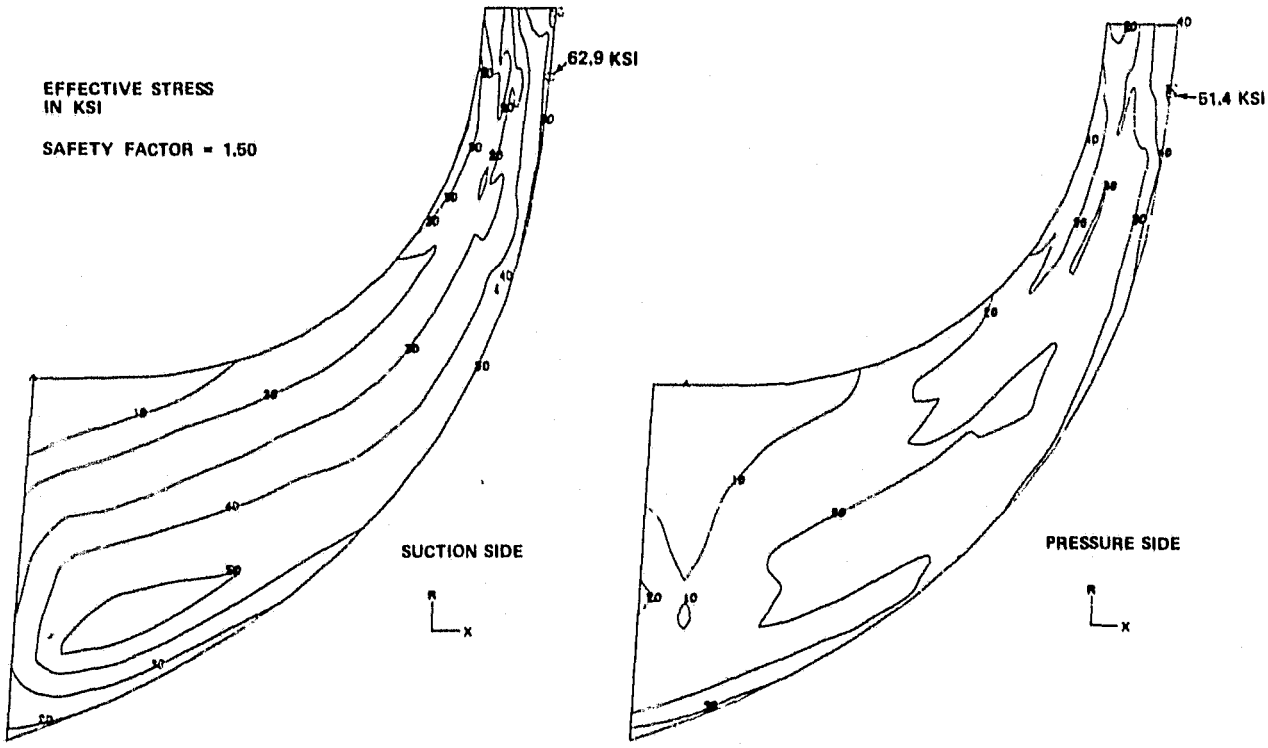

Figure 33. Effective Stress Distribution for NASA Impeller Blade at 105-Percent Speed.

2.6.3 Rotor Cyclic Life Calculation

The cyclic life of the impeller was determined using the stress simulation results discussed earlier. The critical locations of the impeller were the disk bore (maximum stress = 96.4 ksi) and the inducer region of the blade (maximum stress = 60 ksi). The disk bore became the dominant area because of its higher peak stress.

Below the proportional limit, the loading was purely cyclic (i.e., from 0 ksi to 96.4 ksi then back to 0 ksi). Figure 34 illustrates the life diagram for room-temperature Ti-17 and revealed a life in excess of 10,000 cycles. The impeller disk bore was calculated to reach an approximate temperature of 150°F while operating. (The fatigue strength of titanium at 150°F is similar to room-temperature titanium.)

Since the blade inducer region can be subject to mild vibratory response -- typically ±5 ksi (although ±10 ksi was considered for fatigue calculations), the combined loading in the inducer region was also plotted in Figure 34. It fell below the 10^7 cycle endurance limit.

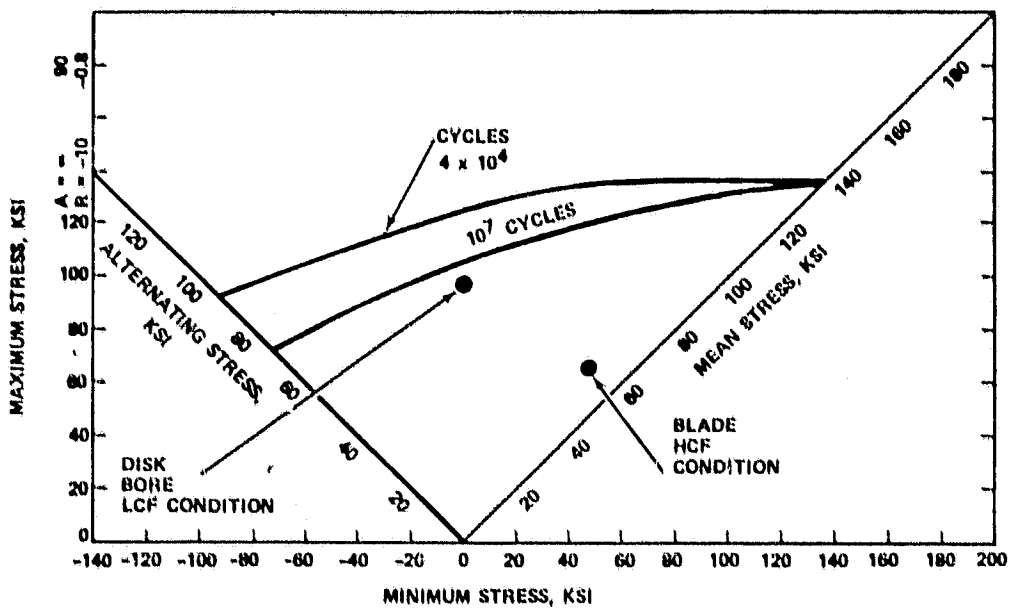

Figure 34. Life Diagram for Titanium. [Note: Diagram for Ti-6Al-4V (Shown) Is Conservative Relative to Ti-17 Strength.]

2.6.4 Calculation of Moment of Inertia

Inertia properties were calculated within the finite-element analysis program used to evaluate impeller stresses. The calculation was an integration of the element inertias. The results of the computer analysis are shown in Table 3.

2.6.5 Rotor-Dynamics Analysis

Computer program "RODA" was used to analyze the rotating system critical speeds and dynamic response. The model for rotor-dynamics analysis of the scaled-impeller rotating group is shown in Figure 35; the upper half represents the mass model, and the lower half represents the stiffness model. Squeeze-film dampers are provided for the four bearings. The bearing loads due to unbalance were already shown in Figures 26 and 27. (The peak load of less than 100 pounds on any bearing satisfied the design criterion for a 500-hour bearing life.)

TABLE 3. COMPUTER MECHANICAL ANALYSIS.

SCALED AFAPL IMPELLER BLADED DISK,JAN 81 100 PERC.RIG SPEED=36366RPM RPM= 36366.00

HUB AREA PROPERTIES--AREA	11.4027	IN**2	MASS PROPERTIES--MASS	.0626	LB-SEC2/IN
RBAR	2.0949	IN	WEIGHT	24.1645	LB
ZBAR	5.5642	IN	I(P)	.5353	LB-IN-SEC2
			I(D)	.3373	LB-IN-SEC2
			RBAR	0.0000	IN
			ZBAR	5.6965	IN

BLADE AREA PROPERTIES--AREA	5.2345	IN**2	MASS PROPERTIES--MASS	.0069	LB-SEC2/IN
RBAR	3.6834	IN	WEIGHT	2.6473	LB
ZBAR	4.7087	IN	I(P)	.0834	LB-IN-SEC2
			I(D)	.0441	LB-IN-SEC2
			RBAR	3.2953	IN
			ZBAR	5.2687	IN

(MASS PROPERTIES ARE FOR ALL BLADES)

TOTAL PROPERTIES-----MASS	.0694	LB-SEC2/IN	KINETIC ENERGIES		
WEIGHT	26.8118	LB	-ALL BLADES	604500.	IN-LB
I(P)	.6186	LB-IN-SEC2	-------DISC	3881300.	IN-LB
I(D)	.3826	LB-IN-SEC2	------TOTAL	4485800.	IN-LB
RBAR	2.7135	IN			
ZBAR	5.6542	IN			

SPEED OF ROTATION = 36366 RPM

FREE RING RADIUS 2.3571 IN

AVERAGE TANGENTIAL STRESS COMPONENTS,KSI

DISC	33.6
BLADES	4.6
FORCES	0.0
TOTAL	38.2

AVERAGE ULTIMATE STRESS = 121.2 BURST RATIO (K=.85) = 1.642
YIELD STRESS = 111.1 YIELD RATIO (K=1.0) = 1.706

NOTE
1. BURST RATIO = SQRT(K*ULT/AVE TAN)
2. YIELD RATIO = SQRT(K*YLD/AVE TAN)
3. FREE RING RADIUS = SQRT(AVE TAN DISC/RHO*RPM**2)

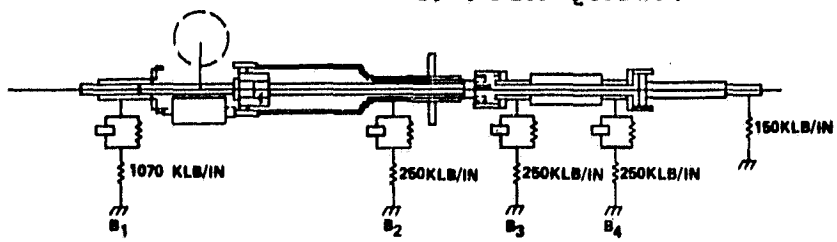

RESONANCE NO.	PERCENT DESIGN SPEED	CRITICAL SPEED*(RPM)
1	8	2,823
2	17	6,217
3	25	9,013
4	31	11,434
---	70	25,456
---	100	36,366
---	120	43,639
5	148	53,704
6	161	58,530

*FOR CRITICAL SPEED CALCULATION, THE SUPPORTING STIFFNESSES AT THE FOUR HYDRAULIC-MOUNTED BEARINGS ARE OBTAINED FROM THE UNBALANCE RESPONSE ANALYSIS.

Figure 35. Rotor Dynamics Model and Critical Speeds for NASA Compressor.

Predicted critical speeds are also listed in Figure 35. Compared to the operating speed of 36,366 rpm, a 48-percent margin exists for the "bent shaft" frequency (5th critical). The mode shapes at the critical speeds are plotted in Figure 36. For these results, the squeeze films were represented by springs having the stiffness estimated from the unbalance response analysis. These spring rates are as follows:

Bearing	Oil Film Spring Rate, klb/in.	Bearing Plus Static Structure Spring Rate, klb/in.	Bearing Plus Static Structure Plus Oil Film Spring Rate, klb/in.
B1	4	1070	4
B2	11	250	10.5
B3	9	250	8.7
B4	14	250	13.3

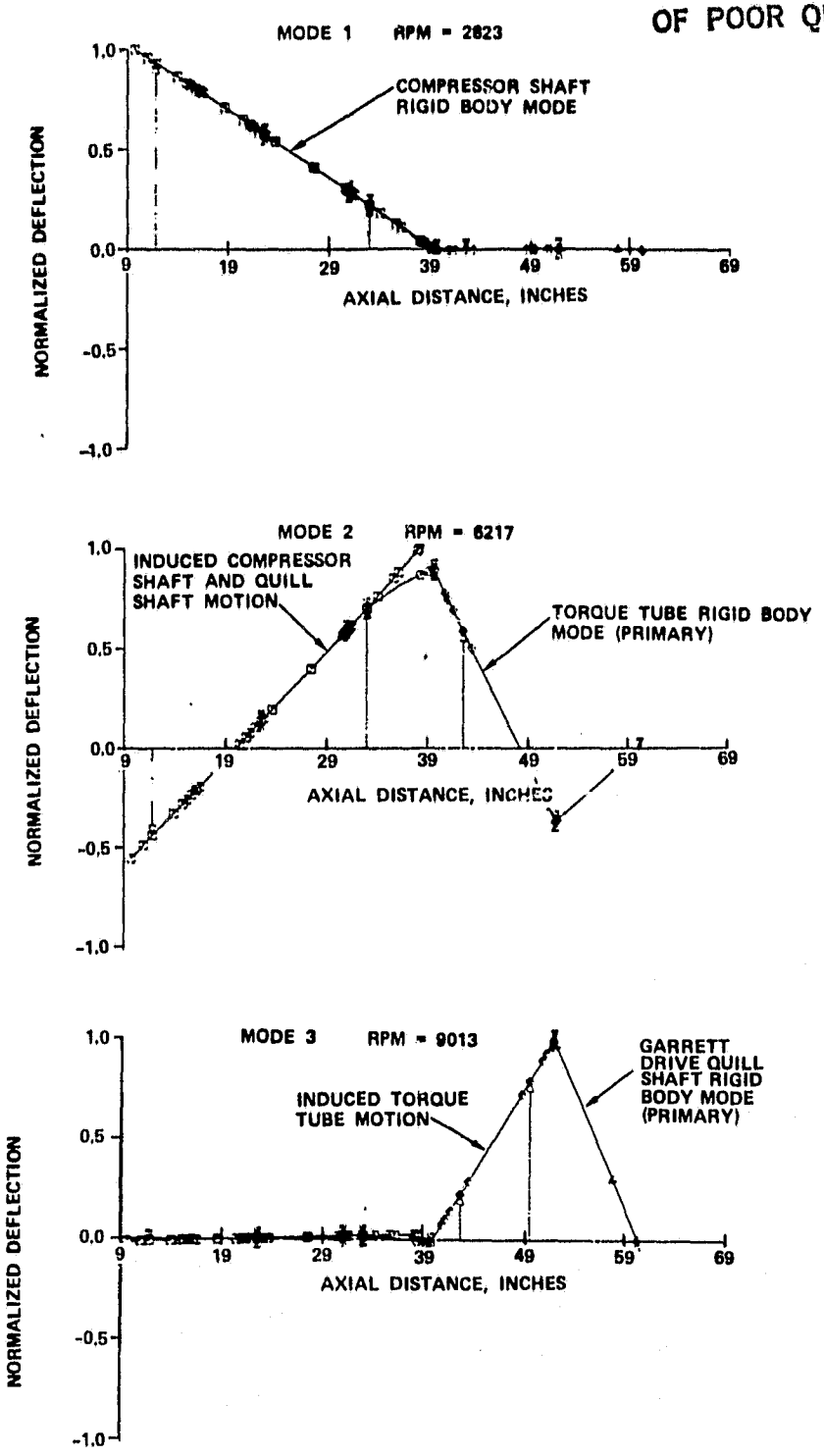

NOTE: DEFLECTIONS NORMALIZED TO LARGEST DEFLECTION.

Figure 36. Critical-Speed Mode Shapes for the NASA Scaled Compressor (Sheet 1 of 2).

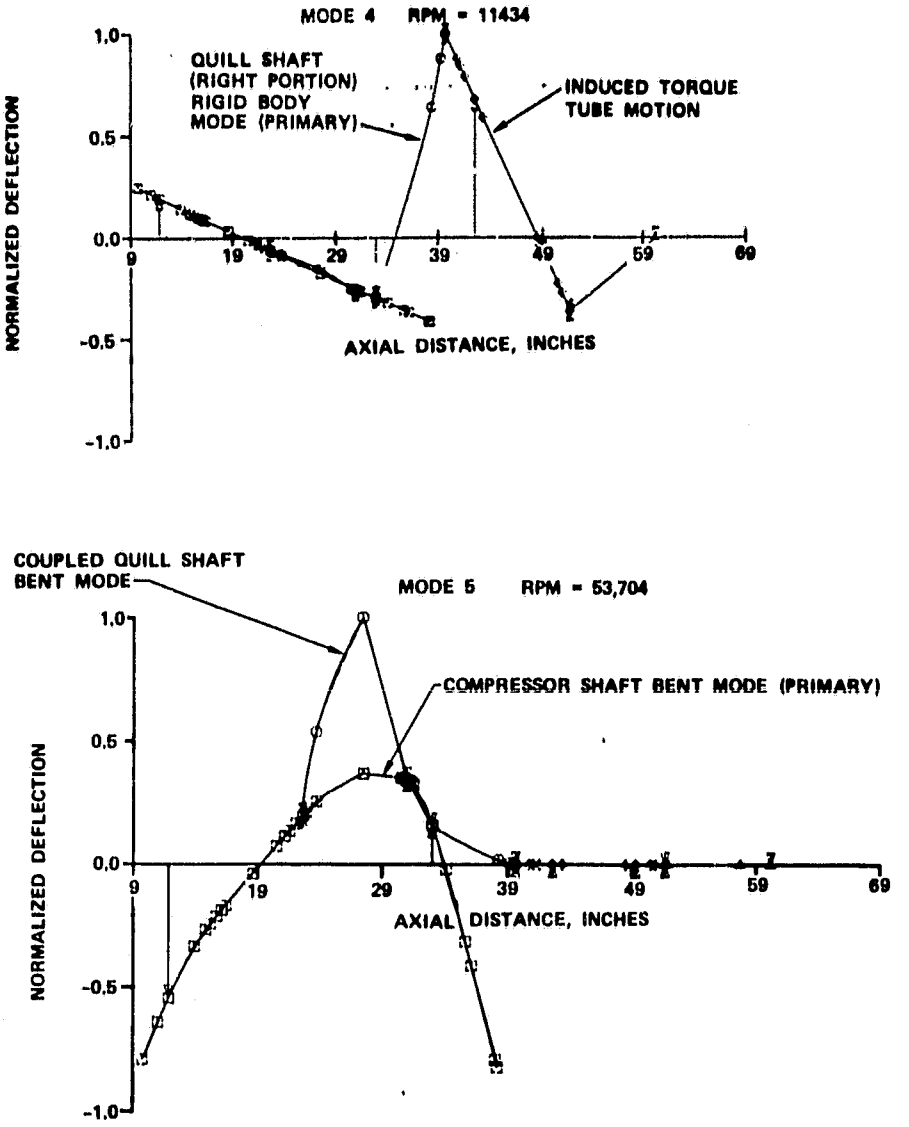

NOTE: DEFLECTIONS NORMALIZED TO LARGEST DEFLECTION.

Figure 36. Critical-Speed Mode Shapes for the NASA Scaled Compressor (Sheet 2 of 2).

3.0 TEST RIG DESCRIPTION

The final design for the NASA test rig is illustrated in Figure 37. The design supports the compressor section with a straddle-mount bearing system consisting of a forward roller bearing and an aft ball (thrust) bearing.

Integrated into the test rig shafting is a clearance-control mechanism that allows the impeller-to-shroud axial clearance to be varied at any time regardless of rotating speed or compressor setting. (This eliminates the need for sensitive impeller-to-shroud shimming.) In addition, the combination of a thrust-measurement ring and a thrust balance piston allows the thrust on the aft ball bearing to be monitored and controlled.

The test rig is instrumented as shown in Figure 38. Included is the instrumentation needed for analyzing compressor aerodynamic performance and monitoring test rig operation.

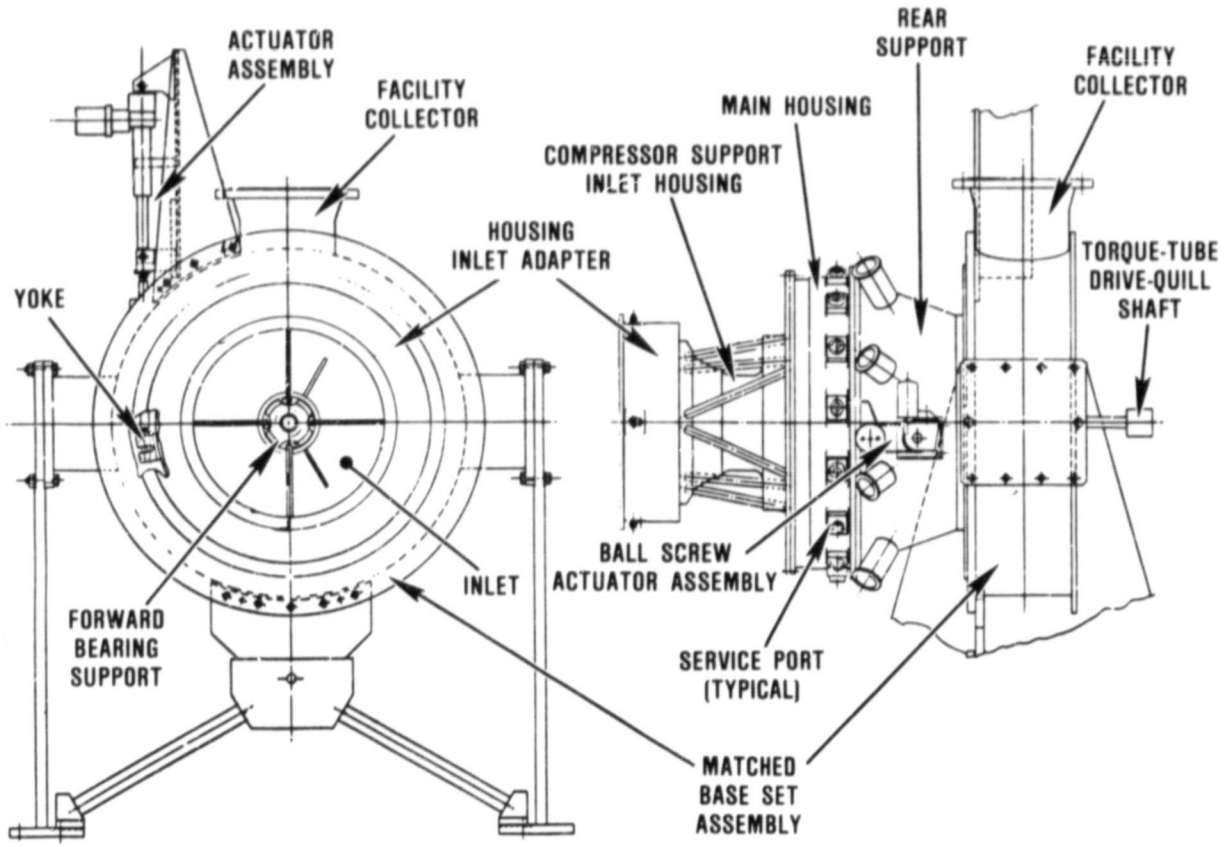

Figure 37. Test Rig Design for NASA 10-lb/sec Compressor.

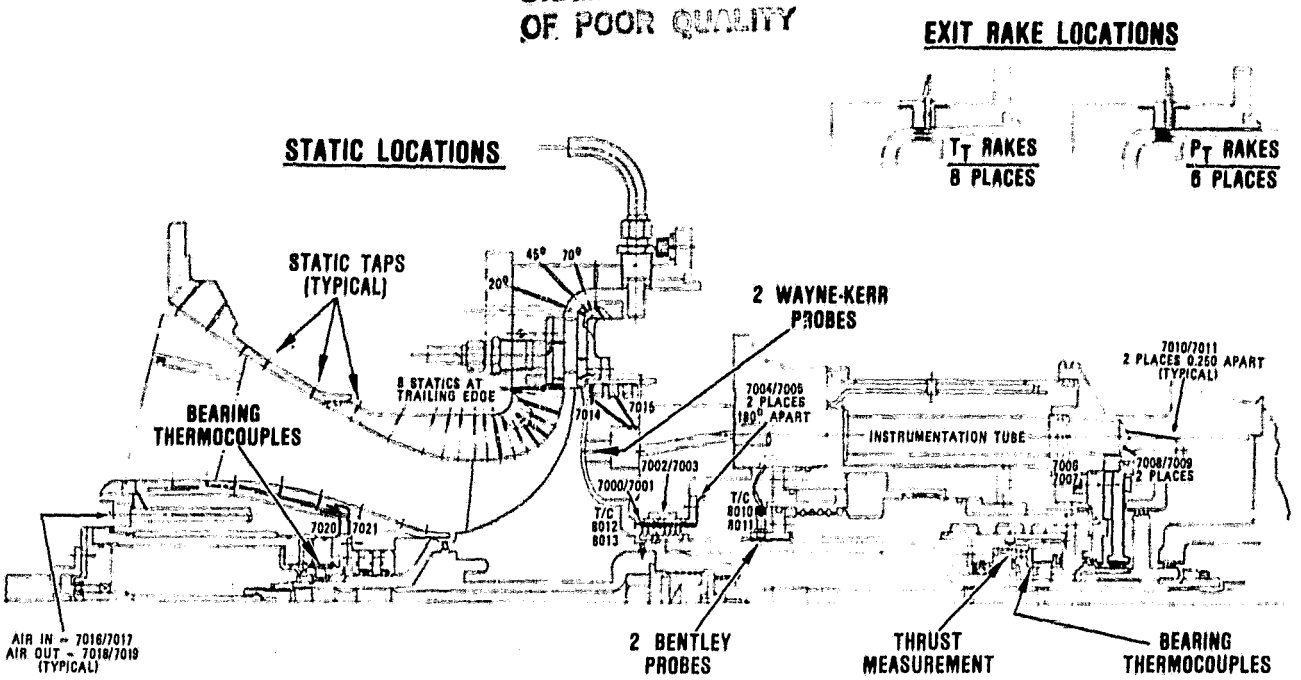

Figure 38. Test Rig Instrumentation Summary.

The assembly of the test rig is described in detail in the assembly procedures, Garrett Report 21-4632. The rig is comprised of the following main assemblies:

- The housing inlet adapter and compressor support inlet housing (Figure 39), which provide for aerodynamically smooth intake of air to the compressor and mechanical support of the front of the driveshaft
- The main housing and rear support (Figure 40), which provide for test-rig services and variable clearance control (see also Figure 41)
- The matched base set (Figure 42), which supports the entire rig, permits throttle control, and attaches to the facility air collector
- The torque-tube (Figure 43), which couples to the facility drive
- The shafting and compressor for initial testing (see Figure 44).

Instrumentation calibrations are contained in Figures 45 through 49 and Tables 4, 5, and 6 for reference.

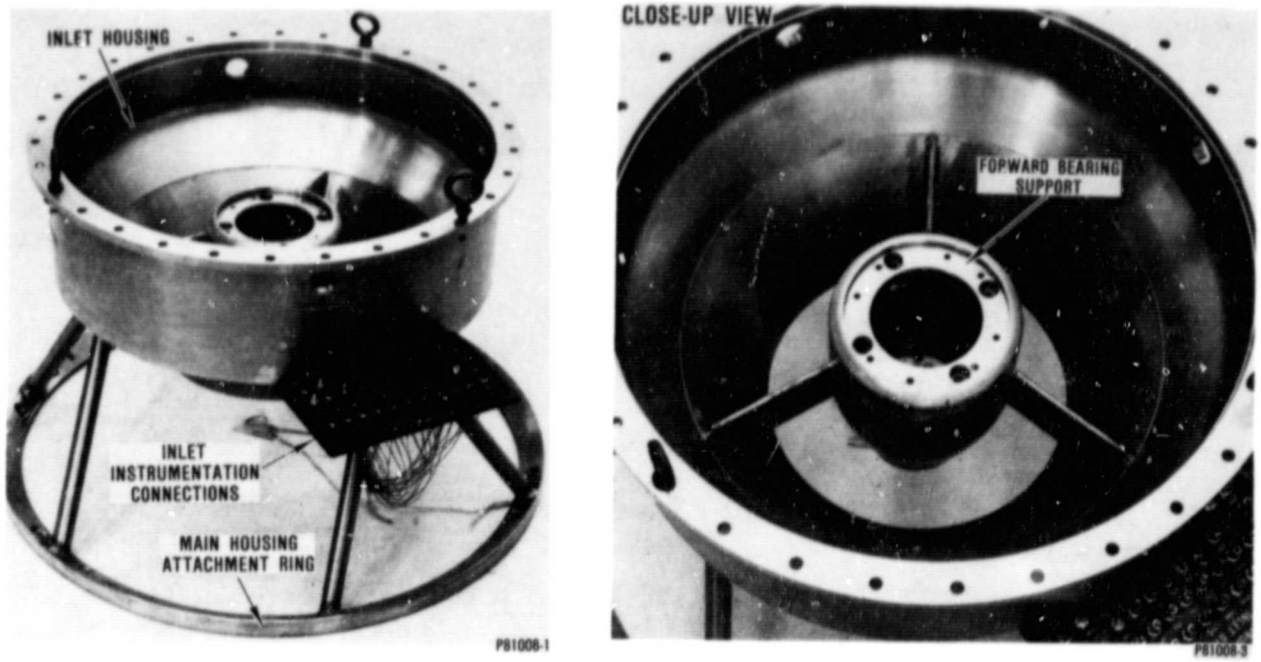

Figure 39. Inlet Housing, Showing Forward Bearing Support.

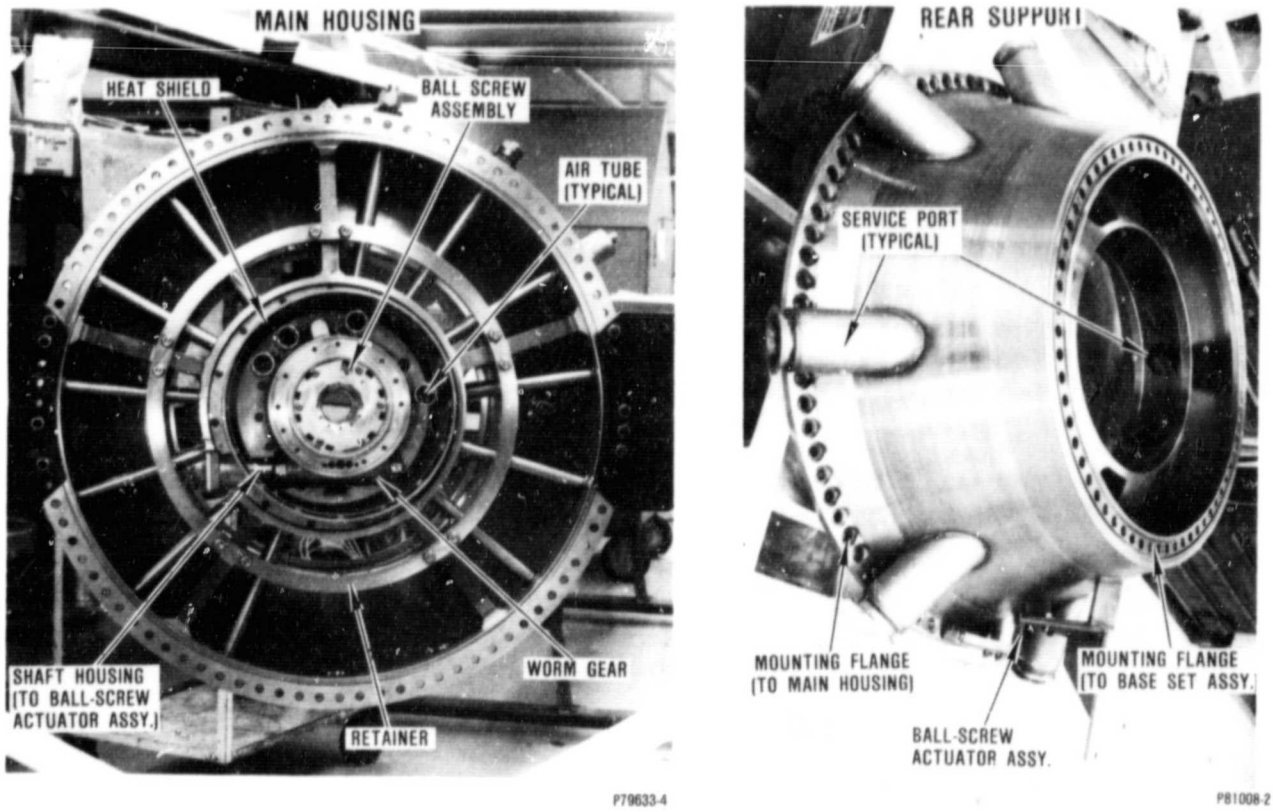

Figure 40. Main Housing and Rear Support.

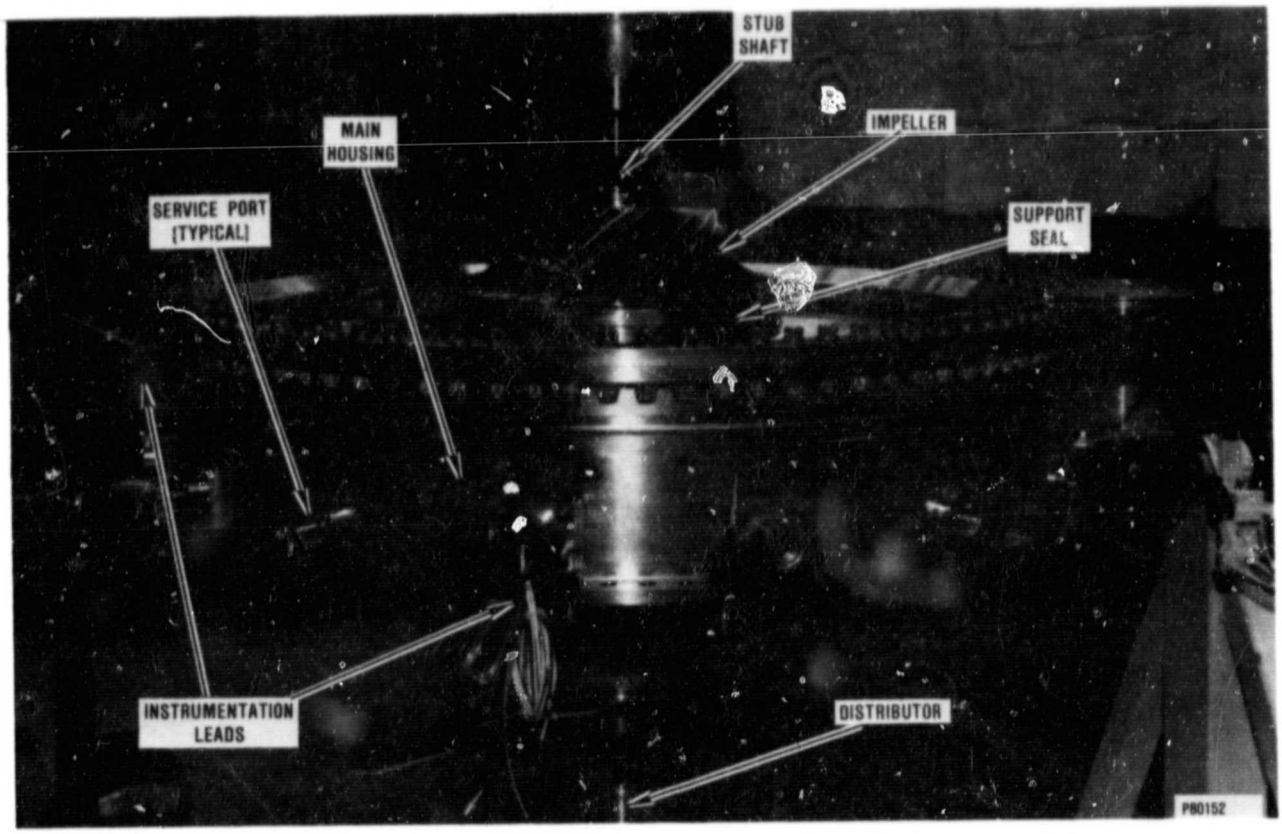

Figure 41. Main Housing, Showing Impeller, Distributor, and Instrumentation Installed.

VIEW FROM REAR

VIEW FROM INLET

Figure 42. Test Rig Matched Base Set.

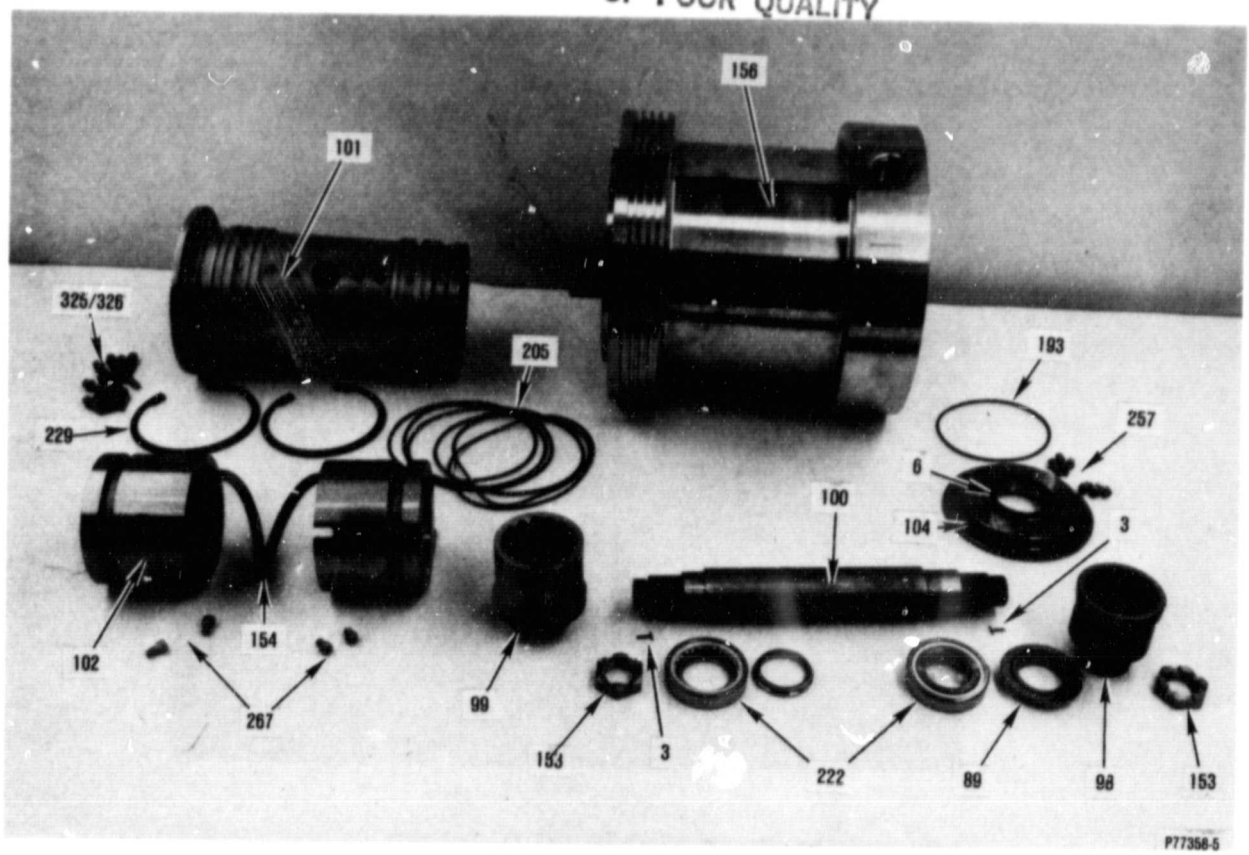

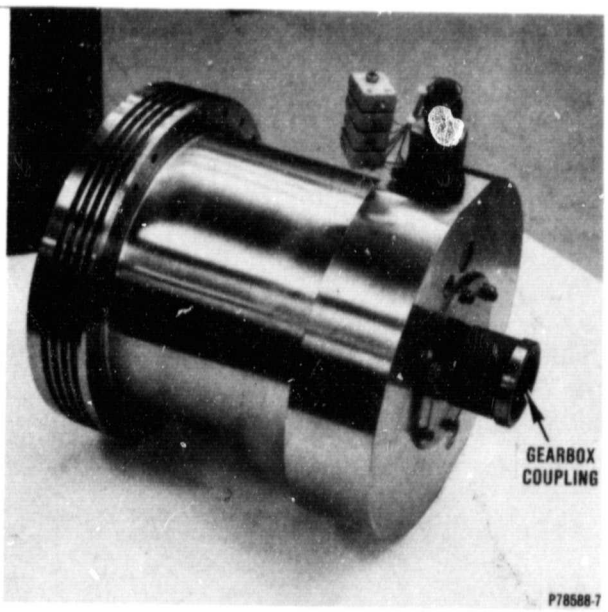

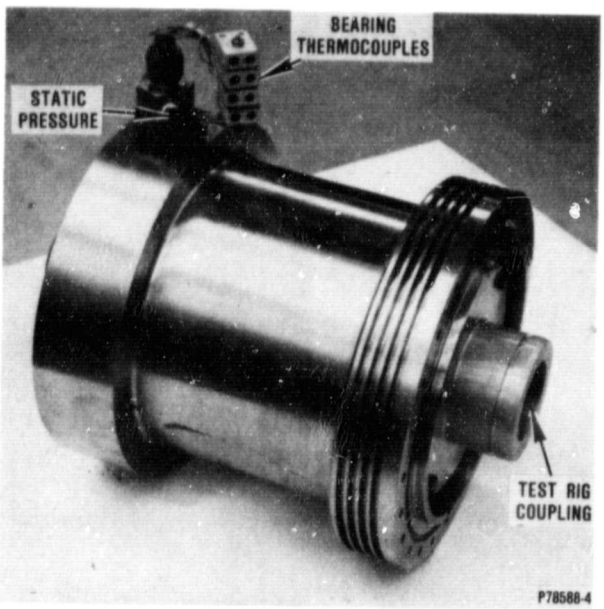

Figure 43. Torque-Tube Hardware and Assembly. (Find Numbers Refer to Drawing 3553131.)

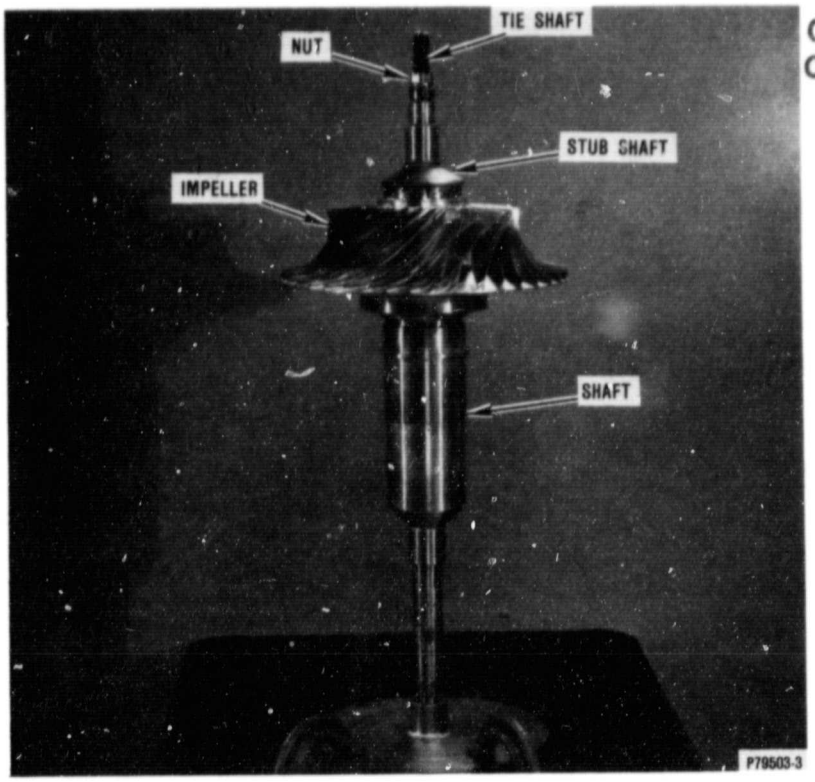

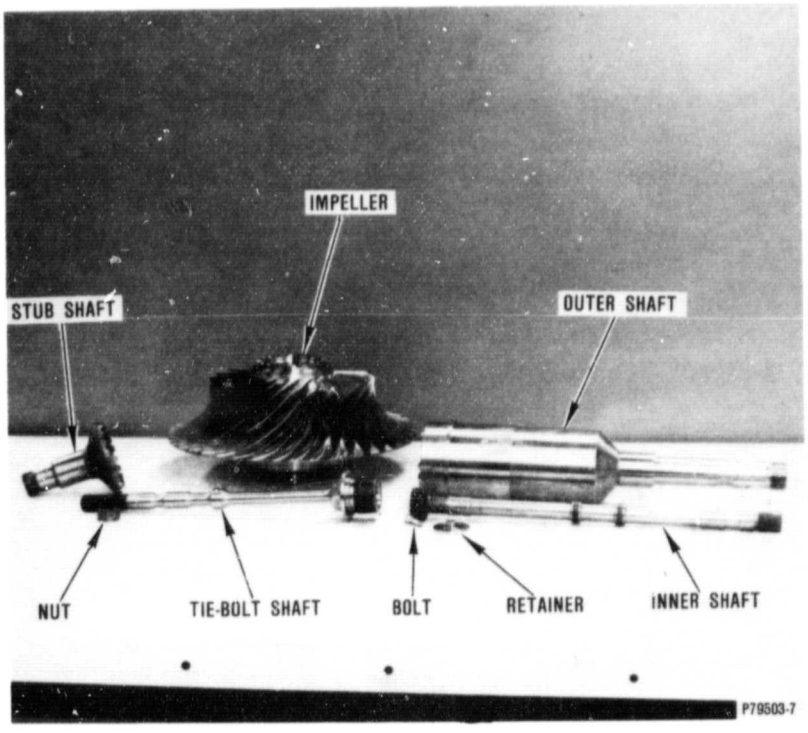

Figure 44. Impeller and Shafting.

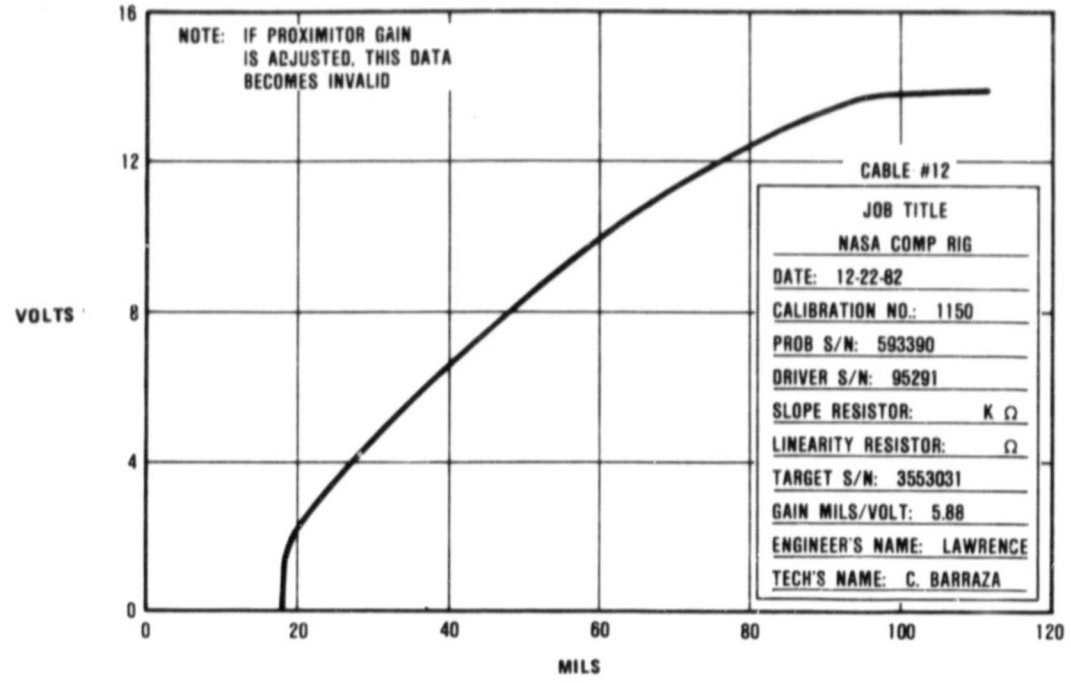

Figure 45. Test Rig Bentley Probe Calibration - Vertical.

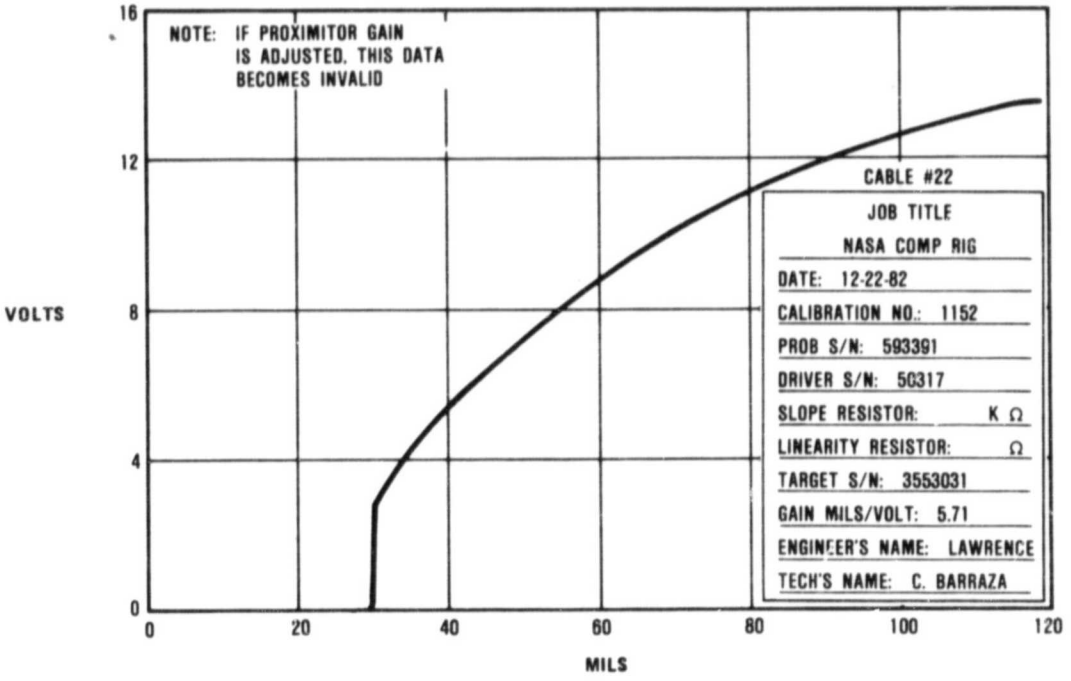

Figure 46. Test Rig Bentley Probe Calibration - Horizontal.

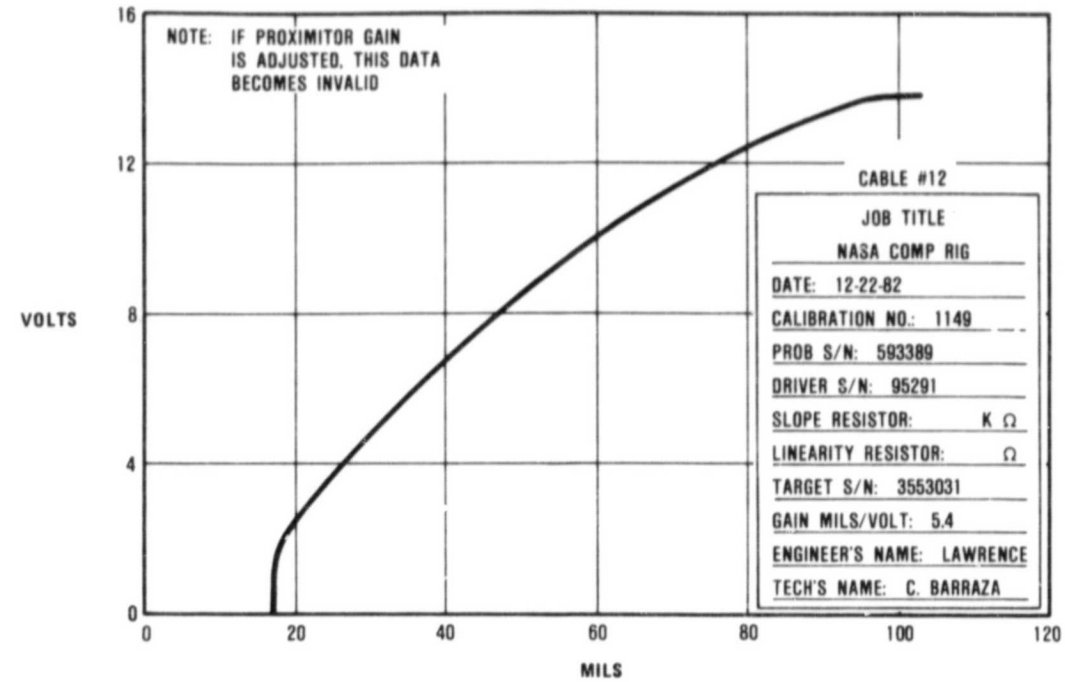

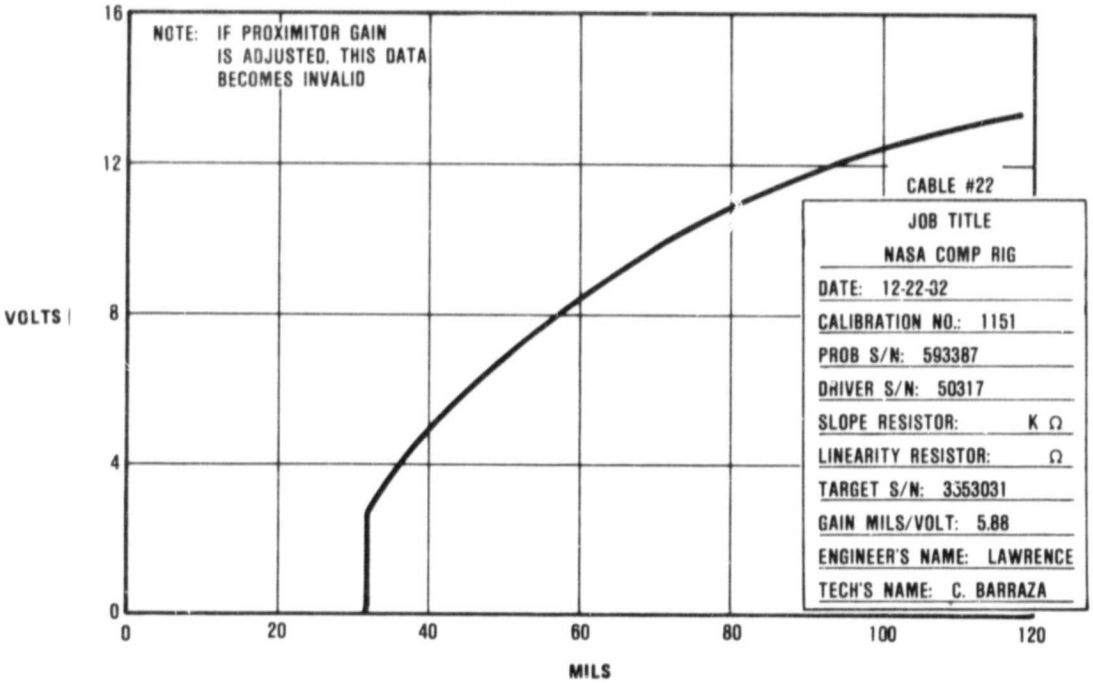

Figure 47. Spare Bentley Probe Calibration.

C.I. Job No. 154
R.I. Job No.
S.I. Job No.
Tech THORMAN
Date 4-27-82

STRAIN GAGE INSTALLATION INFORMATION SHEET

ENGINEERING DATA

Lab Engineer M.V. Merritt Ext 3847
Proj. Engineer P. Sebring Ext 1144
LWO 63703
Unit Name NASA Comp R&S/N
Part Name Thrust Ring S/N
Part Material Steel P/N
Photographs Requested ☐ Yes ☑ No
Mail Photos to: Dept

APPLICATION

☑ Thrust ☐ Dynamic
☐ Torque ☑ Static
☐ Stress ☐ Rotating
☐ Dynamic ☑ Stationary
☐ Other

STRAIN GAGE

Gage Type SA-06-062TT-120 (from print)
Max Temp 350 °F No. of Gages 12

LEADWIRE

Max Temp 350 °F Length 6'
Type Gage

CIRCUIT

☑ Full Bridges ☐ Half Bridge
☐ Single ☐ 2 Wire ☐ 3 Wire

FULL BRIDGE CALIBRATION

Calib Range 2000/65 Cal. Points 20%
No. of Temp Cycles 1
Temp Cycle Range 500 °F to 325 °F
Temp Cycle Increments 50°F

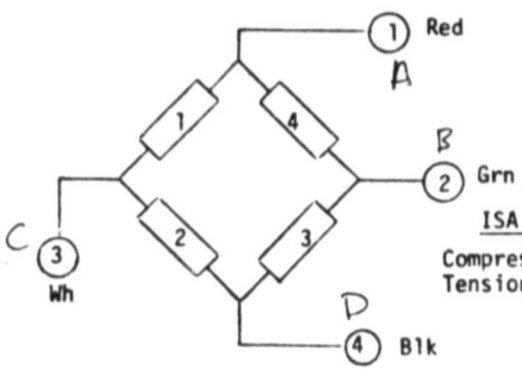

ISA STANDARD
Compression - Negative
Tension - Positive

LABORATORY DATA

STRAIN GAGE

Gage Type EA-06-062TT-120
Gage Factor 2.03 ± 2% Res 120Ω
Adhesive Type 8112
Covering Type ☐ Mithra ☐ Cer 1000
Gage Coat ☐ Armadillo
Type 8112 ☐ Gage Coat ☐ Flame Spray ☐ Other

LEADWIRE

Gage to Terminator .38 GA. FORMVAR
Terminator Out 36 GA TEFLON
Solder Type 420°
☐ Armadillo

IDENTIFICATION

☐ Notches (.020 MGO)
☐ Wire Marker
☒ Color Code ON DWG NO. 3553340
☐ Gage Location Data Attached

AMBIENT NO-LOAD READING

Strain Indicator Type-S/N
Reading w/Bal Out με
Bal Reading w/Zero με

CALIBRATION

Cal. Date Tech
Bridge #1
Resistance Ω Rc = Ω
Across 1 and 2 = με
=
Bridge #2
Resistance Ω Rc = Ω
Across 1 and 2 = με
=

☐ Calibration Data Attached
☒ Temperature Cycle Data Attached
☐ Bridge Wired to ISA Standard

Figure 48. Strain Gage Installation.

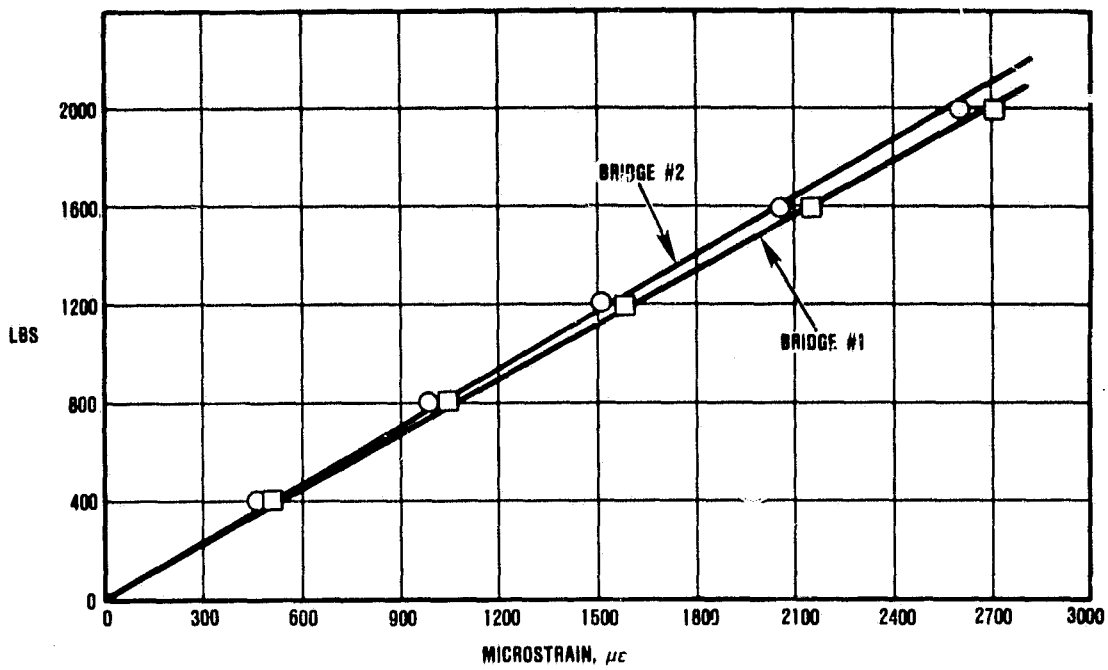

Figure 49. Thrust-Ring Strain Gage Calibration.

TABLE 4. STRAIN GAGE CALIBRATION DATA.

Bridge No. 1
CI No. 154B
Balance: Zero Inst. No. EC412, -10.360 microinch offset
Date: 12/21/82
Bridge Resistance: 478 ohms

Load (Percent)	Load (lbs)	Comp. (με)
0	0	0
20	400	510
40	800	1060
60	1200	1575
80	1600	2140
100	2000	2705
0	0	0

Bridge No. 2
CI No. 154B
Balance: Zero Inst. No. EC432, -10.050 microinch offset
Date: 12/21/82
Bridge Resistance: 478 ohms

Load (Percent)	Load (lbs)	Comp. (με)
0	0	0
20	400	465
40	800	985
60	1200	1505
80	1600	2060
100	2000	2605
0	0	0

TABLE 5. IMPELLER BACKFACE CLEARANCE CALIBRATION.

Clearance (mils)	Wayne-Kerr Probe 1 (voltage)	Wayne-Kerr Probe 2 (voltage)
Touch*	0.571	0.517
0.010	0.651	0.597
0.020	0.731	0.680
0.030	0.814	0.766
0.040	0.892	0.846
0.050	0.970	0.928
0.060	1.049	1.010
0.070	1.123	1.087
0.080	1.196	1.164
0.090	1.264	1.234
0.100	1.332	1.310
0.110	1.392	1.382
0.120	1.463	1.450
0.130	1.549	1.517
0.140	1.631	1.575
0.150	1.703	1.632
0.160	1.788	1.801
0.170	1.906	1.962
0.180	2.010	2.080
0.190	2.090	2.160
0.200	2.140	2.210

*Clearance when impeller contacted backshroud was 0.010 inch at probe location.

TABLE 6. EXIT THERMOCOUPLE RAKE RECOVERY FACTOR.

Probe No.	Element No.	Rec. Fac*
1	1	0.00250
	2	0.00208
	3	0.00047
2	1	0.00126
	2	0.00162
	3	0.00160
3	1	0.00072
	2	0.00153
	3	0.00079
4	1	0.00087
	2	0.00064
	3	0.00085
5	1	0.00016
	2	0.00028
	3	0.00090
6	1	0.00132
	2	0.00136
	3	0.00098
7	1	0.00133
	2	0.00107
	3	0.00218
8	1	0.00148
	2	0.00094
	3	0.00314

Probes were calibrated on the vacuum tunnel at conditions:

$M = 0.30$

$T_T = 87°F$ (Avg)

*The recovery factor is calculated using the following formula:

$$R.F. = \frac{T_{T\ True} - T_{T\ Element}}{T_{T\ Element}}$$

All temperatures are absolute.

$T_{T\ True}$ is an average of 4 total temperature probes located in a low mach area of the tunnel (inlet).

All recovery factors listed are averages of four data scans. Data scatter was low.

4.0 TEST RIG MECHANICAL INTEGRITY

Prior to shipment to NASA in January, 1983, the test rig components were subjected to analysis and mechanical integrity verification. The torque-tube sub-assembly was checked for mechanical operation to 60,000 rpm. All pressurized components were proof-pressure-checked to 450 psia. All compressor components were carefully inspected, balanced, and check-balanced; the impeller also completed holographic inspection. The collector/throttle-valve assembly was checked for proper actuation at temperatures to 800°F. And the test rig was checked for proper operation.

4.1 Torque-Tube Mechanical Check Run

The torque-tube hardware was assembled according to GTEC Assembly Drawing 3553131 and was installed in a test fixture, as shown in Figure 50. The oil baffle was installed on the torque tube, as shown in Figure 51, to improve the oil scavenge system around the ball spline. The test fixture set-up included an air turbine starter as a drive motor, an oil-supply source, oil scavenge, and torque-tube vibration monitoring equipment (accelerometers). A strip chart recorder was used to record torque-tube rotational speed (rpm), oil flow (gpm), torque-tube vertical vibration (mils), and torque-tube horizontal vibration (mils). Vibration was also monitored on a real-time analyzer.

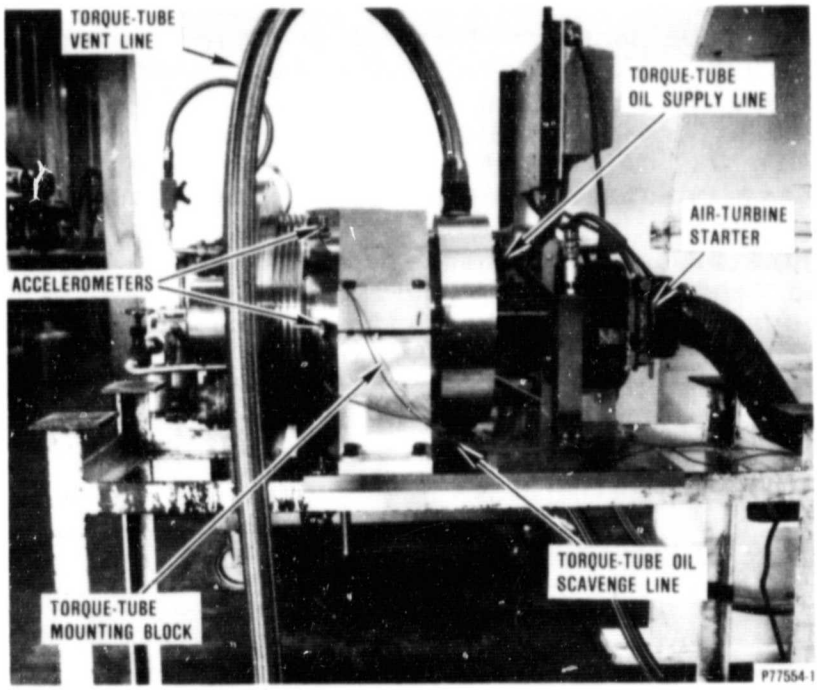

Figure 50. Torque-Tube Installed in Test Fixture.

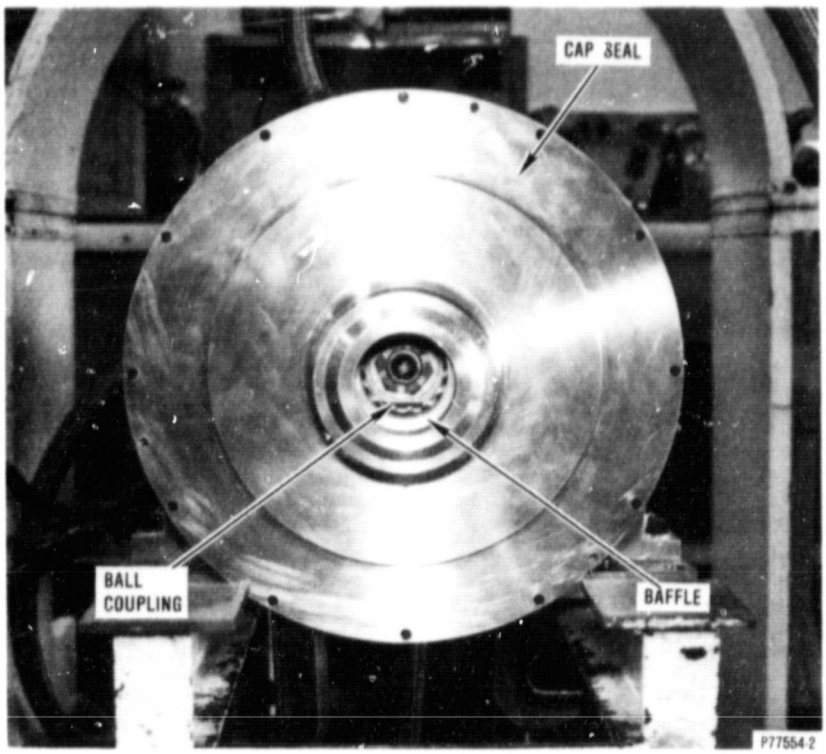

Figure 51. Oil Baffle Installation.

The torque tube was accelerated in speed increments of 5,000 rpm, up to 60,000 rpm. Visual data was recorded at each speed increment for speed, vibration, oil supply pressure, oil flow, oil inlet temperature, and oil scavenge temperature. This data is presented in Table 7. After the incremental acceleration was completed, a steady constant acceleration to 60,000 rpm was accomplished. (The strip chart recording of this acceleration is presented in Figure 52.) Additional testing of the torque-tube indicated that the vent line was not necessary and that, in some cases, the scavenge system was improved without the vent.

GTEC considered the torque tube to be acceptable for operation in the NASA facility at speeds up to 60,000 rpm. It was shipped to NASA-LeRC, with the recommendation that the torque-tube vent should be capped during operation.

4.2 Hydrostatic Pressure Test

A hydrostatic pressure test was conducted on the internally pressurized components of the test rig. A structural schematic of the hardware involved is shown in Figure 53. Prior to hardware assembly, six bolts from each joint (A, B, C, D, and E) were arbitrarily selected and measured. After completion of the pressure test the same bolts were again measured.

TABLE 7. TORQUE-TUBE RECORDED TEST DATA.

Speed (rpm)*	Oil Pressure (psi)	Oil In Temp (°F)	Oil Scavenge Temp (°F)	Oil Flow (gpm)	Vert. Vibration (mils)	Horiz. Vibration (mils)
0	100	66	67	1.17	0	0
5	100	67	70	1.17	0.04	0.01
10	100	68	73	1.17	0.03	0.01
15	100	69	77	1.17	0.02	0.02
20	100	70	81	1.17	0.03	0.03
30	100	77	95	1.17	0.03	0.01
40	100	82	112	1.26	0.03	0.03
45	100	87	124	1.29	0.02	0.02
50	100	87	128	1.21	0.02	0.02
55	100	89	139	1.15	0.05	0.03
60	100	97	147	1.20	0.05	0.03

*X1000

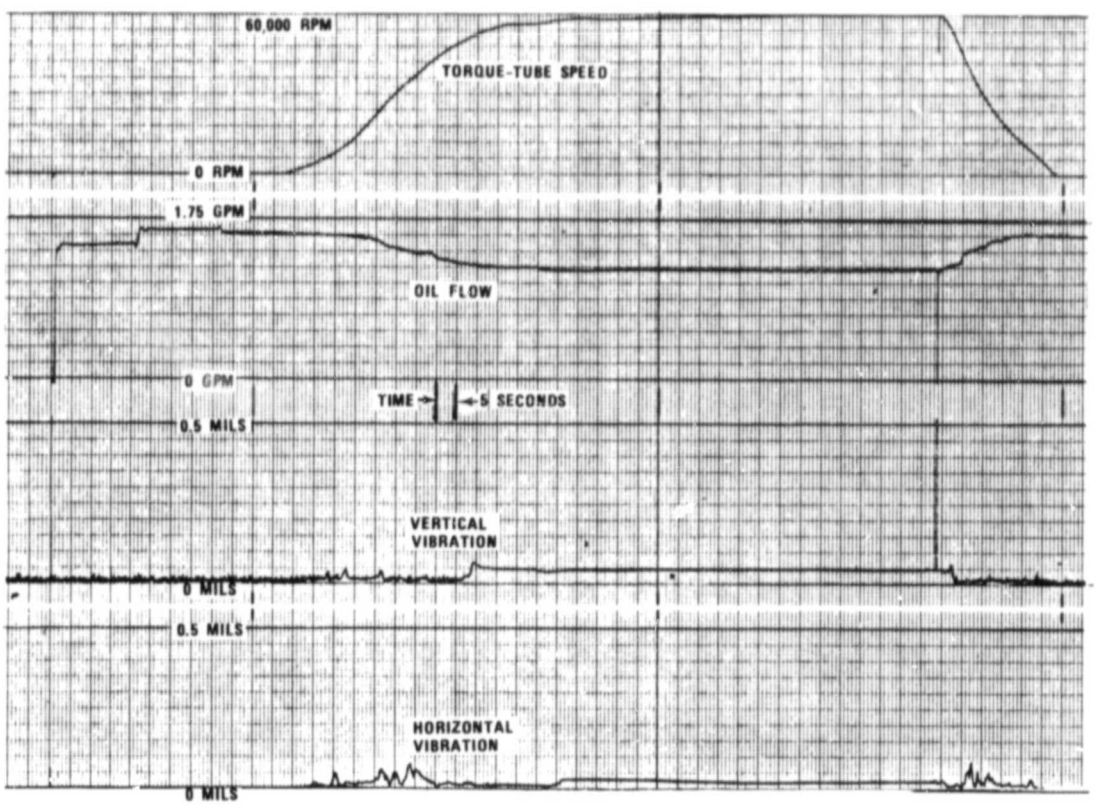

Figure 52. Torque-Tube Acceleration Data.

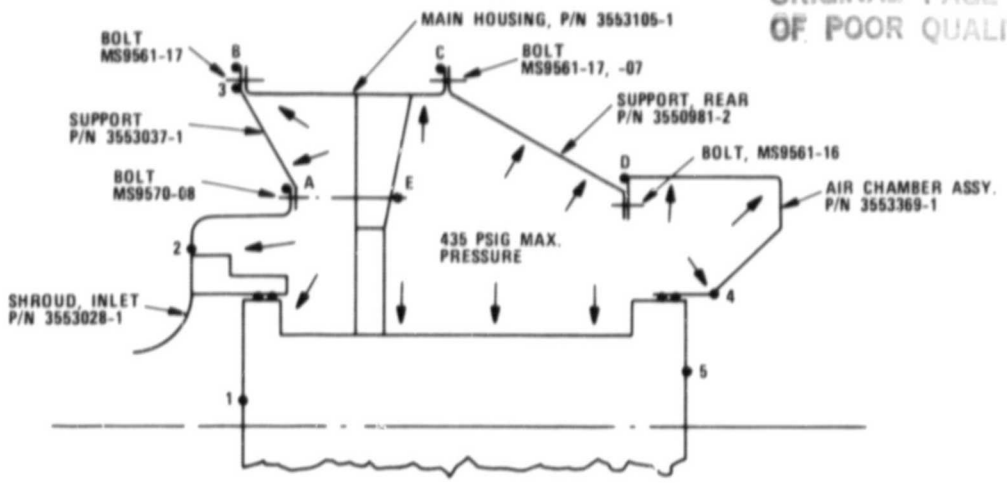

Figure 53. Test Rig Structural Schematic (Not to Scale).

The hardware was assembled incorporating "blank-off" hardware to seal normally open passages. The assembled pressure vessel is shown in Figure 54 prior to testing. Three dial indicators were used to record structure deflections at the various internal pressures.

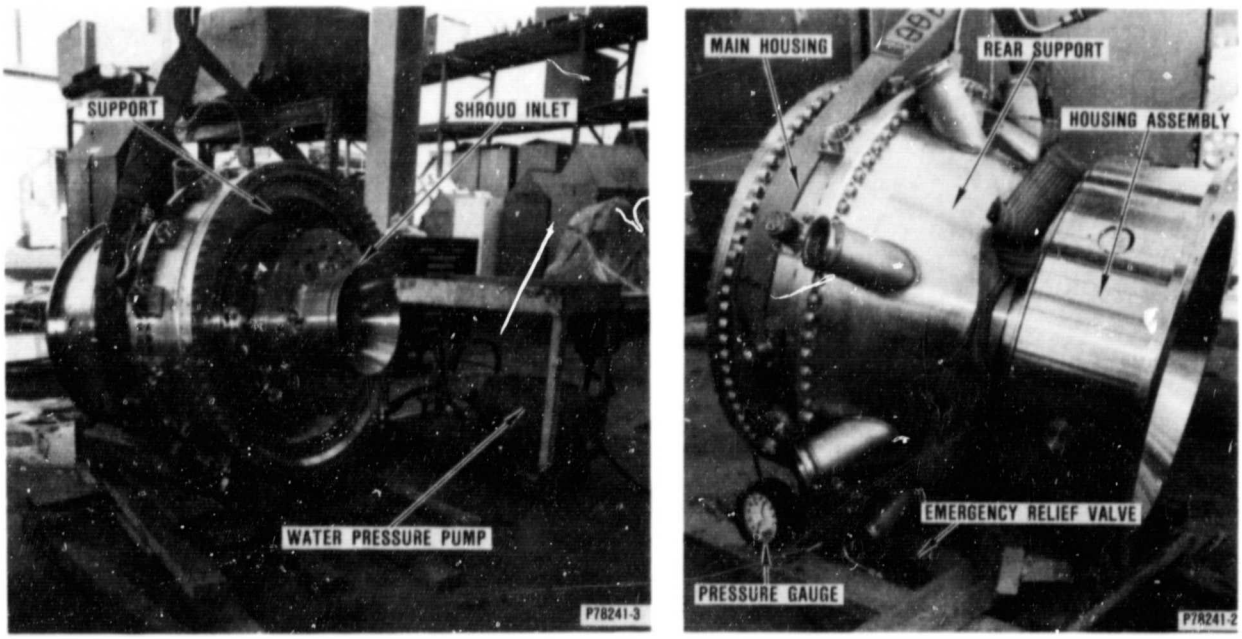

Figure 54. Hydrostatic Pressure Test.

4.2.1 Test Results

The test rig was pressurized with water, and dial indicator readings were recorded at various pressure increments during the hydrostatic pressure test. The tabulated readings for each dial indicator (and their positions) are shown in Table 8. Although some permanent set was recorded by all three dial indicators, a review of the stress-strain relationship for AISI 347 CRES (see Figure 55) showed that none of the components exceeded the 0.2-percent yield stress.

TABLE 8. DIAL INDICATOR READINGS (INCH).

PRESSURE (PSIA)	DIAL INDICATOR LOCATION		
	1	2	3
15	0	0	0
115	0.003	0.001	-0.001
215	0.006	0.002	-0.002
315	0.009	0.0035	-0.003
365	0.0105	0.0045	-0.004
415	0.0130	0.0055	-0.005
435	0.0160	0.0065	-0.006
450	0.0185	0.0073	-0.006
415	0.0180	0.0065	-0.006
315	0.0150	0.0050	-0.006
215	0.0120	0.0035	-0.0025
115	0.0085	0.0020	-0.0010
15	0.0050	0.0005	+0.001

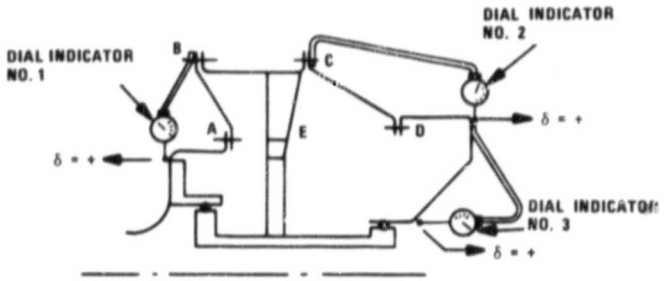

STRUCTURAL SCHEMATIC OF RIG AND DIAL INDICATOR POSITIONS

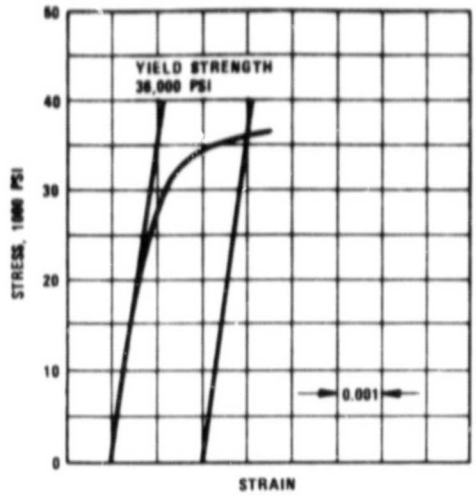

Figure 55. Typical Stress-Strain Curves in Tension for Annealed Stainless Steels of the 300 Series.

The measured deflections versus internal pressure at the three dial indicator locations were plotted. The proportional limit of the component was determined from the point where the deflection/pressure plots became nonlinear. This deflection point was then transferred to the stress/strain curve for the material, giving the stress versus deflection plots (Figures 56, 57, and 58). None of the components exceeded the 0.2-percent yield strength.

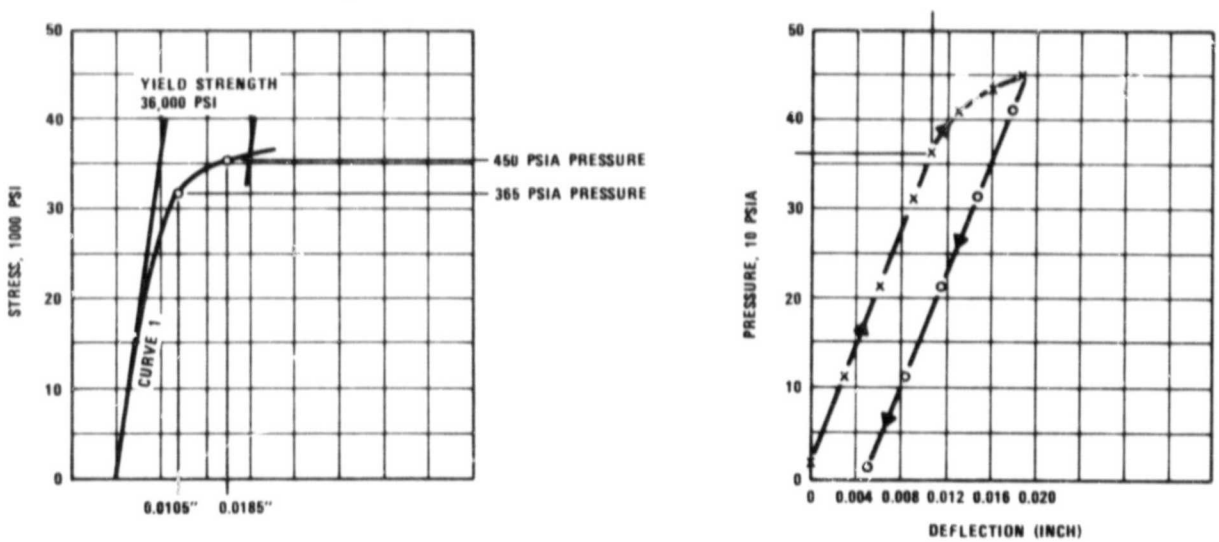

Figure 56. Dial Number 1 Indications for Stress Versus Deflection (left) and Pressure Versus Deflection (right).

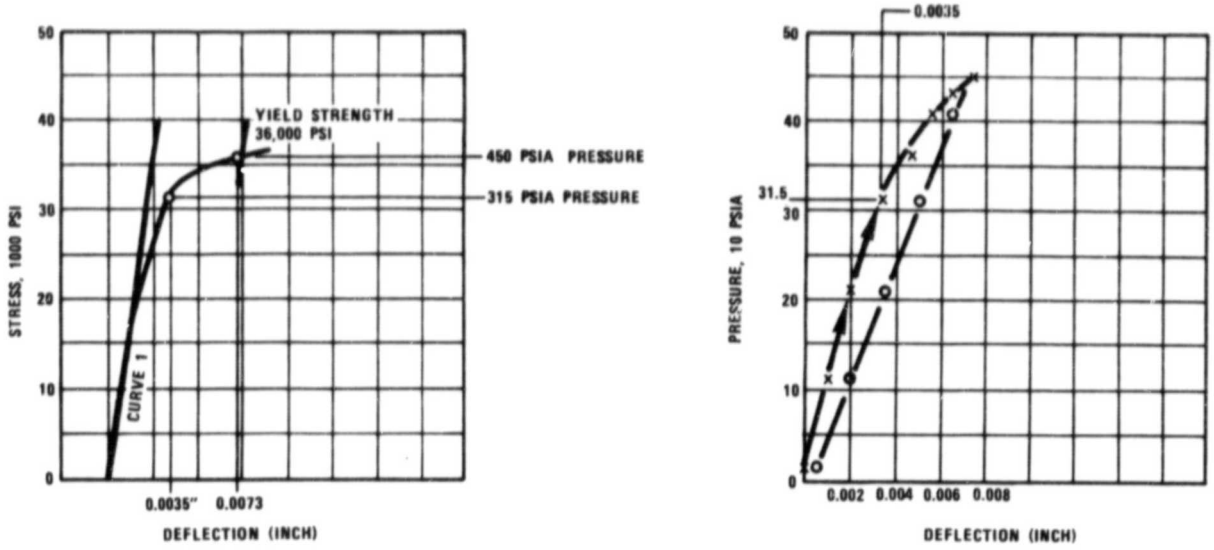

Figure 57. Dial Number 2 Indications for Stress Versus Deflection (left) and Pressure Versus Deflection (right).

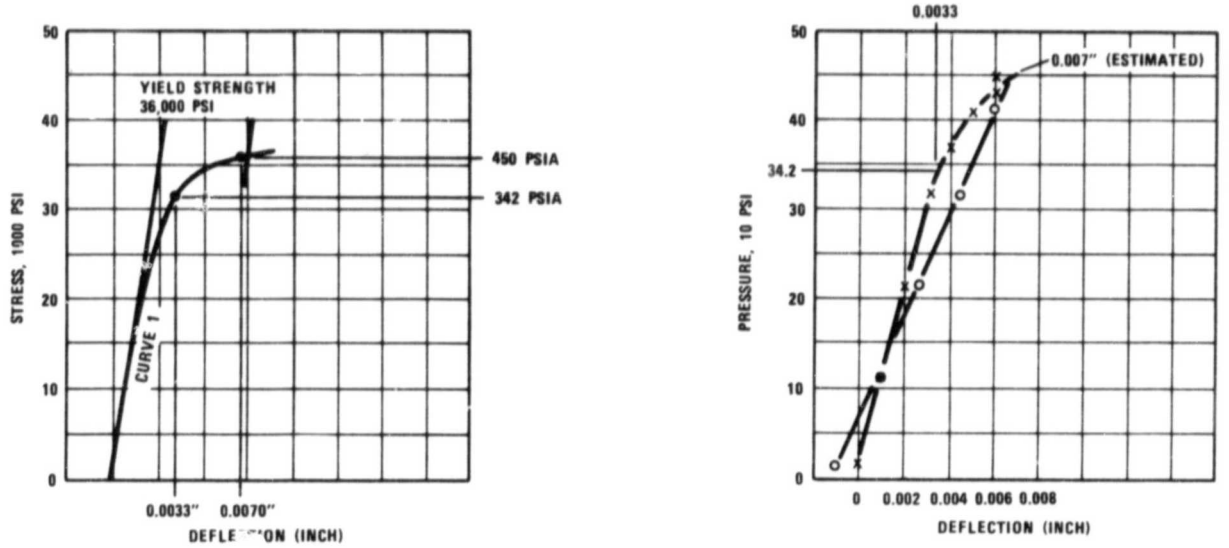

Figure 58. Dial Number 3 Indications for Stress Versus Deflection (left) and Pressure Versus Deflection (right).

After completion of the test, the free length of each bolt (measured prior to the test) was again measured to verify that yielding had not occurred. The comparison of bolt lengths before and after the pressure test are presented in Table 9. All measured bolt strains were substantially below the 0.2-percent yield strain.

TABLE 9. BOLT LENGTHS BEFORE AND AFTER PRESSURE TESTING.

	JOINT A		JOINT B		JOINT C		JOINT D		JOINT E	
BOLT NO.	BEFORE (INCHES)	AFTER (INCHES)	BEFORE (INCHES)	AFTER (INCHES)	BEFORE (INCHES)	AFTER (INCHES)	BEFORE (INCHES)	AFTER (INCHES)	BEFORE (INCHES)	AFTER (INCHES)
1	1.5678	1.5682	2.1342	2.1342	2.1290	2.1293	2.0660	2.0661	4.6289	4.6290
2	1.5649	1.5651	2.1352	2.1352	2.1354	2.1359	2.0680	2.0691	4.6300	4.6298
3	1.5678	1.5679	2.1270	2.1270	2.1298	2.1302	2.0692	2.0698	4.6307	4.6306
4	1.5674	1.5674	2.1334	2.1334	2.1351	2.1352	2.0695	2.0698	4.6293	4.6292
5	1.5650	1.5650	2.1401	2.1401	2.1414	2.1410	2.0683	2.0685	4.6333	4.6298
6	1.5687	1.5688	2.1311	2.1311	2.1386	2.1387	2.0669	2.0671	4.6324	4.6324
7	---	---	---	---	---	---	---	---	4.6324	4.6324
8	---	---	---	---	---	---	---	---	4.6290	4.6291
9	---	---	---	---	---	---	---	---	4.6316	4.6316
10	---	---	---	---	---	---	---	---	4.6324	4.6320

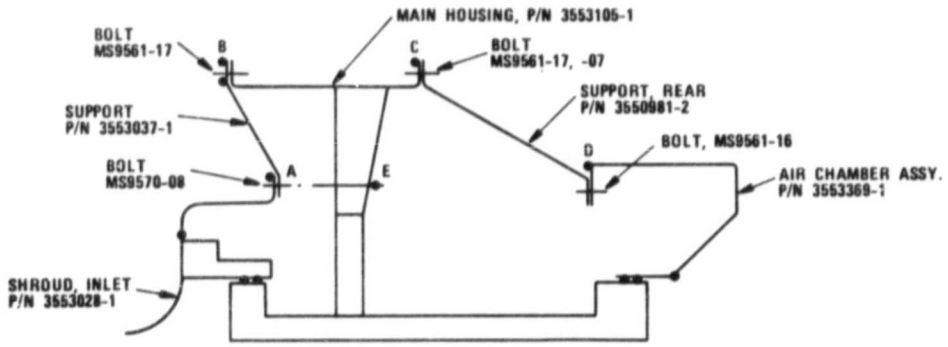

The diameters of all pilot circles were measured for the five pressure-vessel components after completion of the pressure testing. Table 10 compares the measured diameters to the diameters specified on the engineering drawings. The resulting calculated strains were all well below the 0.2-percent yield strain.

4.2.2 Conclusions

The pressure vessel components demonstrated the capability to sustain an internal pressure of 450 psia and all test objectives were successfully met.

- Stress levels in all pressure vessel components remained below their 0.2-percent yield strength at an internal pressure of 450 psia.
- At pressures up to 300 psia, all component stress levels remained below their elastic limit, ensuring that no permanent deformation would result from operating at pressures of 300 psia or less.

TABLE 10. MEASURED PILOT DIAMETERS OF PRESSURE VESSEL COMPONENTS AFTER PRESSURE TESTING.

Part Number	Pilot Dia. Location	Post-Test Dia. (Inches)	Specified Dia. (Inches)	Permanent Strain (IN./IN.)
3553369-1	Joint "D"	21.920	21.914/21.919	0.00027/0.00005
3553028	Joint "A"	18.915	18.912/18.914	0.00016/0.00005
3553037	Joint "B"	32.510	32.501/32.504	0.00027/0.00018
	Joint "A"	18.913	18.912/18.914	+0.00005
3553105	Joint "B"	32.505	32.501/32.504	0.00012/0.00003
	Joint "C"	32.498	32.497/32.500	0.00003/0.0000
3550981	Joint "C"	32.495	32.501/32.504	0.0000
	Joint "D"	21.912	21.910/21.915	0.00009/0.0000

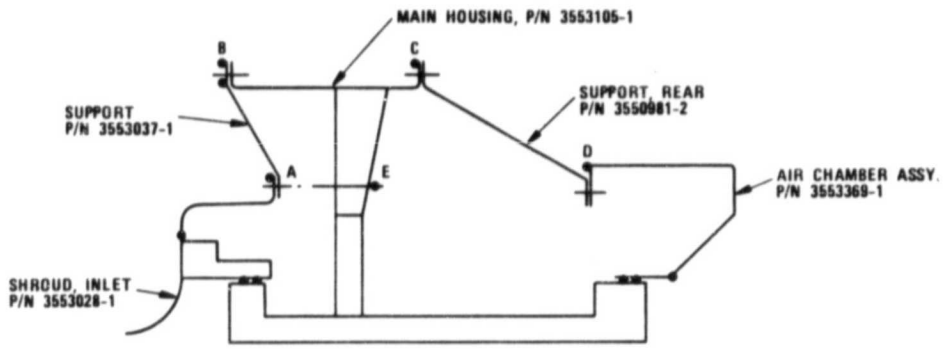

- The support retained a permanent deformation of 0.005 inch in the axial direction (outer flange relative to inner flange) after completion of the pressure test. However, the 0.2-percent yield stress was not exceeded.*

4.3 Impeller Inspection and Holography

The impeller (Figure 59) was inspected against the tooling and layout drawings on a sideview comparator. The inspection showed that the contour and thickness of the exit region of the main and splitter blades was excellent. However, three areas along the

*The permanent set occurred because the stress-strain relationship for austenitic stainless steels (all test components were AISI 347 CRES) departs from proportionality at relatively low values of stress and there is no sharp yield point. It is standard practice, therefore, to determine the yield strength at 0.2-percent offset on the stress-strain curve. This value lies considerably higher than the proportional limit.

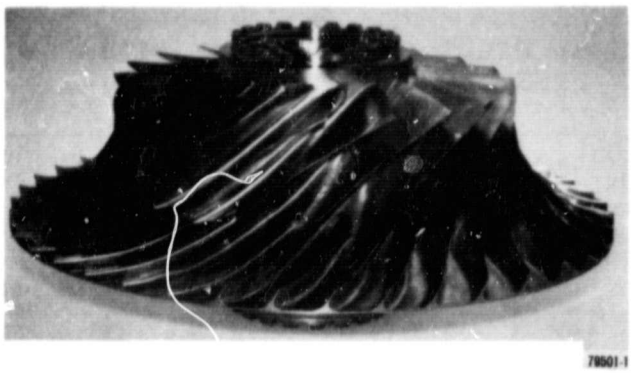

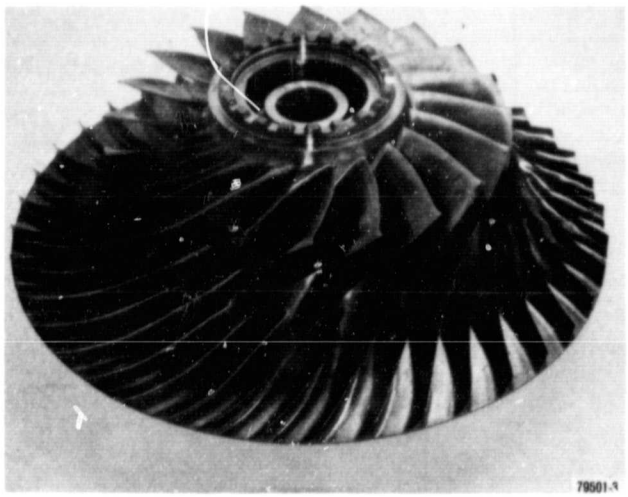

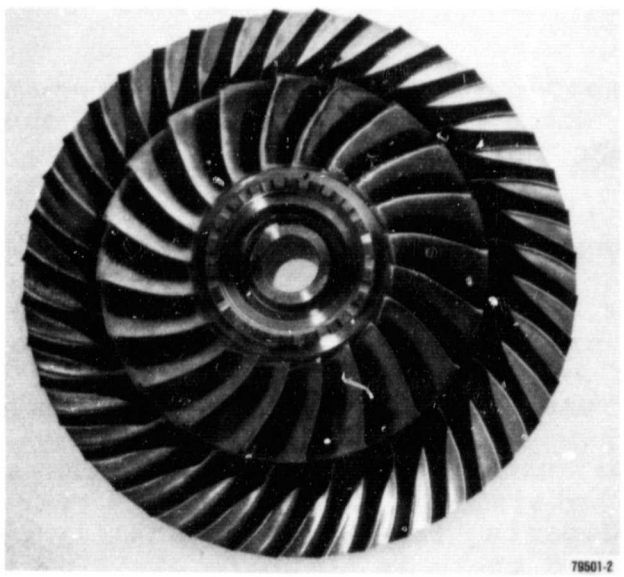

Figure 59. NASA Scaled Impeller.

shroud line -- i.e., the main-blade inducer, splitter-blade inducer, and main blade immediately downstream of the "knee" region -- had excessive blade thickness. These areas were restored to blueprint dimensions by handfinishing the extra material. Inducer throat measurements were taken at three different radii, as shown in Table 11.

Following this inspection, holography was performed to determine the impeller's exact vibratory characteristics. The frequencies investigated ranged from 0 to 15,000 Hz for the full blade and splitter and from 0 to 12,000 Hz for the backplate. (During testing, all blades were damped out except the blade under examination.)

TABLE 11. INDUCER THROAT MEASUREMENTS.

THROAT	RADIUS		
	4.075 (INCH)	3.32 (INCH)	2.715 (INCH)
1	0.607	0.543	0.429
2	0.605	0.544	0.425
3	0.606	0.544	0.427
4	0.604	0.543	0.430
5	0.606	0.538	0.430
6	0.604	0.537	0.432
7	0.604	0.542	0.429
8	0.603	0.544	0.435
9	0.601	0.539	0.429
10	0.602	0.541	0.427
11	0.599	0.537	0.420
12	0.602	0.542	0.429
13	0.604	0.540	0.430
14	0.604	0.547	0.432
15	0.603	0.545	0.431
16	0.604	0.547	0.428
17	0.602	0.545	0.427
18	0.605	0.545	0.432
19	0.603	0.543	0.432
20	0.604	0.545	0.431
AVG	0.6036	0.5426	0.429
σ_N	0.0018	0.0030	0.003
MAX-MIN	0.007	0.010	0.015
(MAX-AVG)/AVG	0.004	0.008	0.014
(MIN-AVG)/AVG	-0.008	-0.010	-0.021

Computer Program "ISOVIB" had been used to predict vibratory frequencies of the blade and splitter. The holographic results compared favorably, as follows:

Mode	ISOVIB Prediction (380°F, 36,366 rpm), Hz	ISOVIB Prediction (380°F, 0 rpm), Hz	ISOVIB Prediction (70°F, 0 rpm), Hz	Holography Results (70°F, 0 rpm), Hz
1	2416	2072	2175	2145
2	3980	3720	3906	3971
3	4782	4493	4718	4860
4	5531	5135	5391	5326
5	6211	5903	6198	6601

The first four modes predicted for 0-rpm speed and 380°F temperature were within 5 percent of the measured values. This was expected due to the lower modulus at 380°F (relative to the 70°F-temperature at which the holographic testing was performed). The corresponding computer-generated Campbell diagram for the full blade is presented in Figure 60.

Furthermore, as illustrated in Figure 61 for measured frequencies of the full blade and splitter, 100-percent-speed interference points for the first three modes were found to be 3.9/rev, 6.56/rev, and 7.9/rev. (100-percent-speed points were chosen to be the same as 0-speed points). Figure 62 compares the photographed mode shapes and frequencies to those predicted.

Holographic testing also verified computer program "DABLE's" calculation of backplate vibratory frequencies, as follows:

Nodal Diametric	Vibratory Frequencies, Hz	
	Predicted (70°F, 0 rpm)	Measured (70°F, 0 rpm)
Umbrella		4333
2	3736	3827
3	4083	4146
4	4384	4393
5	4734	4697
6	5174	4757
7	5713	
8	6348	6247
9	7069	6931
10	7866	7975
11	8729	8023

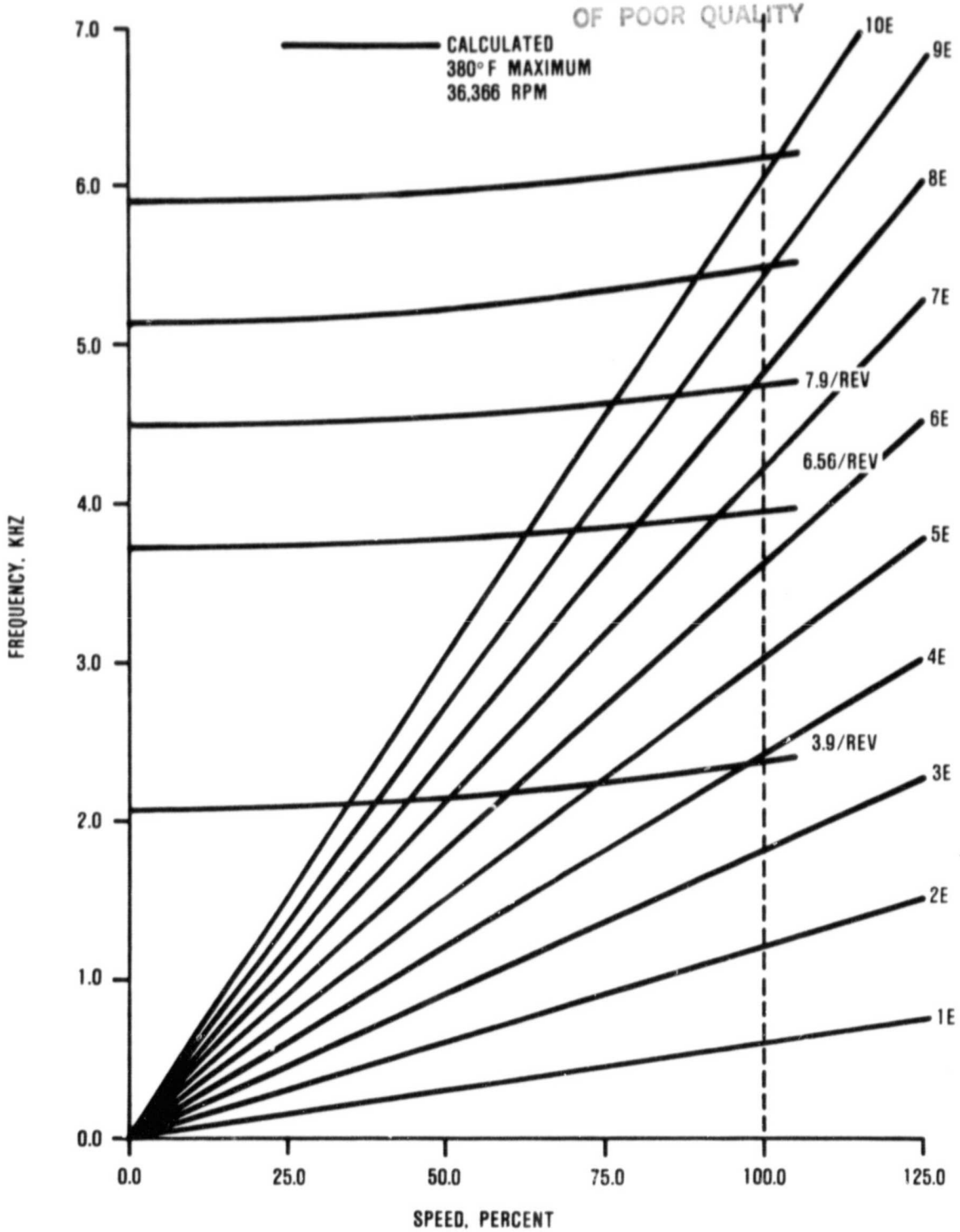

Figure 60. Campbell Diagram for Full Blade and Splitter.

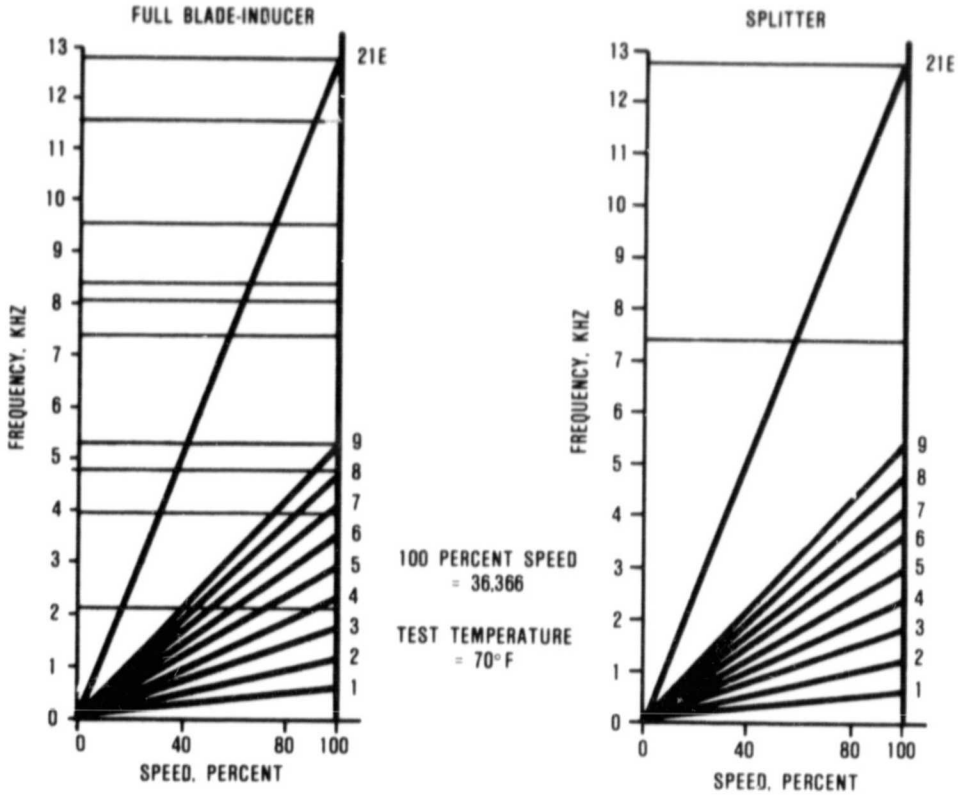

Figure 61. Holographic Results for NASA Scaled Impeller.

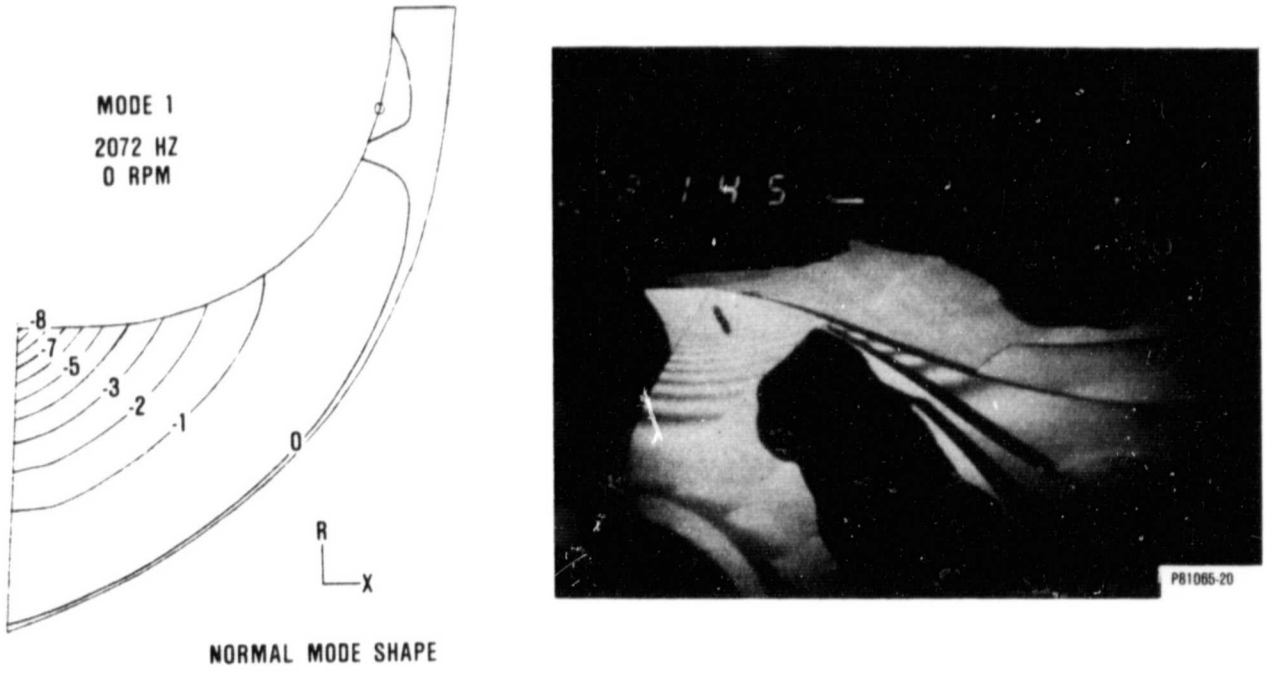

Figure 62. Comparison of Predicted Mode Shapes to Holography Photographs (Sheet 1 of 3).

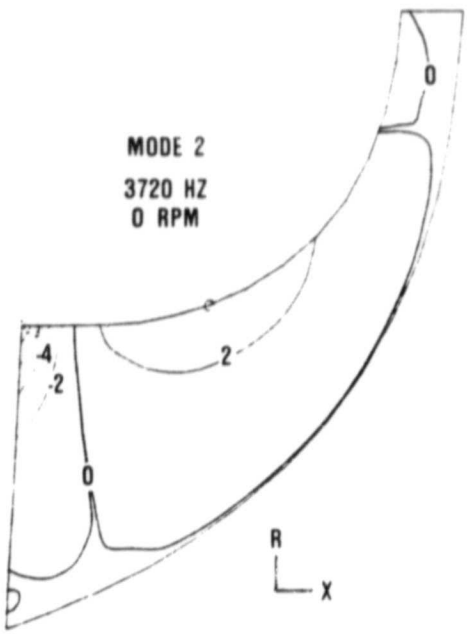

NORMAL MODE SHAPE

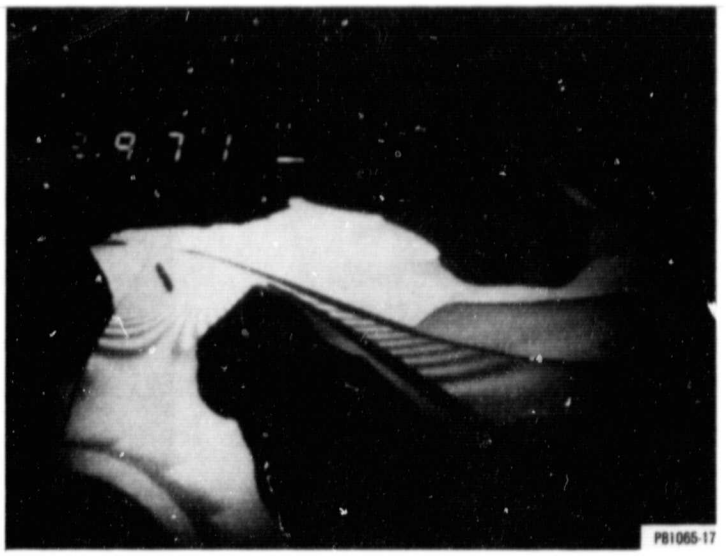

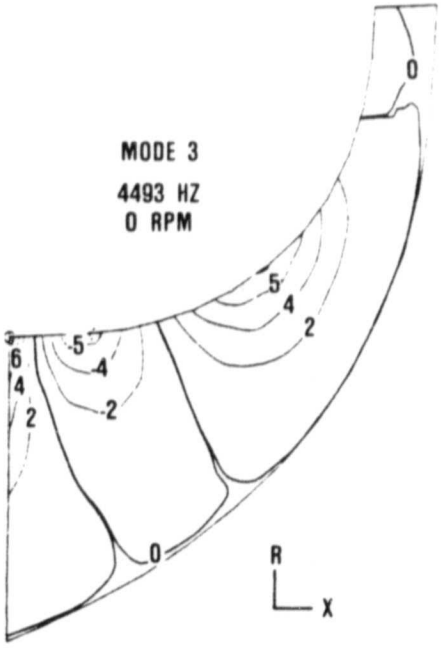

NORMAL MODE SHAPE

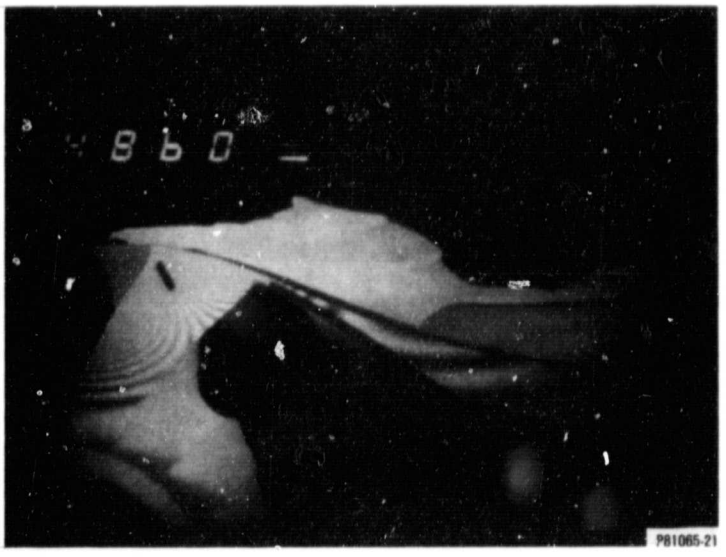

Figure 62. Comparison of Predicted Mode Shapes to Holography Photographs (Sheet 2 of 3).

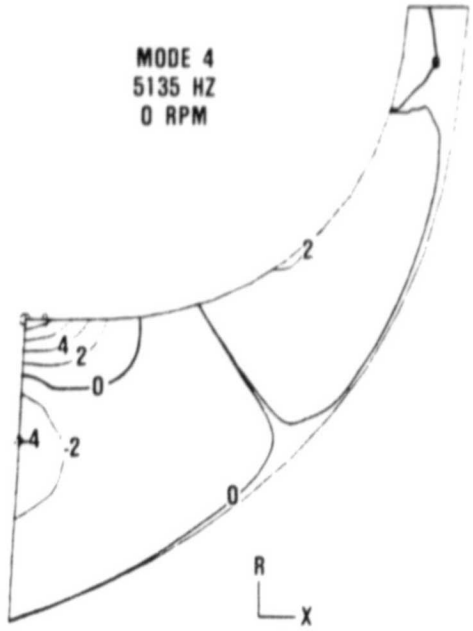

NORMAL MODE SHAPE

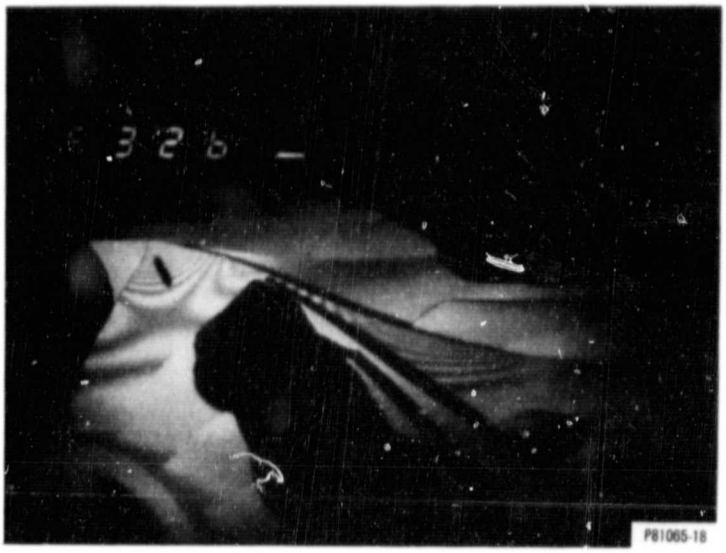

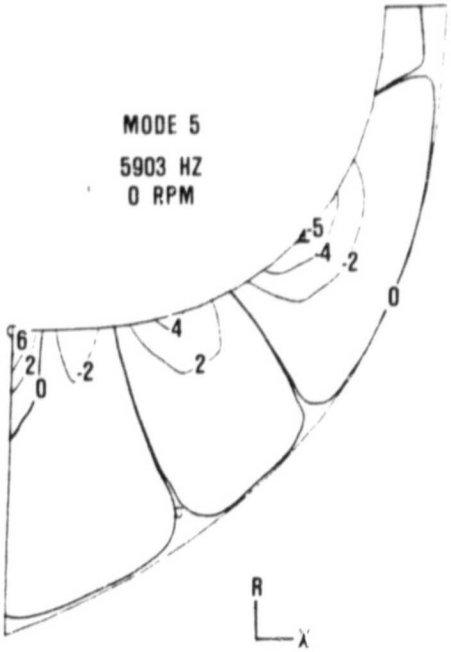

NORMAL MODE SHAPE

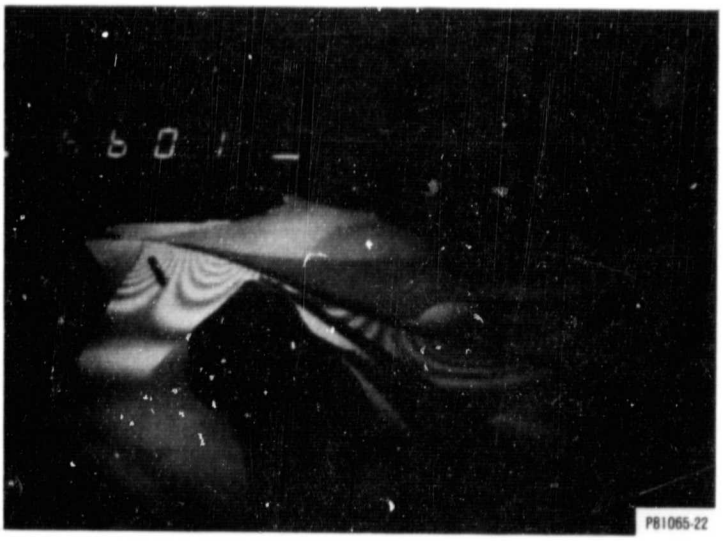

Figure 62. Comparison of Predicted Mode Shapes to Holography Photographs (Sheet 3 of 3).

These values are also plotted on the interference diagram, Figure 63; and Figure 64 shows the backplate modes excited during holography. As shown in Figure 64, the backplate has a 28-percent frequency margin above 100-percent speed; this margin is sufficient to prevent blade/disk coupling within the operated range.

The major impact of the holographic testing was to confirm a predicted strong tendency for 4/rev excitation. (Accordingly, the rig had not been designed with four, evenly spaced inlet struts or instrumentation probes near the inlet.) Holography also indicated possible 21/rev interference excited by the wake from the diffuser vanes; however, the tendency of a centrifugal compressor to stiffen could not be accounted for in the holographic testing and should push this frequency above the 21/rev interference point.

4.4 Diffuser Inspection

Figure 65 illustrates the inspection criteria for the diffuser. All 42 passage throat widths were measured, as summarized in Table 12. Polar plots of the individual throat width variation

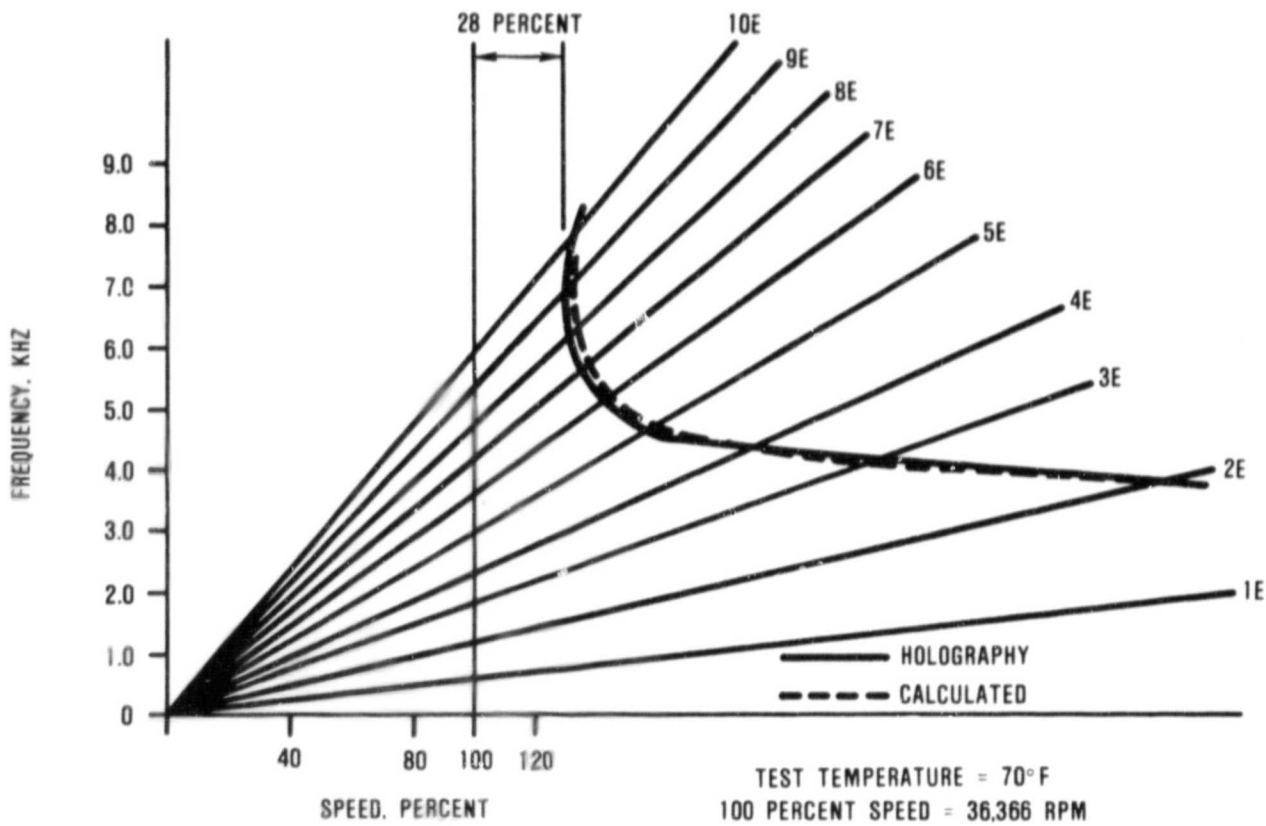

Figure 63. Backplate Holography Results for NASA Impeller.

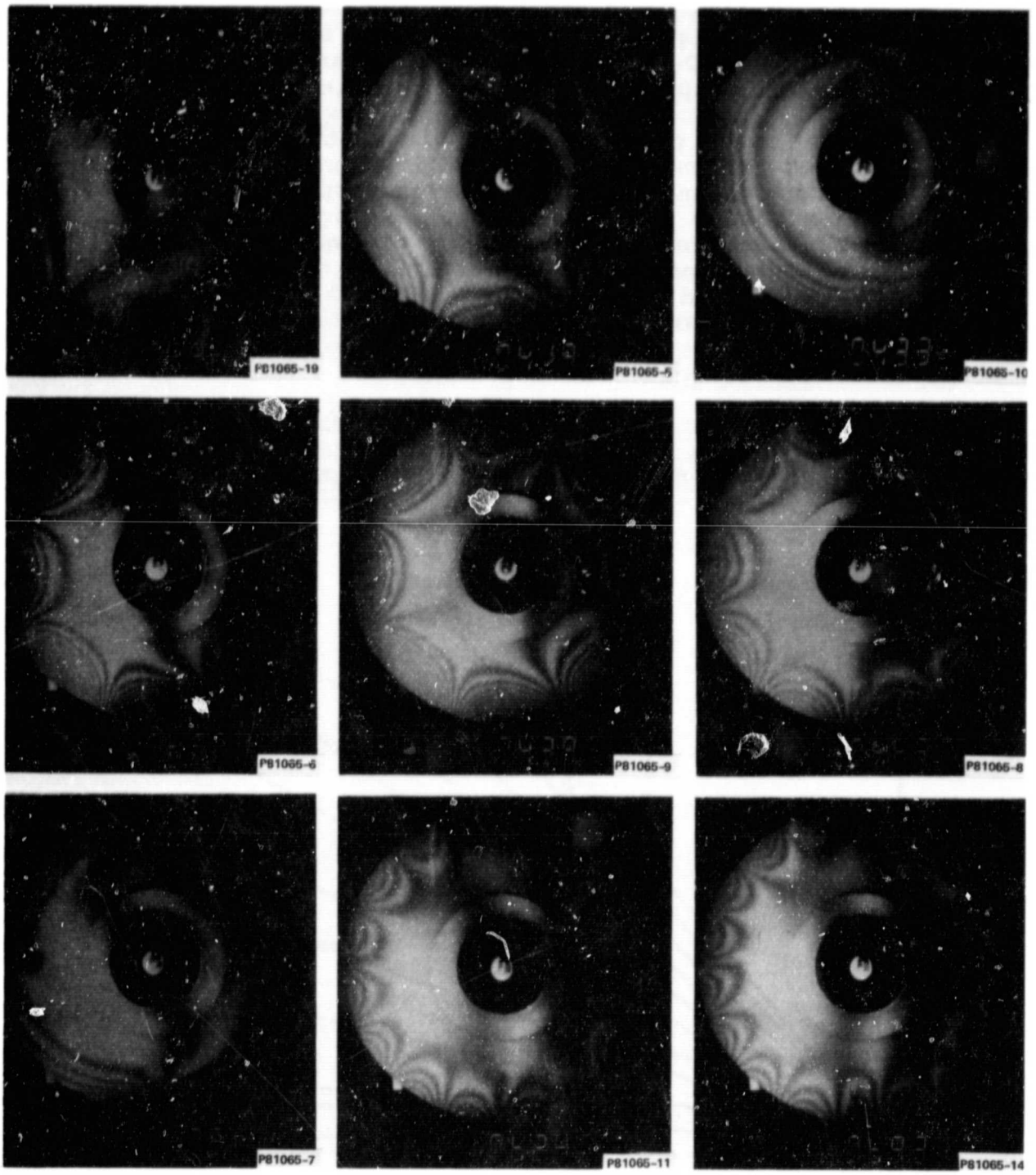

Figure 64. Disk Backplate Holography Results for NASA Impeller (Sheet 1 of 2).

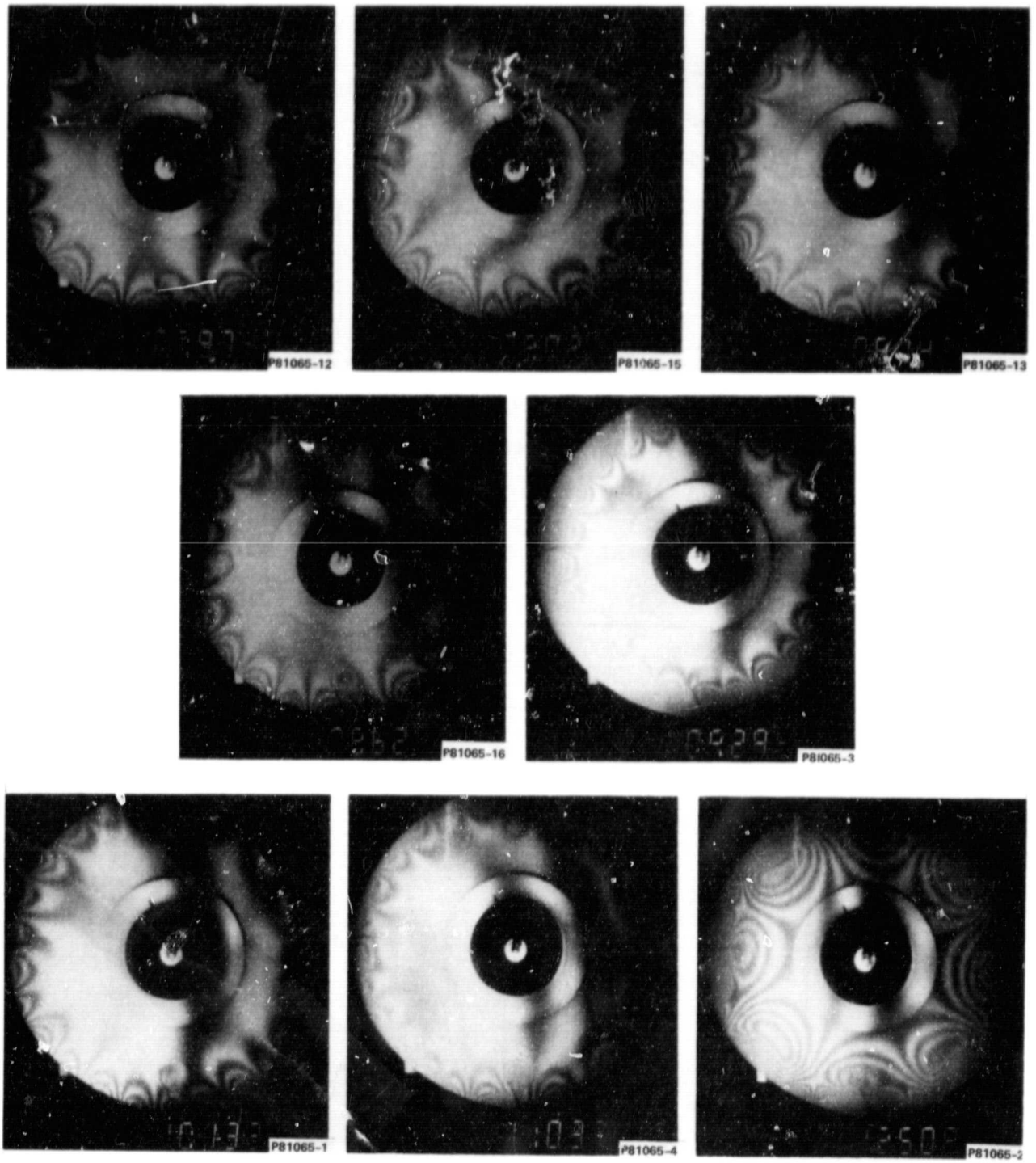

Figure 64. Disk Backplate Holography Results for NASA Impeller (Sheet 2 of 2).

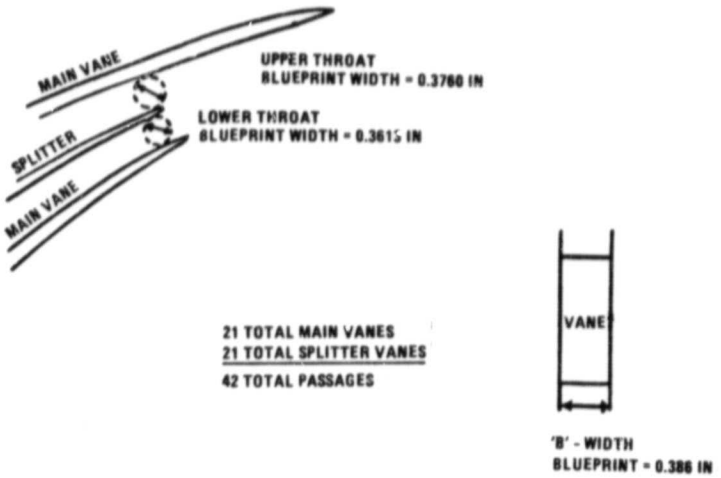

Figure 65. Vane Diffuser Throat Area.

TABLE 12. SUMMARY OF MEASURED THROAT WIDTHS.

UPPER (BLUEPRINT = 0.3670")		LOWER (BLUEPRINT = 0.3613")	
PASSAGE	DIAMETER	PASSAGE	DIAMETER
2	.372	1	.353
4	.370	3	.361
6	.372	5	.369
8	.371	7	.362
10	.377	9	.366
12	.366	11	.362
14	.373	13	.358
16	.368	15	.360
18	.376	17	.366
20	.377	19	.355
22	.369	21	.361
24	.376	23	.358
26	.372	25	.361
28	.378	27	.356
30	.375	29	.357
32	.377	31	.365
34	.382	33	.354
36	.378	35	.358
38	.378	37	.355
40	.369	39	.360
42	.372	41	.357

and total throat width variation are shown in Figure 66. A summary of diffuser measurement averages and variations is presented in Table 13. The diffuser was well within production hardware tolerance and acceptable for testing.

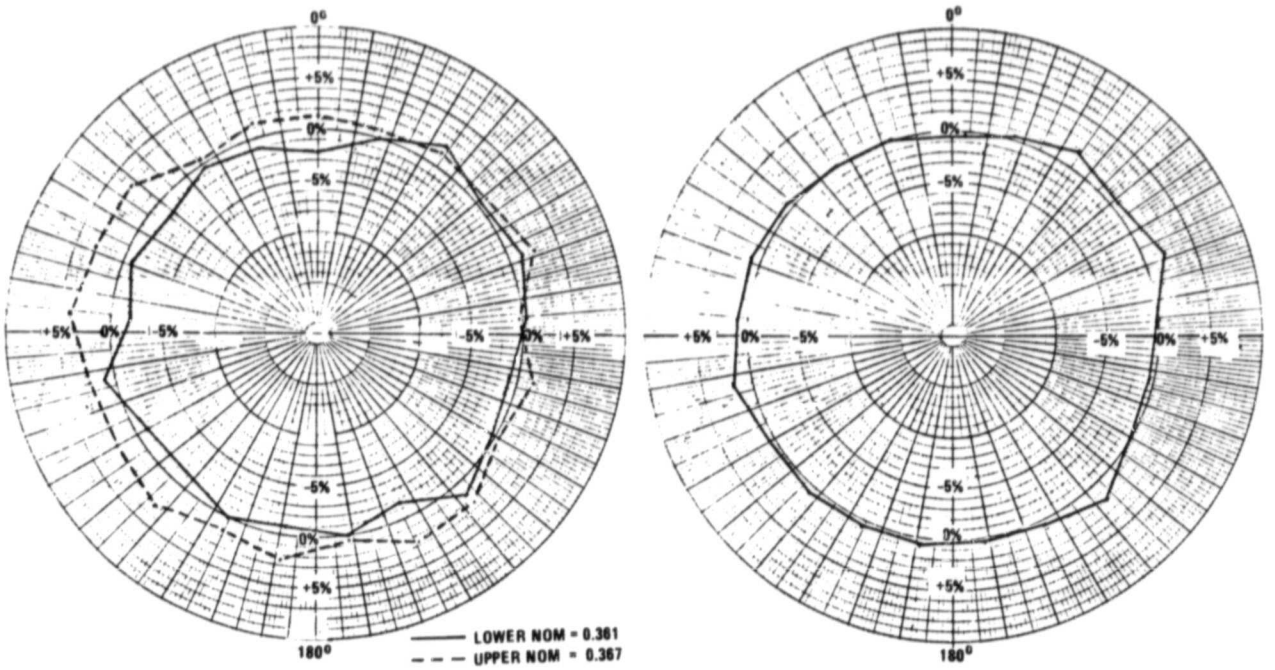

Figure 66. NASA 10-Lb/Sec Diffuser Total Throat Width Variation.

TABLE 13. MEASUREMENT AVERAGES AND VARIATIONS.

UPPER THROAT WIDTH		LOWER THROAT WIDTH	
NOMINAL	.367 (DESIGN)	NOMINAL	.361 (DESIGN)
AVERAGE	.3737	AVERAGE	.3597
MAXIMUM	.382	MAXIMUM	.369
MINIMUM	.366	MINIMUM	.353
STANDARD DEVIATION	.0040	STANDARD DEVIATION	.0042
AREA UPPER / AREA NOMINAL	1.008	AREA LOWER / AREA NOMINAL	.9860

"B"- WIDTH - NOMINAL = .386 (DESIGN)
AVG = .382 ± .001

TOTAL THROAT AREA / DESIGN THROAT AREA = .997

MAXIMUM 2θ = 7.26°	MAXIMUM 2θ = 4.51°
MINIMUM 2θ = 6.44°	MINIMUM 2θ = 3.90°
NOMINAL 2θ = 6.70° (DESIGN)	NOMINAL 2θ = 4.37° (DESIGN)

4.5 Rotating Group Runout and Check Balance

The rotating group was assembled for runout measurements and a check balance. The assembly was set up on the forward roller-bearing and aft ball-bearing surfaces for a runout check. The results are shown in Figure 67.

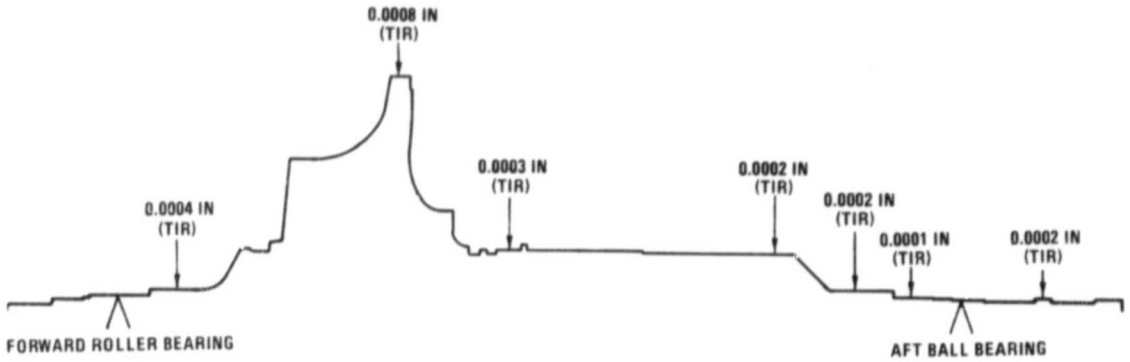

Figure 67. Rotating Group Run-Outs.

The assembly was then set up in a balance machine, again on the bearing surfaces, for a two-plane dynamic balance check. The rotating group weight is 40.3 lbs, and the center of gravity is 6.55-inches aft of the forward roller bearing. The total combined unbalanced limit is 0.129 in-oz (assuming an eccentricity of 0.0002 inch). The allowable unbalance limits are 0.0889 in-oz for the forward roller-bearing plane and 0.0401 in-oz for the aft ball bearing plane. Figure 68 shows that the results of the check-balance were well within the specified limits.

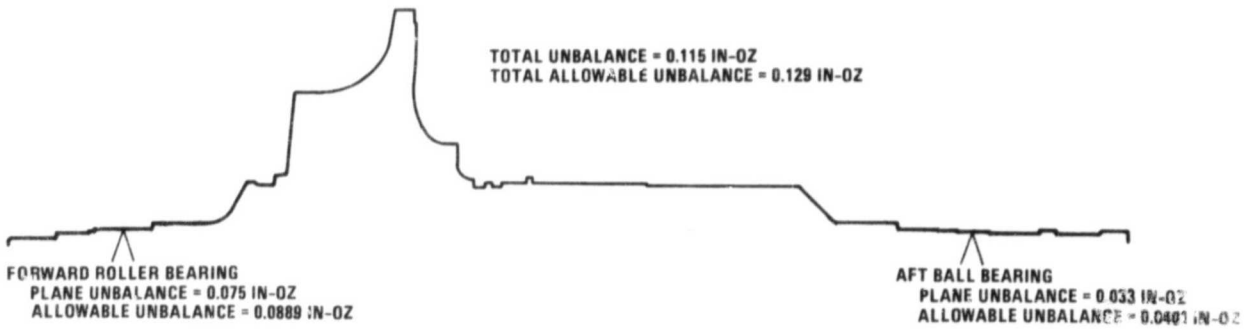

Figure 68. Rotating Group Check Balance.

4.6 Collector/Throttle-Valve

The collector and throttle valve were assembled in accordance with Drawing 3553131. The collector was pictured previously in Figure 42, and the throttle-valve stationary housing assembly (with the air passages "blanked off") was shown in previous Figure 54. The other main parts in the collector/throttle-valve assembly were the throttle valve itself -- an outer ring that rotates on bearings around the stationary housing -- and a screw assembly (operated by an electrically driven actuator motor) that controls flow by aligning the throttle valve slots with respect to the holes in the stationary housing. The wide-open choked flow rates and plenum leakage flows with the throttle valve fully closed are shown in Figure 69.

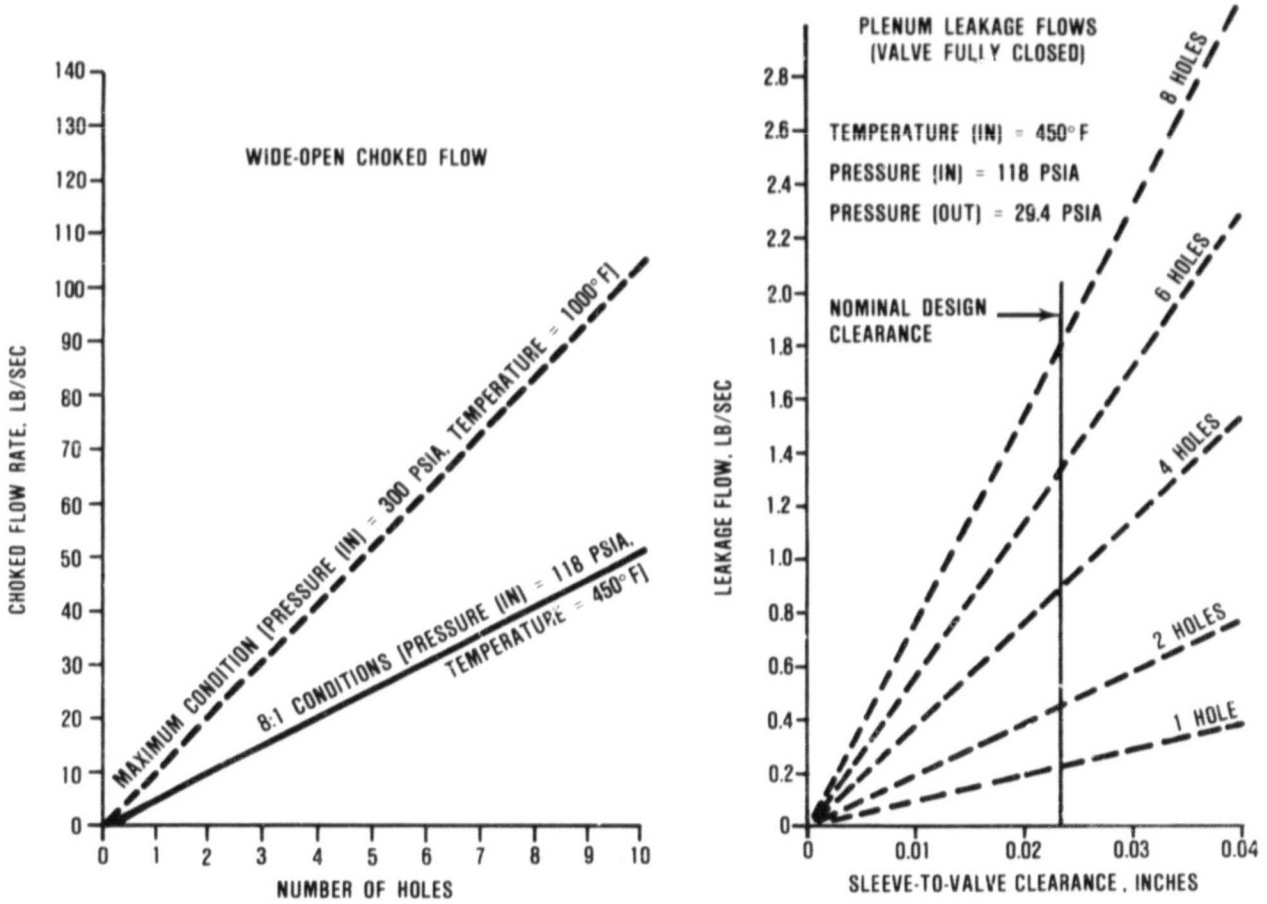

Figure 69. Flow Versus Number of Holes in the Throttle Valve.

The collector assembly was subjected to a thermal cycle test to verify predicted centerline growth and actuator operation. The test setup consisted of blank-off plates, an input line for hot air, cooling water lines, tooling for measuring thermal growth, and thermocouples to measure air temperature, water temperature, and collector leg temperatures at various locations. The test setup is shown in Figure 70.

The capacity of the hot-air supply was limited to approximately 700°F. Thermal growth data was recorded for different cooling-water flows, and data is presented in Table 14. [It should be noted that the thermocouples (T_1-T_6) were biased by periodic shade or sun effects due to overhead obstructions.] The vertical deflection for the design cooling-water flow is plotted against the predicted thermal growth in Figure 71.

A post-test inspection revealed several problems with the throttle valve assembly (Figure 72). At peak temperature, there was interference at the interface of the shaft and yoke; as a result, the yoke was modified. Several bearings failed due to excessive radial loading caused by the stationary housing thermally expanding quicker than the throttle valve; the outside diameter of the stationary housing was modified to increase the housing-to-bearing clearance. Interference between the actuator guide and the two actuator antirotation clevis was noted; dry-lubrication was applied to the interfacing surfaces to eliminate this problem. Finally, a very light lubricating oil that had been applied to the link shaft during assembly became coked and caused interference during high-temperature operation; this surface was cleaned and dried.

Following modification, the collector/throttle valve assembly was assembled with all new bearings. It was then connected to an improved hot-air source, and mechnical operation through the entire actuator stroke was verified at air temperatures up to 800°F. A post-test inspection revealed no other problems.

4.7 Test Rig Mechanical Check-Run

After all components were checked for proper operation, the compressor test rig was installed in a GTEC compressor test cell. Figure 73 shows the installation. A facility plenum was used to collect the thrust-balance exhaust air. Only instrumentation necessary for rig protection or data-point verification was hooked-up. Roller- and thrust-bearing temperatures were monitored, as were respective oil-in and oil-out temperatures; and thrust-balance load was measured for the thrust bearing. In addition, the following instrumentation was used:

- External accelerometers
- Radial clearance probes

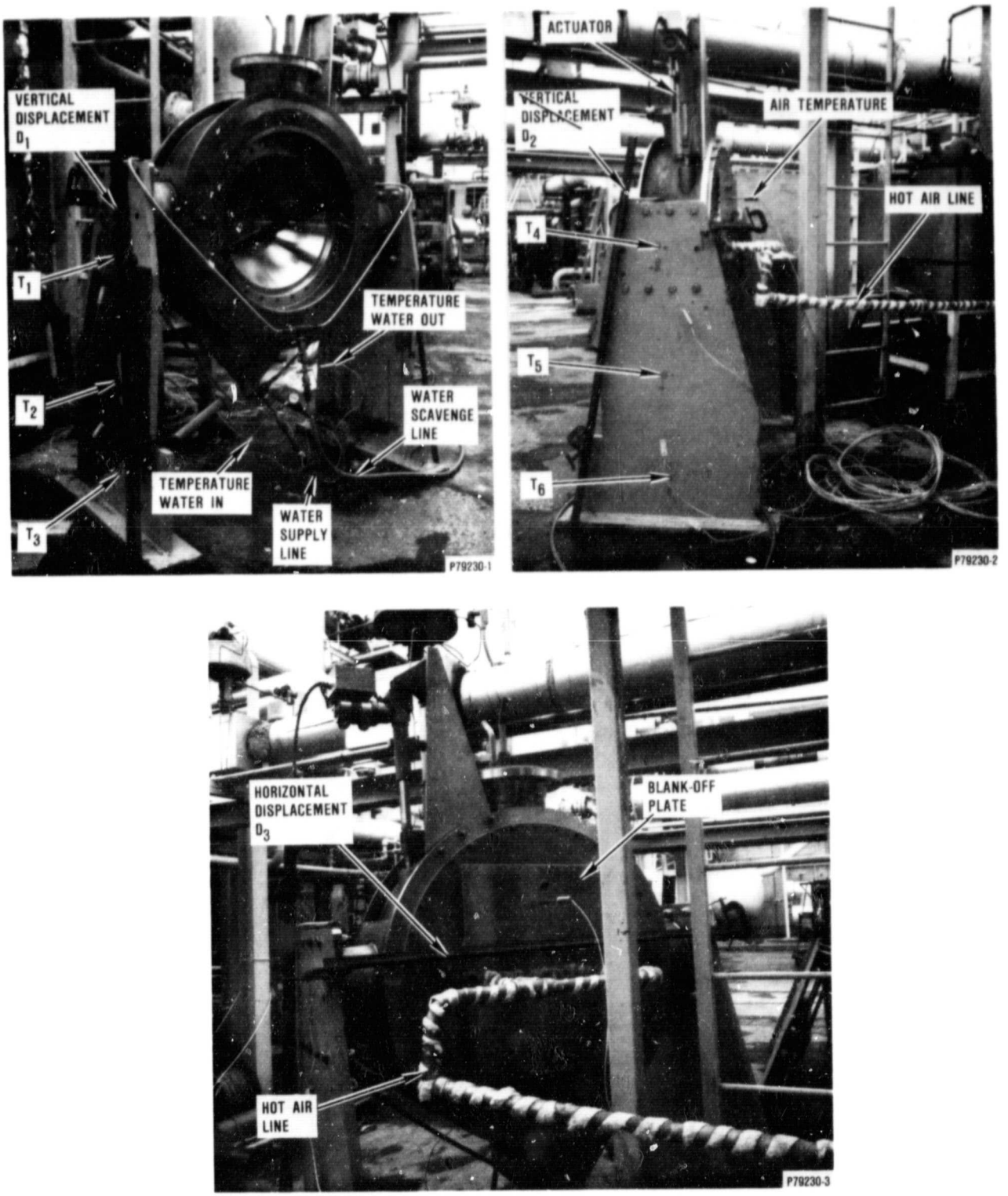

Figure 70. Collector Thermal Test Setup.

TABLE 14. COLLECTOR THERMAL GROWTH DATA.

	Total Cooling Water Flow		
	2 GPM	1 GPM	0.5 GPM
Collector Leg Temperature (°F)			
T_1	93	100	105
T_2	107	118	126
T_3	99	109	113
T_4	100	98	100
T_5	113	114	119
T_6	108	110	111
Air Temperature (°F)	663	688	690
Vertical Thermal Growth (inches)			
D_1	0.007	0.0075	0.017
D_2	0.007	0.009	0.014
Horizontal Thermal Growth (inches)			
D_3	0.086	0.091	0.097
Temperature Cooling Water (°F)			
In	80	75	85
Out	80	80	90

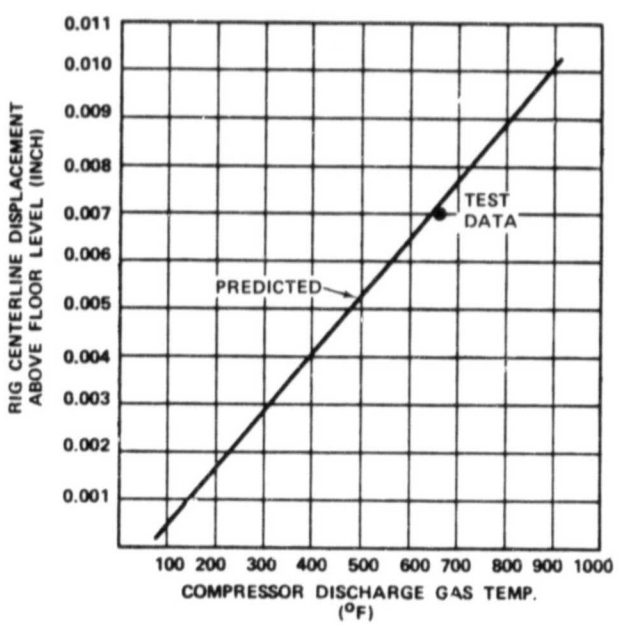

Figure 71. Test Rig Vertical Thermal Growth.

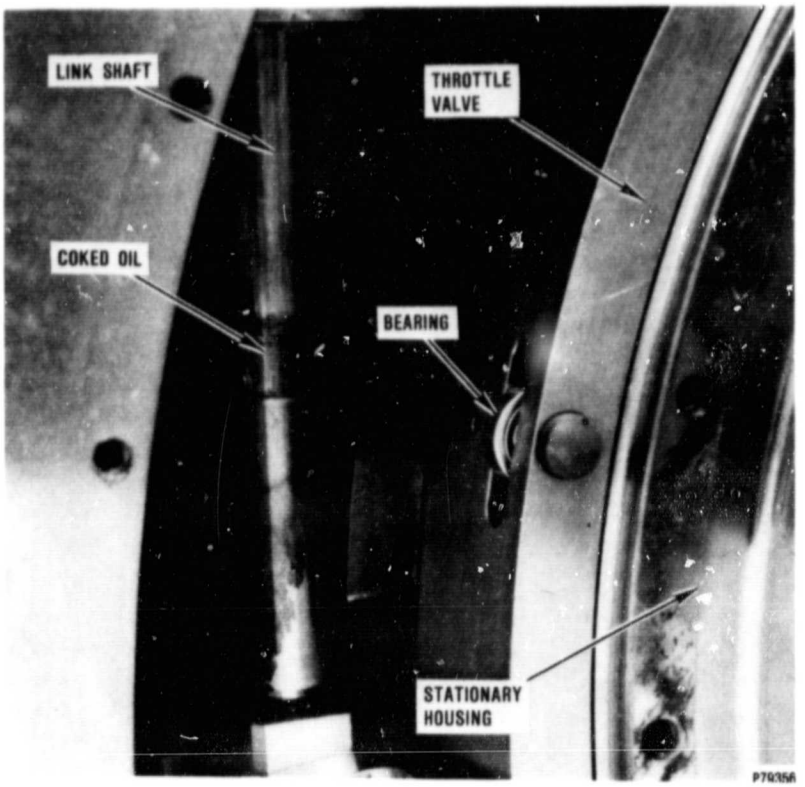

Figure 72. Throttle Valve Assembly.

- Axial clearance probes
- Impeller backface clearance probes
- Bentley probes.

Instrumentation was connected to a computer system used for recording "scans" and establishing data points. The system contained reference pressures and temperatures to ensure accurate data collection. In addition, two eight-channel strip charts and a 14-channel tape recorder were necessary to record various data.

After the test rig was installed and the instrumentation hooked up, a vacuum check and pressure check were accomplished to verify proper operation of the instrumentation and to check for leaks. The test rig was pressurized to 10 psi and a computer scan was taken to verify operation of connected static pressures. Flanges and instrumentation lead-outs were checked for leaks. And a vacuum of -2 in. Hg was applied to the test rig to double check the operation of connected static pressures.

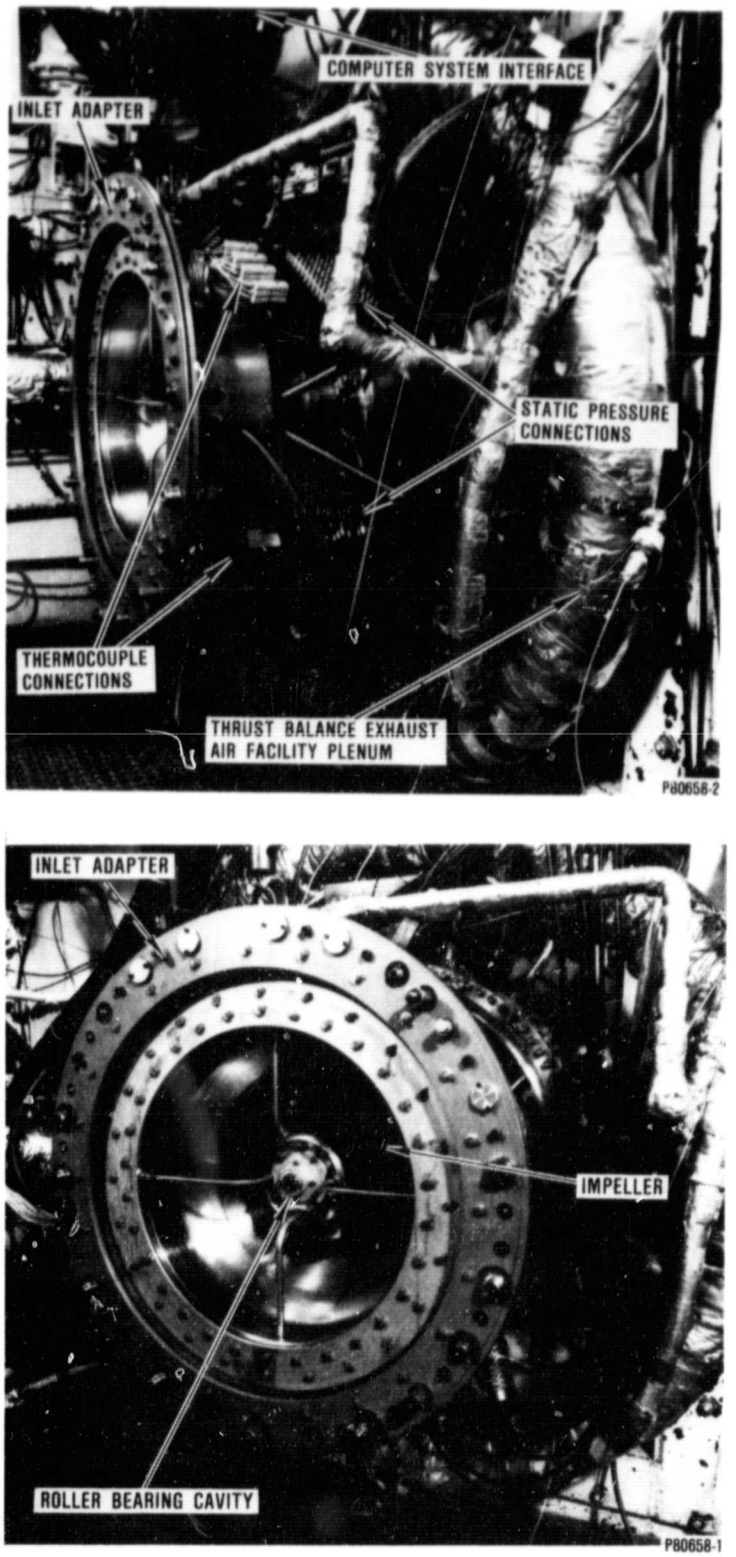

Figure 73. NASA Test Rig Installation.

4.7.1 Test Procedure

NASA personnel arrived at Garrett after the test cell installation was complete. Final test rig assembly procedures and test cell installation procedures were discussed in detail.

A test sequence for the mechanical check-run was jointly developed by Garrett and NASA personnel. This test sequence was designed to verify proper test-rig mechanical operation with minimum risk to test-rig hardware. The procedure below was followed to verify mechanical operation of the test rig.

(a) Prior to slow roll, all instrumentation (including clearance probes, compressor vibration, load measurement, and strain gages) was checked for proper connection and calibration. The rotating group was moved aft by two to three turns to ensure axial clearance. Discharge valve "open," recording instrumentation "on," oil flow, cooling air flow, and thrust-balance air-flow capability were verified.

(b) During slow roll, operation of the clearance-control spindle was verified; and a 0.035-inch minimum axial impeller clearance was established. Furthermore, it was verified that Wayne-Kerr probes indicated adequate clearance (0.020+ inch). Then when speed stabilized, all manual and scan data were recorded and proper instrumentation operation was verified.

(c) The rig was then accelerated to the 8,000-10,000-rpm range, while 0.035-inch minimum axial impeller clearance was maintained. When speed stabilized, manual and scan data were recorded and proper instrumentation operation was verified. (Maximum allowable vibration during steady-state operation was 0.5 mil.)

(d) The rig was then accelerated to 20,000 rpm, again maintaining 0.035-inch minimum axial impeller clearance. When speed stabilized, manual and scan data were recorded. (Maximum allowable vibration during steady-state operation is 0.3 mil; and the allowable range for operating thrust is 500-1200 lbs.)

(e) The rig was then successively accelerated to 25,000 rpm, 30,000 rpm, 36,366 rpm (100 percent), and 38,200 rpm (105 percent), adhering to the same procedure as (d) above.

(f) The rig was then slowly decelerated to 36,366 rpm, at which time axial impeller clearance was decreased to 0.009 inch (design clearance). When speed stabilized, manual and scan data were recorded. (Maximum allowable

vibration during steady-state operation is 0.3 mil; and the allowable range for operating thrust is 500-1200 lbs.) Axial impeller clearance was then increased to 0.035 inch.

(g) The rig was then slowly decelerated first to 30,000 rpm, then to 20,000 rpm. At each speed, data was recorded when rig speed stabilized. [0.035-inch clearance was maintained, as were the vibration and thrust range noted in (f) above.]

(h) Prior to shutdown, maximum cooling air was turned on, and thrust-balance air was turned off.

(i) After shutdown and roll down, manual and scan data were recorded, cooling air and oil were left on for one-half hour minimum, and the rig was checked for obvious oil leaks.

After completion of the check-out procedure, the test rig was restarted and throttled from choke to surge at 80- and 100-percent speeds, simulating performance speed lines. For the surge points, the impeller-to-shroud clearance was increased to 0.018-inch minimum for safety. Computer scans were taken at various points along the speed lines and the data transmitted to NASA personnel. Computer scans for compressor choke flow were recorded at 60-, 70-, and 90-percent speeds.

Several test-rig operational characteristics were also established. The axial clearance was moved from a minimum of 0.009 inch to a maximum of 0.035 inch at 100-percent speed to verify proper operation of the clearance-control spindle. The axial clearance was also adjusted at all other speed points. The clearance-control spindle responded as expected and without incident.

At NASA's request, an emergency shutdown was accomplished from 100-percent speed. (This data was to establish NASA's own emergency shutdown procedure, particularly the maximum allowable roll down time). The strip chart data from the Garrett emergency shutdown is shown in Figure 74.

4.7.2 Test Rig Operation

The test rig operated smoothly and as expected. The check-out procedure to 105-percent speed was completed without incident. The test rig was run at 100-percent speed for a significant period of time to record various data.

The following instrumentation ranges were expected and recorded at 100-percent speed with the corresponding maximum-allowable steady-state values:

Instrumentation	Expected Range	Maximum Allowable	100-Percent Speed (Actual Data)
Speed, rpm	0-38,200	39,500	36,366
Compressor Vibration, mil	0-0.5	1.0	0.1
Axial Clearance, inch	0.009-0.045	0.009-0.045	0.011 (minimum)
Radial Clearance, inch	0.002-0.010	0.001	0.009 (minimum)
Wayne-Kerr Probes, inch	0.020+	0.015	*
Balance Piston Air Pressure, psig	0-150	200	96 (maximum)
Rear Bearing Cavity Pressure, psig	-1 to -5	+15	+6 (maximum)
Thrust Load, lbs	0-1200	1500	1000 (maximum**)
Roller Bearing Air In, psig	8 to 12	5 to 15	10
Roller Bearing Air Out, psig	-1 to 5	-5 to -1	-2

*Instrumentation not working
**Calibration offset, value shown is approximate

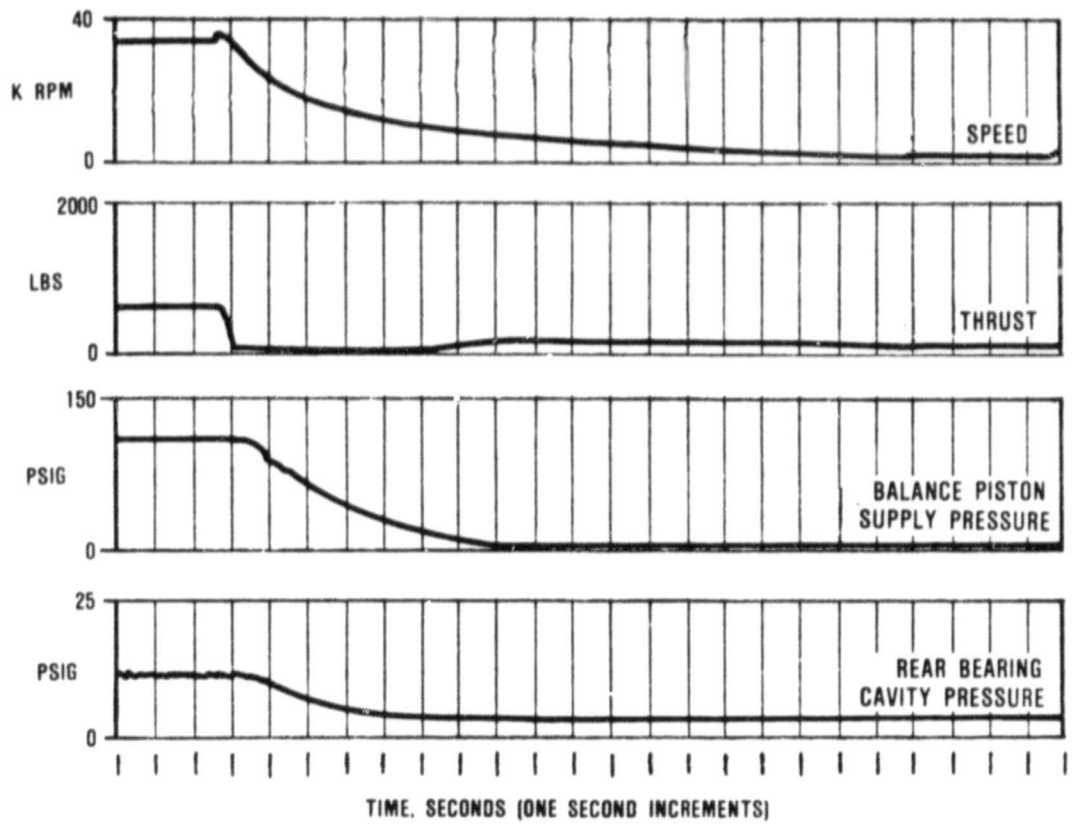

Figure 74. Emergency Shut-down Strip Chart Data (Sheet 1 of 2).

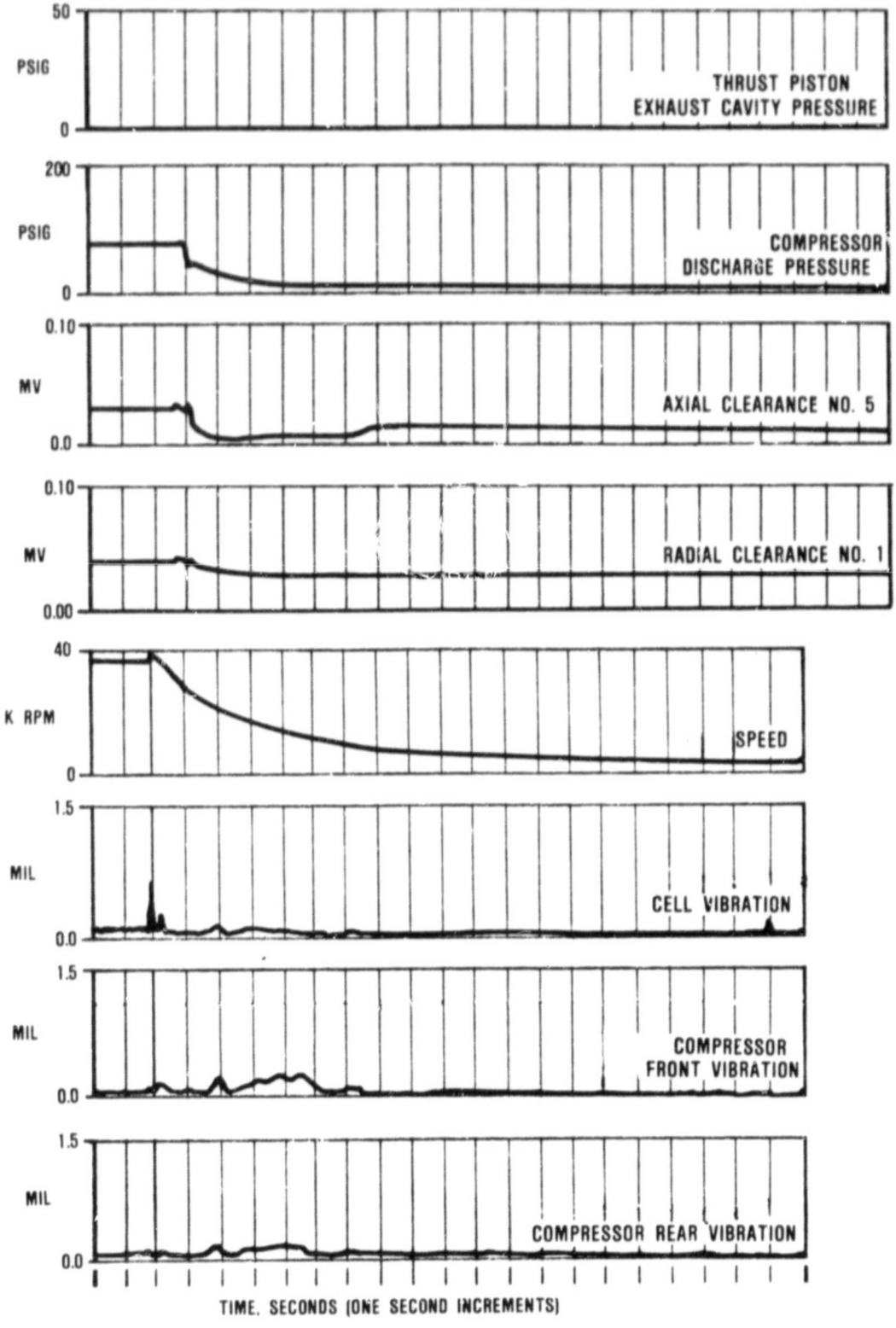

Figure 74. Emergency Shut-down Strip Chart Data (Sheet 2 of 2).

5.0 CONCLUSIONS AND RECOMMENDATIONS

It can be concluded from the mechanical check-run of the test rig and the functional check of the torque-tube and throttle-valve assemblies that all of the hardware is operating as designed. The operating characteristics of the test rig and general test rig "behavior" were as expected. When assembled and installed in the NASA facility, the test rig and throttle valve assembly will provide the vehicle for a wide range of compressor tests and evaluations.

Garrett recommends that the torque-tube be run initially with the torque-tube vent capped. The torque-tube scavange system operated better in this condition than when the torque tube was vented to ambient.

Also, Garrett recommends that NASA design and install new Bentley probes during an appropriate test rig teardown. Currently, Bentley replacement requires the teardown of the thrust-bearing cavity and clearance-control mechanism. If a special adapter configuration were designed, the Bentley probes could be installed through P/N 3553034 Support Seal (F/N 78) from the outside (diffuser exit area). See Figure 75. Installing the Bentley probes in the Support Seal would eliminate the need for a clearance-control teardown for Bentley replacement.

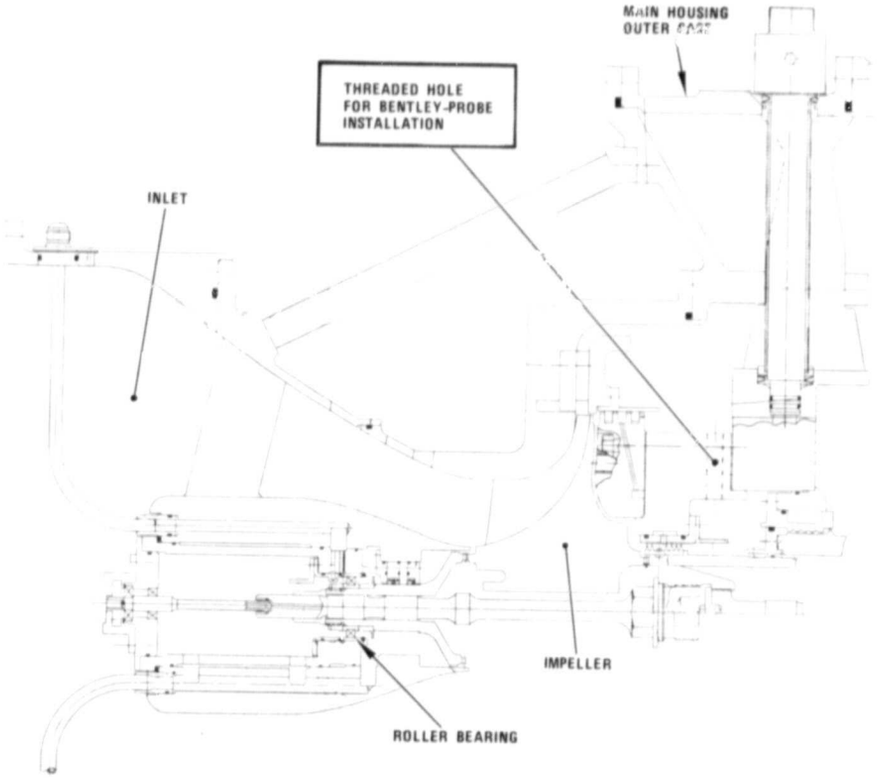

Figure 75. Recommended Bentley Probe Installation.

REFERENCES

1. Hermann Schlichting. Boundary Layer Theory. (Translated by J. Kestin.) 4th Edition. New York: McGraw-Hill, 1960.

2. J.A. Broadstone. Control of Surface Quality. Unpublished Paper Available from Surface Checking Gage Company, Hollywood, CA.

C-2